OAK RIDGE NATIONAL LABORATORY
operated by
UNION CARBIDE CORPORATION • NUCLEAR DIVISION
U.S. ATOMIC ENERGY COMMISSION

ORNL - TM - 3257

FEB 10 1972

DATE ISSUED: [redacted]

ENGINEERING DEVELOPMENT STUDIES FOR MOLTEN-SALT BREEDER REACTOR PROCESSING NO. 7

L. E. McNeese

ORNL-TM-3257

Contract No. W-7405-eng-26

ENGINEERING DEVELOPMENT STUDIES FOR MOLTEN-SALT BREEDER REACTOR PROCESSING NO. 7

L. E. McNeese

FEBRUARY 1972

OAK RIDGE NATIONAL LABORATORY
Oak Ridge, Tennessee 37830
operated by
UNION CARBIDE CORPORATION
for the
U.S. ATOMIC ENERGY COMMISSION

Reports previously issued in this series are as follows:

ORNL-4365	Period ending July 1968
ORNL-4366	Period ending September 1968
ORNL-TM-3053	Period ending December 1968
ORNL-TM-3137	Period ending March 1969
ORNL-TM-3138	Period ending June 1969
ORNL-TM-3139	Period ending September 1969
ORNL-TM-3140	Period ending December 1969
ORNL-TM-3141	Period ending March 1970

CONTENTS

CONTENTS (Continued)

SUMMARIES

ANALYSIS OF THE FLUORINATION--REDUCTIVE EXTRACTION AND METAL TRANSFER FLOWSHEET

Recently obtained data on the distribution of several rare earths between molten salt and bismuth containing reductant have been used in additional calculations made to identify the important operating parameters in the flowsheet and to determine the optimum operating conditions. The behavior of fission products more noble than uranium in the fluorination--reductive extraction process has also been considered, and the effects of these materials on the reactor breeding ratio have been calculated. Calculations were also carried out to determine the heat generation rates associated with the decay of halogen fission products that will be removed by fluorination.

DEVELOPMENT OF A FROZEN-WALL FLUORINATOR: DESIGN CALCULATIONS FOR INDUCTION HEATING OF A FROZEN-WALL FLUORINATOR

Calculations were made to show the effects of coil current, frequency, wall temperature, and fluorinator diameter on the thickness of the frozen salt film in a continuous fluorinator that employs high-frequency induction heating. An approximate analysis of the dynamics of frozen film formation was carried out, and methods for controlling the frozen film thickness were examined. Calculations were also carried out to estimate the power requirements for a 5-ft-long experimental fluorinator that employs rf heating.

DEVELOPMENT OF THE METAL TRANSFER PROCESS

The first engineering experiment (MTE-1) for studying the removal of rare earths from single-fluid MSBR fuel salt by the metal transfer process was completed during this reporting period. The main objective of the experiment was to demonstrate the selective removal of rare earths (La and Nd) from a fluoride salt mixture containing thorium fluoride. The experiment was performed at 660°C in a 6-in.-diam carbon-steel vessel,

which contained two compartments interconnected at the bottom by a pool of molten bismuth that was saturated with thorium. One compartment contained fluoride salt to which 2 mCi of ^{147}Nd and a sufficient quantity of LaF_3 to produce a concentration of 0.38 mole % had been added. The second compartment contained LiCl.

The distribution coefficients for the rare earths between the fluoride salt and the thorium-saturated bismuth were relatively constant throughout the run and were in agreement with expected values. The distribution coefficients for the rare earths between the LiCl and the thorium-saturated bismuth were higher than anticipated during the first part of the run but approached the expected values near the end of the run.

Approximately 50% of the lanthanum and 25% of the neodymium originally present in the fluoride salt were removed during the run. The rates at which the rare earths were removed are in close agreement with expected removal rates; however, the rare earths did not collect in the lithium-bismuth solution (with which the LiCl was contacted) as expected. Instead, most of the rare earths were found in a 1/8-in.-thick layer of material located at the interface between the LiCl and the thorium-saturated bismuth. It is believed that the presence of oxide in the system may account for the accumulation of the rare earths at this point.

STUDY OF THE PURIFICATION OF SALT BY CONTINUOUS METHODS

The system was charged with 28 kg of salt (66-34 mole % $LiF-BeF_2$), and ten flooding runs were carried out using hydrogen and argon. During these runs, salt flow rates of 50 to 400 cm^3/min were used with argon and hydrogen flow rates of up to 7.5 and 30 liters/min, respectively. The temperature of the column was 700°C in each case. The pressure drop across the column increased linearly with increased gas flow rate; however, the salt flow rate had only a minor effect on pressure drop. The maximum flow rate possible with the present system is about 19% of the calculated flooding rate.

SEMICONTINUOUS REDUCTIVE EXTRACTION EXPERIMENTS IN A MILD-STEEL FACILITY

Following routine H_2-HF treatment of the bismuth and the salt in the system, the phases were transferred to the respective feed tanks. Then 90 g of purified LiF-UF_4 eutectic salt was added to the salt phase to produce a UF_4 concentration of about 0.0003 mole fraction for the first mass transfer run (UTR-1). Hydrodynamic performance during the 140-min run was excellent, and ten pairs of bismuth and salt samples were taken. The column was operated at 62% and 76% of flooding (at a bismuth-to-salt volumetric flow rate ratio of unity); nevertheless, virtually none of the uranium was extracted from the salt due to an operational difficulty that prevented reductant from being added to the bismuth.

Dissolution of thorium in the bismuth feed tank in preparation for the second mass transfer experiment proceeded slowly as the result of poor mixing in the tank. In run UTR-2, 95% of the uranium was extracted from the salt. The run was made with a 200% excess of reductant over the stoichiometric requirement and with bismuth and salt flow rates of 247 ml/min and 52 ml/min, respectively. These flow rates are equivalent to about 77% of flooding. This experiment represents the first known demonstration of the continuous extraction of uranium from molten salt into bismuth containing reductant. The results indicate that high uranium removal efficiencies can be obtained in a packed column having a reasonable length.

MEASUREMENT OF AXIAL DISPERSION COEFFICIENTS IN PACKED COLUMNS

We have continued our measurements of axial dispersion in packed columns during the countercurrent flow of fluids having high densities and a high density difference. These experiments (which use mercury and water) were intended to simulate the conditions in packed columns through which bismuth and molten salt are in countercurrent flow. Results reported

previously for a 2-in.-ID column packed with 3/8-in. Raschig rings are compared with data obtained during this reporting period for 1/4-in. Raschig rings, 1/4-in. solid cylinders, and 1/2-in. Raschig rings. In each case, the axial dispersion coefficient was independent of the dispersed-phase (mercury) flow rate. Dispersion coefficients for 3/8- and 1/2-in. packing were also independent of the continuous-phase (water) flow rate; their values were 3.5 and 4.8 cm^2/sec, respectively. Data for the 1/4-in. packing indicate that the dispersion coefficient is inversely proportional to the continuous-phase flow rate. The data obtained during this study are compared with a published correlation of axial dispersion coefficient data. The present data are found to be in good agreement with the published correlation; this is remarkable since the correlation was developed from data obtained with systems having density differences between one and two orders of magnitude less than the density difference of the mercury-water system.

1. INTRODUCTION

A molten-salt breeder reactor (MSBR) will be fueled with a molten fluoride mixture that will circulate through the blanket and core regions of the reactor and through the primary heat exchangers. We are developing processing methods for use in a close-coupled facility for removing fission products, corrosion products, and fissile materials from the molten fluoride mixture.

Several operations associated with MSBR processing are under study. The remaining parts of this report describe: (1) optimized conditions for operation with the combined flowsheet that utilizes both fluorination--reductive extraction and the metal transfer process, and results of calculations showing the effect of noble-metal removal time on reactor breeding performance and the heat generation rates associated with decay of the halogen fission products; (2) results of calculations that show the sensitivity of the frozen film thickness in a continuous fluorinator heated by high-frequency induction heating to coil current, frequency, wall temperature, and fluorinator diameter; (3) results of the first engineering experiment for demonstrating the metal transfer process for removal of rare-earth fission products from fluoride salt mixtures; (4) studies of the continuous purification of salt; (5) experiments made in a mild-steel reductive extraction facility to demonstrate the extraction of uranium from molten salt by countercurrent contact with bismuth containing reductant; and (6) measurements of axial dispersion in packed columns during the countercurrent flow of mercury and water. This work was carried out in the Chemical Technology Division during the period April through June 1970.

2. ANALYSIS OF THE FLUORINATION--REDUCTIVE EXTRACTION AND METAL TRANSFER FLOWSHEET

M. J. Bell L. E. McNeese

A flowsheet that uses fluorination--reductive extraction and the metal transfer process for removing protactinium and the rare earths from the fuel salt of a single-fluid MSBR has been described previously.[1] Calculations to identify the important operating parameters in this flowsheet and to determine the optimum operating conditions have been continued using recently obtained data on the distribution of several rare earths between molten salt and bismuth containing reductant. The behavior of fission products more noble than uranium in the fluorination--reductive extraction process has also been considered, and the effects of these materials on the reactor breeding ratio have been determined by means of calculations. Calculations were also carried out to determine the heat generation rates associated with the decay of halogen fission products that will be removed by fluorination. These items are discussed in detail in the remainder of this section.

2.1 Distribution of Rare-Earth and Alkaline-Earth Elements Between Molten Salt and Bismuth Containing Reductant

Ferris and co-workers[2] have continued to measure the equilibrium distribution of fission product and actinide elements between molten salt and bismuth containing reductant. They have found that, at a given temperature, the distribution coefficient for element M, defined as

$$D_M = \frac{\text{mole fraction of M in bismuth phase}}{\text{mole fraction of M in salt phase}},$$

can be expressed as

$$\log D_M = n \log X_{Li} + \log K_M^* ,$$

where

X_{Li} = the mole fraction of lithium in the bismuth phase,

n = the valence of M in the salt phase, and

$\log K_M^*$ = a constant.

Plots of the $\log K_M^*$ values vs reciprocal absolute temperature are linear over the temperature range 625-750°C, as shown in Fig. 1. Thus, the temperature dependence of $\log K_M^*$ can be expressed as $\log K_M^* = A + B/T$. Values of the constants A and B used in the present flowsheet calculation are shown in Table 1 for several elements. These data indicate that the distribution of the rare earths is relatively insensitive to temperature and that the distribution coefficients for a given element are about the same, regardless of whether lithium chloride or lithium bromide is used as the salt phase.

2.2 Isolation of Protactinium Using Fluorination--Reductive Extraction

Calculations were made for selecting optimum operating conditions for the protactinium isolation system. Optimum conditions were tentatively assumed to be those resulting in the minimum partial fuel cycle cost. The partial fuel cycle cost includes the following components of the fuel cycle cost which are associated with the isolation of protactinium: (1) bismuth and uranium inventories in the protactinium decay tank, (2) the loss of bred uranium resulting from inefficient protactinium isolation, (3) the cost of ^7Li reductant required to extract uranium and protactinium from the fuel salt, and (4) the cost of BeF_2 and ThF_4, which must be added to the system in order to maintain a constant fuel salt composition. An interest rate of 14% per annum was used to compute inventory charges, and the value of ^{233}U was taken to be \$12/g. The following costs were used for chemicals: bismuth, \$5/lb; ThF_4, \$6.50/lb; BeF_2, \$7.50/lb; and ^7Li metal, \$55/lb.

Values that were obtained for the partial fuel cycle cost include only those charges directly related to the isolation of protactinium and include no contribution either for fluorination of the fuel salt to remove

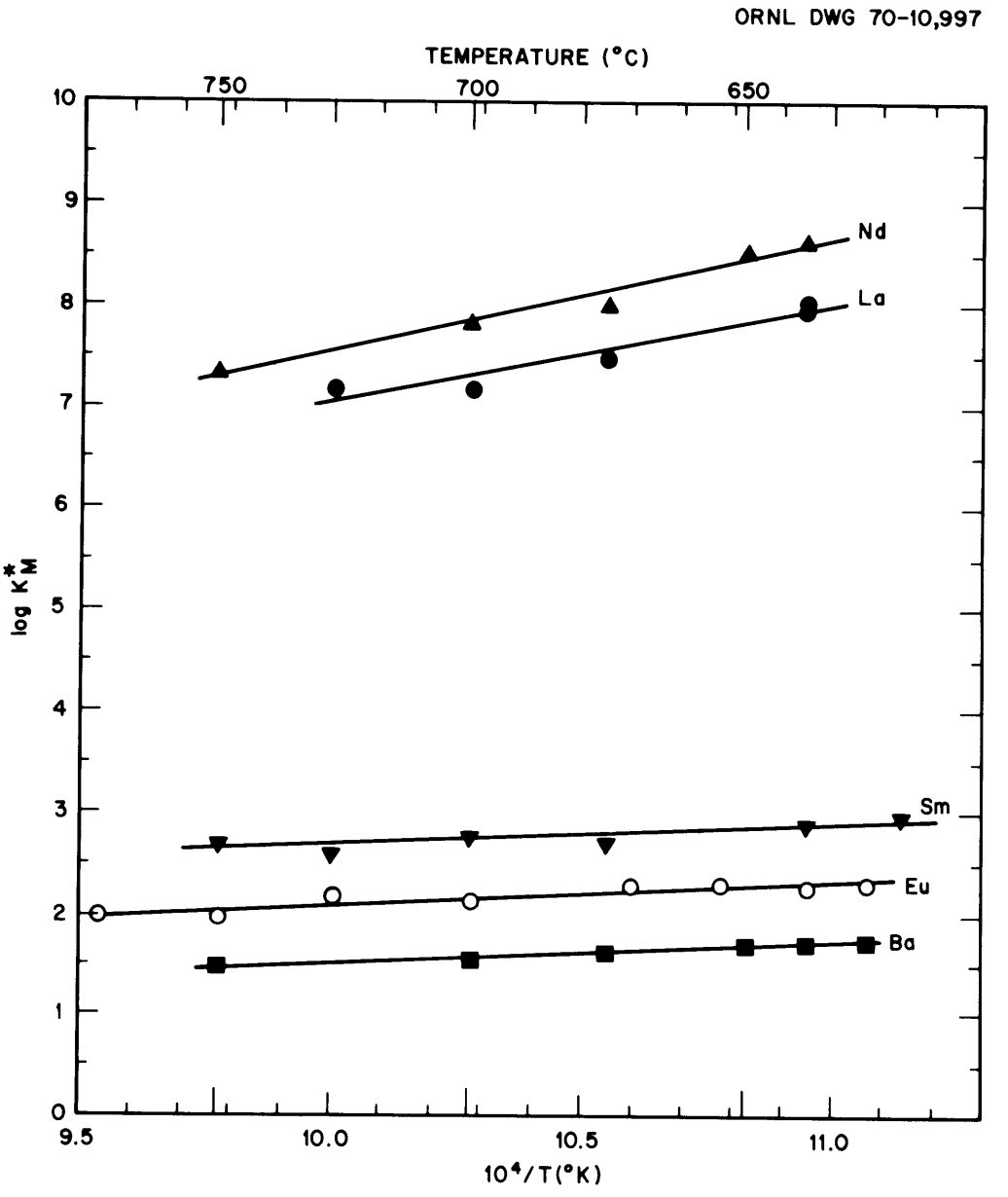

Fig. 1. Effect of Temperature on the Values of log K_M^* Obtained for Several Elements Using LiCl as the Salt Phase.

Table 1. Temperature Dependence of log K_M^* for Several Elements:

$$\log K_M^* = A + B/T \ (^\circ K)$$

(Temperature range: 625 to 750°C)

Salt	Element	A	B	Std. Dev. of log K_M^*
LiCl	Ba^{2+}	-0.6907	2,189	0.02
	La^{3+}	-2.6585	9,697	0.1
	Nd^{3+}	-3.3568	10,900	0.08
	Sm^{2+}	0.7518	1,950	0.05
	Eu^{2+}	-0.1584	2,250	0.05
LiCl-LiF (97.55-2.45 mole %)	Pm^{3+}	-1.2356	8,536	0.33
LiBr	Ba^{2+}	-0.0733	1,333	0.02
	Nd^{3+}	4.046	4,297	0.1

uranium or for removal of fission products (notably zirconium) in the protactinium isolation system.

The effect of the number of equilibrium stages in the extraction columns above and below the protactinium decay tank on the partial fuel cycle cost is shown in Fig. 2. In the final selection of the number of stages for these columns, one must consider the expense associated with an increased number of stages. The decision to use two stages below and five stages above the protactinium decay tank was made because a larger number of stages results in only a small decrease in cost. For a reductant feed rate of 429 equiv/day and a thorium concentration in the bismuth entering the column equal to 90% of the thorium solubility at 640°C, the bismuth-to-salt volumetric flow rate ratio in the columns is 0.14. The required column diameter is 3 in. if the column is packed with 3/8-in. molybdenum Raschig rings.

The effects of changes in the reductant addition rate and in the volume of the protactinium decay tank on the partial fuel cycle cost are shown in Fig. 3. The capital cost of the decay tank, a relatively expensive equipment item, will also influence the final choices for the tank volume and the reductant feed rate; however, this cost has not yet been taken into consideration. Values of 161 ft^3 for the decay tank volume and 429 equiv of reductant per day were selected as optimum. Decreasing the reductant feed rate from 429 equiv/day to 400 equiv/day reduces the partial fuel cycle cost by 2% and increases the inventory charge on bismuth in the decay tank by about 5%. The effect of the operating temperature on the performance of the protactinium isolation system, as shown by changes in the partial fuel cycle cost, is given in Fig. 4. A minimum partial fuel cycle cost of 0.0453 mill/kWhr is observed for the following conditions: a temperature of 640°C, a column having two stages below and five stages above the protactinium decay tank, a decay tank volume of 161 ft^3, and a reductant addition rate of 429 equiv/day. These conditions, which have been chosen as the reference processing conditions, result in a protactinium removal time of 10.7 days and a uranium inventory of 12.7 kg (about 0.67% of the reactor inventory) in the protactinium

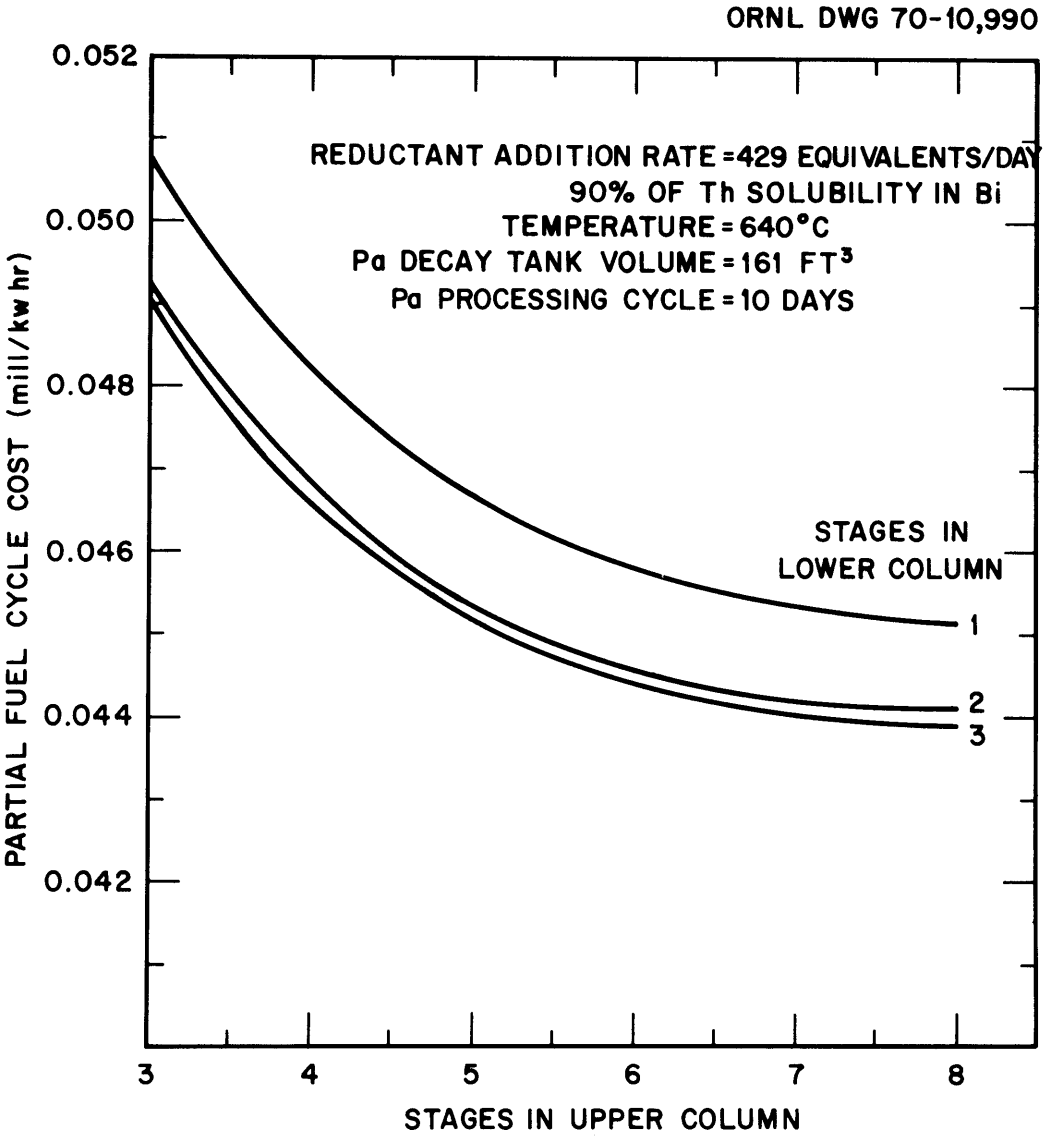

Fig. 2. Partial Fuel Cycle Cost for the Protactinium Isolation System as a Function of the Number of Stages in the Extractors Above and Below the Protactinium Decay Tank.

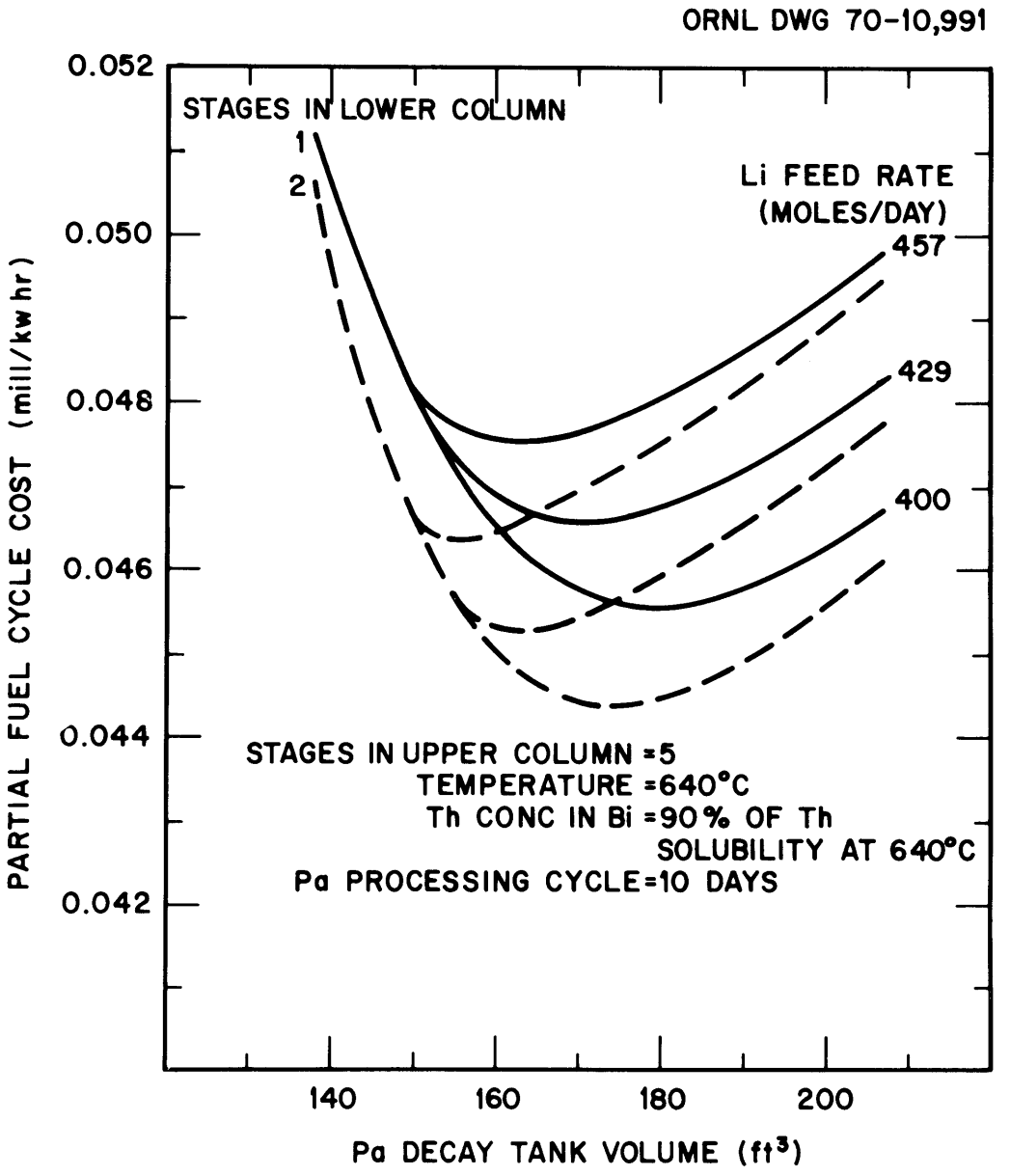

Fig. 3. Partial Fuel Cycle Cost for the Protactinium Isolation System as a Function of the Protactinium Decay Tank Volume and the Reductant Addition Rate.

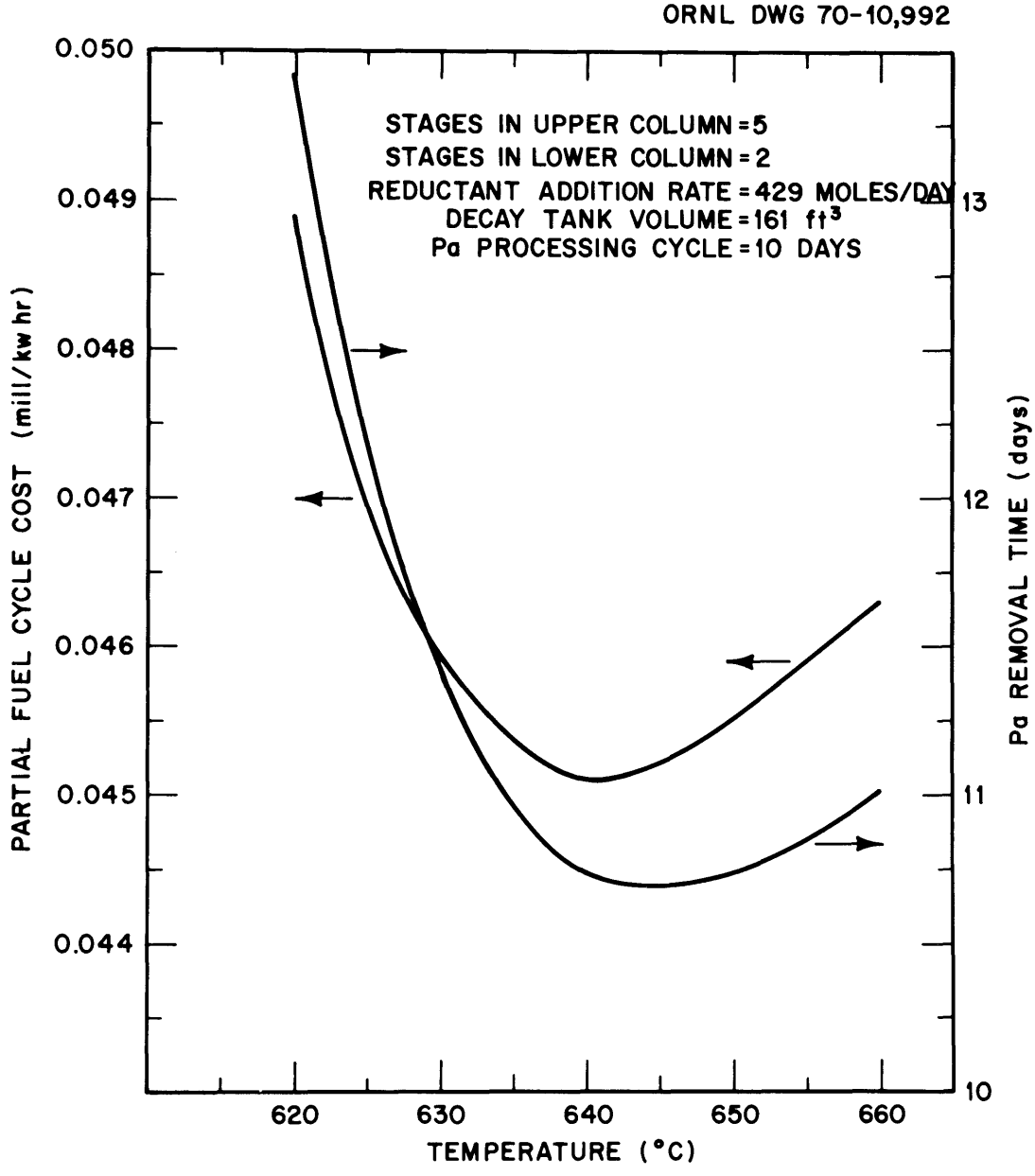

Fig. 4. Protactinium Removal Time and Partial Fuel Cycle Cost for Protactinium Isolation System as a Function of Temperature.

decay tank. The components of the partial fuel cycle cost are as follows: bismuth inventory charge, 0.0097 mill/kWhr; uranium inventory charge, 0.003 mill/kWhr; loss in ^{233}U due to inefficient protactinium isolation, 0.0013 mill/kWhr; ^{7}Li metal consumption, 0.0151 mill/kWhr; and BeF_2 and ThF_4 addition, 0.0163 mill/kWhr.

2.3 Removal of Noble Metals with the Fluorination--Reductive Extraction Flowsheet

Previous calculations of fission product inventories and poisoning in an MSBR have assumed that most of the noble metals (Se, Nb, Mo, Tc, Ru, Rh, Pd, Ag, Sb, and Te) have been removed from the fuel salt on a short (50-sec) cycle by being plated out on metal surfaces or by being transported to the off-gas system as a "smoke." As a result of these assumptions, the neutron poisoning by these materials was negligible; however, the heat load on the off-gas system was increased by about 10 MW. A more conservative assumption with regard to both neutron poisoning and heat generation in the processing plant would be that a significant fraction of these materials will remain in the fuel salt and will be removed in the processing plant. Accordingly, we have made calculations to estimate the neutron poisoning caused by these materials in the event that they remain in the fuel salt. These calculations assumed a chemical processing system in which protactinium was removed by fluorination--reductive extraction on a 10-day cycle and the rare earths were removed on a 25-day cycle by the metal transfer process. Many of the noble metals (i.e., Se, Nb, Mo, Tc, Ru, Sb, and Te) form volatile fluorides during fluorination and can be separated with varying degrees of difficulty from UF_6 by sorption on materials such as NaF. The remaining materials (Ga, Ge, Rh, Pd, Ag, Cd, In, and Sn) are relatively soluble in bismuth and will be extracted into the bismuth with the same removal time as Pa.

In these calculations, the removal time of the individual noble-metal elements was varied from 2.5 to 640 days, and the effect of this variation on the reactor performance was determined. Figure 5 shows the

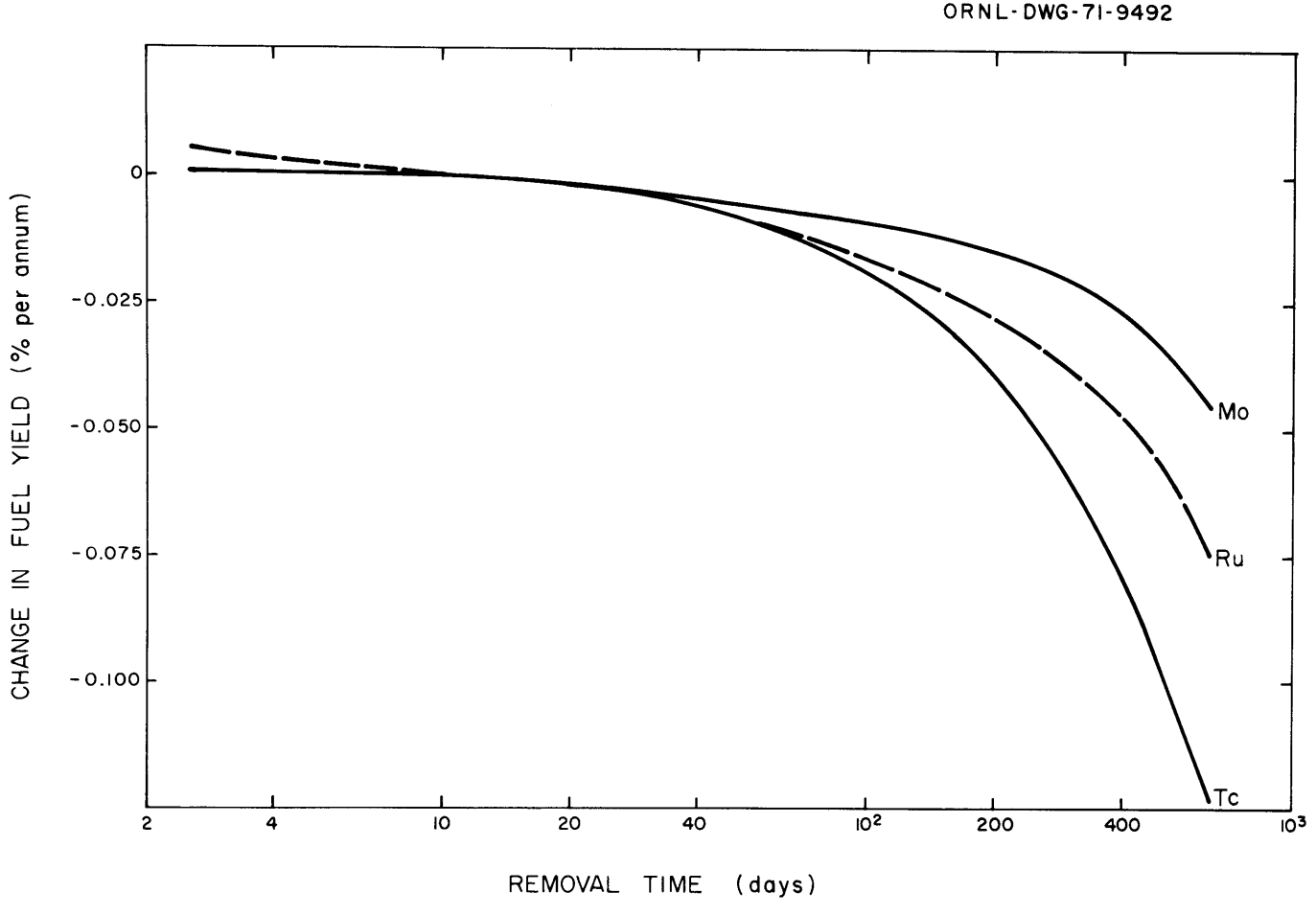

Fig. 5. Effect of Removal Time on Fuel Yield for Noble Metals That Form Volatile Fluorides.

effect of the removal time for important noble metal elements which form volatile fluorides on the fuel yield of an MSBR. The elements that have the most effect on neutron poisoning are Tc, Ru, and Mo; Se, Sb, Nb, and Te have virtually no effect. The curves in Fig. 5 are relatively flat for removal times shorter than about 100 days, indicating that the removal efficiency for an individual element may be as low as 10% without seriously impairing reactor performance. Figure 6 shows the effect of removal time on the fuel yield for elements with nonvolatile fluorides. Here, a relatively large decrease in fuel yield is associated with long removal times for Rh, while the elements Cd, Pd, and Ag have only a small effect. Negligible effects were observed for Ga, Ge, In, and Sn. In these calculations, a 10-day removal time for all noble metals was taken as the reference condition. For this condition, the total neutron poisoning (Ψ) for the noble metals is 0.0010 absorption per fissile absorption. The principal isotopes contributing to this poisoning are: ^{105}Rh, $\Psi = 0.00085$; ^{113}Cd, $\Psi = 0.00005$; ^{99}Tc, $\Psi = 0.00003$; and ^{103}Rh, $\Psi = 0.00002$.

If the noble metals are removed on a 10-day cycle, their combined thermal power will be 0.98 MW. The heat load on the fluorinator off-gas system will depend on the fractions of noble-metal fluorides that are collected in this system and their residence time. The important heat sources among noble metals having volatile fluorides are given in Table 2. The maximum amount of heat that could be produced in the UF_6 separation system, assuming that these isotopes were collected with 100% efficiency and retained indefinitely would be 0.95 MW. Similar data are shown in Table 3 for the noble-metal fission products whose fluorides are not volatile. These isotopes will add a maximum of 30 kW of heat to the bismuth stream in the protactinium isolation system.

2.4 Halogen Removal in the Uranium Removal System

In the fluorination--reductive extraction flowsheet for removal of uranium and isolation of protactinium from MSBR fuel salt, the halogen fission products will be removed as volatile fluorides and will enter the UF_6 separation system with a 10-day removal time. These materials

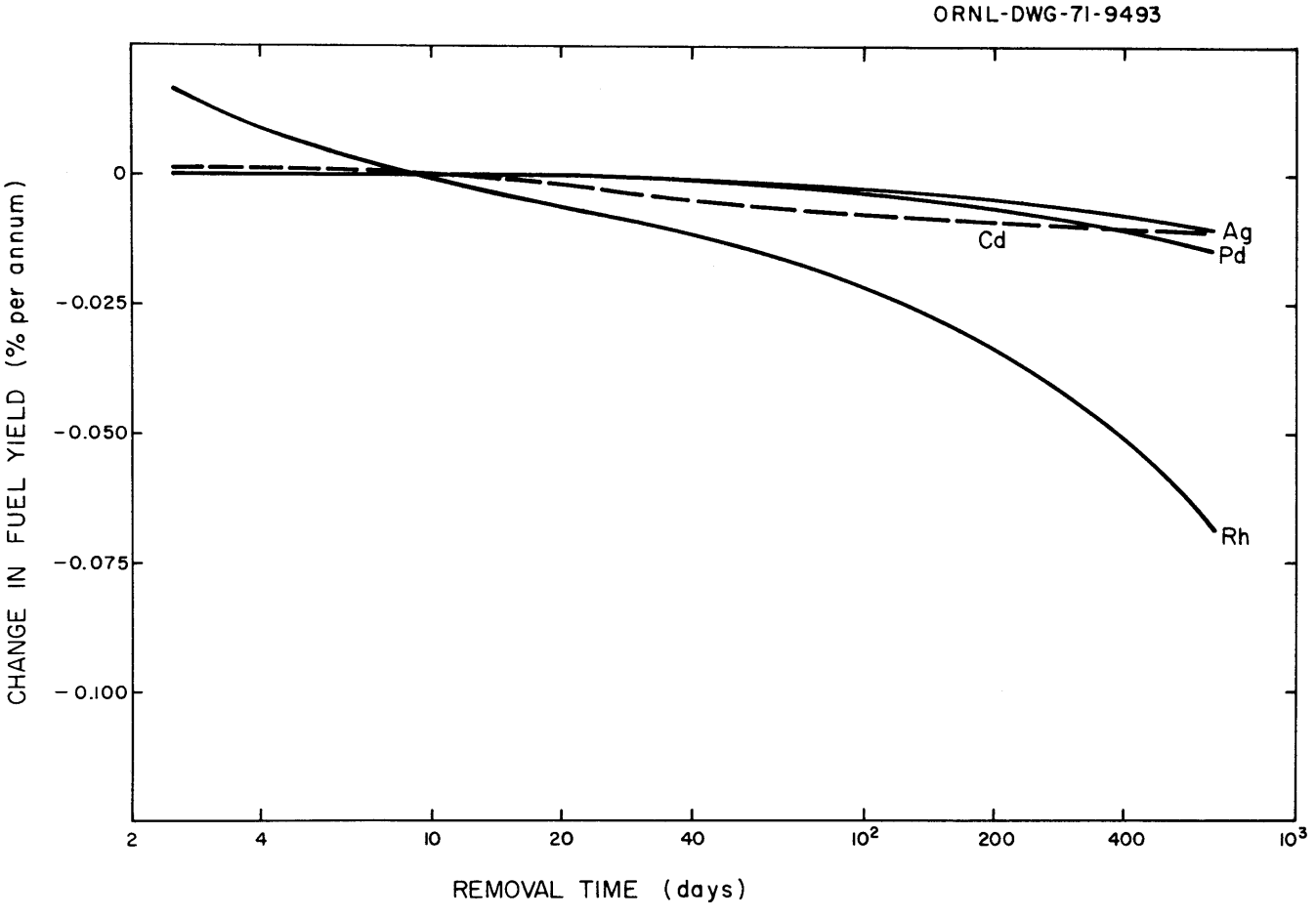

Fig. 6. Effect of Removal Time on Fuel Yield for Noble Metals That Do Not Form Volatile Fluorides.

Table 2. Thermal Power of Isotopes of Noble-Metal Elements That Have Volatile Fluorides

Removal time, 10 days

Isotope	Thermal Power (kW)	Half-Life
^{132}Te	456	78 h
^{99}Mo	139	67 h
^{103}Ru	106	40 d
^{106}Ru	45.1	1.0 y
^{129m}Te	44.6	34 d
^{95}Nb	44.0	35 d
^{127}Sb	27.2	3.9 d
^{131m}Te	18.7	1.2 d
^{134}Te	14.3	42 m
^{126}Sb	12.3	12.5 d
^{129}Sb	10.7	4.5 h
^{133m}Te	9.4	50 m
^{97}Nb	4.5	72 m
^{125}Sb	3.5	2.7 y
^{131}Sb	3.0	25 m
^{127m}Te	3.0	105 d
^{128}Sb	2.8	9.6 h
^{105}Ru	2.2	4.43 h
^{99m}Tc	1.7	6.0 h
^{130}Sb	1.5	39 m

Table 3. Thermal Power of Isotopes of Noble-Metal Elements That Form Nonvolatile Fluorides

Removal cycle, 10 days

Isotope	Thermal Power (kW)	Half-Life
^{126}Sn	20.2	$\sim 10^5$ y
^{125}Sn	5.2	9.62 d
^{129m}Sn	4.9	1 h
^{128}Sn	2.4	62 m
^{127}Sn	2.4	2.1 h
^{105}Rh	1.8	36 h
^{111}Ag	0.56	7.5 d
^{112}Pd	0.48	21.0 h
^{115}Cd	0.47	2.3 d
^{109}Pd	0.18	13.5 h
^{106m}Rh	0.14	2.2 h
^{115m}Cd	0.09	43 d
^{113}Ag	0.08	5.3 h
^{117}Cd	0.07	2.5 h
^{112}Ag	0.07	3.2 h
^{107}Rh	0.03	21.7 m

will contain a number of isotopes which could contribute as much as 0.3 MW to the heat load on the fluorinator--UF_6 collection system. The principal heat sources in this group are given in Table 4. With the exception of ^{131}I, all of the important materials are isotopes of iodine with half-lives of less than 1 day. The maximum rate at which iodine and bromine would be collected in the uranium removal system is 1 g/day.

3. DEVELOPMENT OF A FROZEN-WALL FLUORINATOR: DESIGN CALCULATIONS FOR INDUCTION HEATING OF A FROZEN-WALL FLUORINATOR

J. R. Hightower, Jr. C. P. Tung

We are continuing to study rf induction heating of molten salt as a method for providing a corrosion-free heat source for an experimental continuous fluorinator in which a film of salt is frozen on the walls to protect against corrosion. A previous study[3] showed that induction heating may be suitable for batch fluorinators, and we have made calcutions and experiments[4] which indicate that induction heating can also be used with a continuous fluorinator.

This section summarizes results of calculations that show the effects of coil current, frequency, wall temperature, and fluorinator diameter on the thickness of the frozen salt film in a continuous fluorinator employing high-frequency induction heating. Methods for controlling the thickness of the frozen film are also discussed. Since the efficiency of heating the salt cannot be reliably calculated, an experiment that uses an aqueous electrolyte as a substitute for molten salt will be carried out in order to measure heating efficiency in equipment similar to the fluorinator.

3.1 Effects of Wall Temperature, Current, Frequency, and Fluorinator Diameter on the Thickness of the Frozen Film

In the proposed fluorinator configuration (designated previously[4] as configuration I), the induction coils are embedded in the frozen salt film

Table 4. Thermal Power of Isotopes of Halogens Removed on a 10-day Cycle

Isotope	Thermal Power (kW)	Half-Life
^{131}I	117	8.05 d
^{133}I	93.2	21 h
^{135}I	66.3	6.7 h
^{132}I	12.8	2.3 h
^{134}I	11.2	53 m
^{84}Br	1.8	32 m
^{83}Br	0.58	24 h
^{87}Br	0.37	5.5 s
^{88}Br	0.14	16 s
^{136}I	0.12	83 s
^{85}Br	0.11	3.0 m
^{86}Br	0.10	54 s
^{82}Br	0.06	35.7 h
^{137}I	0.06	24 s
^{138}I	0.06	6.3 s
^{89}Br	0.04	4.5 s
^{130}I	0.02	12.5 h

near the fluorinator vessel wall. In treating the system mathematically, it was assumed that the molten zone would behave as a solid cylindrical charge in an induction coil and that the effect of bubbles in the molten salt would be negligible.

The heat generation rate in an infinitely long cylindrical charge placed inside an infinitely long coil is given by:

$$P = \frac{2\pi n^2 I^2}{g} \left(\frac{a}{p}\right) \left\{ \frac{\text{ber}\left(\frac{a}{p}\right)\text{ber}'\left(\frac{a}{p}\right) + \text{bei}\left(\frac{a}{p}\right)\text{bei}'\left(\frac{a}{p}\right)}{\left[\text{ber}\left(\frac{a}{p}\right)\right]^2 + \left[\text{bei}\left(\frac{a}{p}\right)\right]^2} \right\}, \qquad (1)$$

where

P = heat generated in molten salt, $W \cdot m^{-1}$,

g = conductivity of molten salt, $\Omega^{-1} \cdot m^{-1}$,

n = coil spacing, turns/m,

I = rms coil current, A,

a = radius of molten salt zone, m,

$p = (2\pi f g \mu)^{1/2}$, m,

f = frequency, Hz,

μ = permeability of salt, assumed to be 4×10^{-7} $Wb \cdot A^{-1} \cdot m^{-1}$,

ber, ber', bei, and bei' are bessel functions.

At steady state, the heat generated in the molten zone will be transferred by conduction through the frozen film that surrounds the molten core of the fluorinator. The equation relating the rate of heat flow to the system dimensions and properties is:

$$Q = \frac{2\pi k(T_i - T_c)}{\ln\left(\frac{r_1}{r_1 - t}\right)}, \qquad (2)$$

where

Q = heat transferred through the salt film, $W \cdot m^{-1}$,

k = thermal conductivity of the frozen salt, $W \cdot m^{-1} \cdot {}^{\circ}C^{-1}$,

t = thickness of the frozen salt film between the molten zone and the inside of the induction coil, m,

r_1 = inside radius of the induction coil, m,

T_i = liquidus temperature of the salt, °C,

T_c = temperature at the induction coil; here we assume that this temperature can be set when, actually, the fluorinator wall temperature is the quantity set.

Combining Eqs. (1) and (2) results in an expression that defines the steady-state frozen film thickness in terms of system properties and the operating variables. Equation (1) contains bessel functions, and it is somewhat cumbersome to use; a more useful approximate equation, valid for $a/p \leq 1.4$, is:

$$P = \frac{2\pi n^2 I^2}{g} \left[0.06077 \left(\frac{a}{p}\right)^{3.988}\right] . \qquad (3)$$

The salt phase, which is assumed to have the composition 68-20-12 mole % LiF-BeF_2-ThF_4, has the following properties:

$g = 1.54\ \Omega^{-1}\cdot cm^{-1}$ at 480°C (ref. 5),

$k = 0.0159\ W\cdot cm^{-1}\cdot °C^{-1}$ at 455°C (ref. 6).

It was assumed that the induction heating generator operated at 400 kHz. Combining Eqs. (2) and (3) and using the above values yields the following expression for the frozen film thickness:

$$\ln\left(\frac{D_1}{D_1 - 2t}\right)(D_1 - 2t)^{3.988} = 6.376 \times 10^5 \frac{\Delta T}{n^2 I^2} , \qquad (4)$$

where

D_1 = the inside diameter of the coil, in. (the equation is valid for $D_1 \leq 5$ in.),

t = the frozen film thickness, in.,

$\Delta T = T_i - T_c$, °C,

n = coil spacing, turns/m,

I = rms coil current, A.

The effect of temperature difference across the frozen film for a range of coil currents was determined from Eq. (4), using an assumed coil spacing of 78.7 turns per meter (2 turns/in.) and a 5-in.-ID coil. The results are shown in Fig. 7. For a constant coil current, the steady-state thickness of the frozen film thickness increases with increasing temperature difference across the film, as would be expected. The sensitivity of the film thickness to changes in temperature difference also increases as the temperature difference increases. Finally, the temperature difference can become so large that a condition is reached in which the heat generated in the molten zone is not sufficient to balance the rate of heat loss from the system and the fluorinator will freeze completely. The thickness of the film at this critical temperature difference is dependent only on the diameter of the fluorinator vessel and the relationship between the heat generated per unit length of fluorinator and the diameter of the molten zone. To illustrate this, assume that the heat generation rate is given by the relation

$$P = \alpha(D_1 - 2t)^b, \tag{5}$$

where

P = heat generation rate, $W \cdot cm^{-1}$,

α,b = constants, and

D_1 and t are as defined for Eq. (4).

If P in Eq. (5) is equated to Q in Eq. (2) (rewritten in terms of diameter rather than radius), the following general equation is obtained:

$$\Delta T = \frac{\alpha}{2\pi k} \ln\left(\frac{D_1}{D_1 - 2t}\right)(D_1 - 2t)^b. \tag{6}$$

The critical film thickness occurs when $dt/d\Delta T \to \infty$, or $d\Delta T/dt = 0$. If an expression for the quantity $d\Delta T/dt$ is determined from Eq. (16) and set

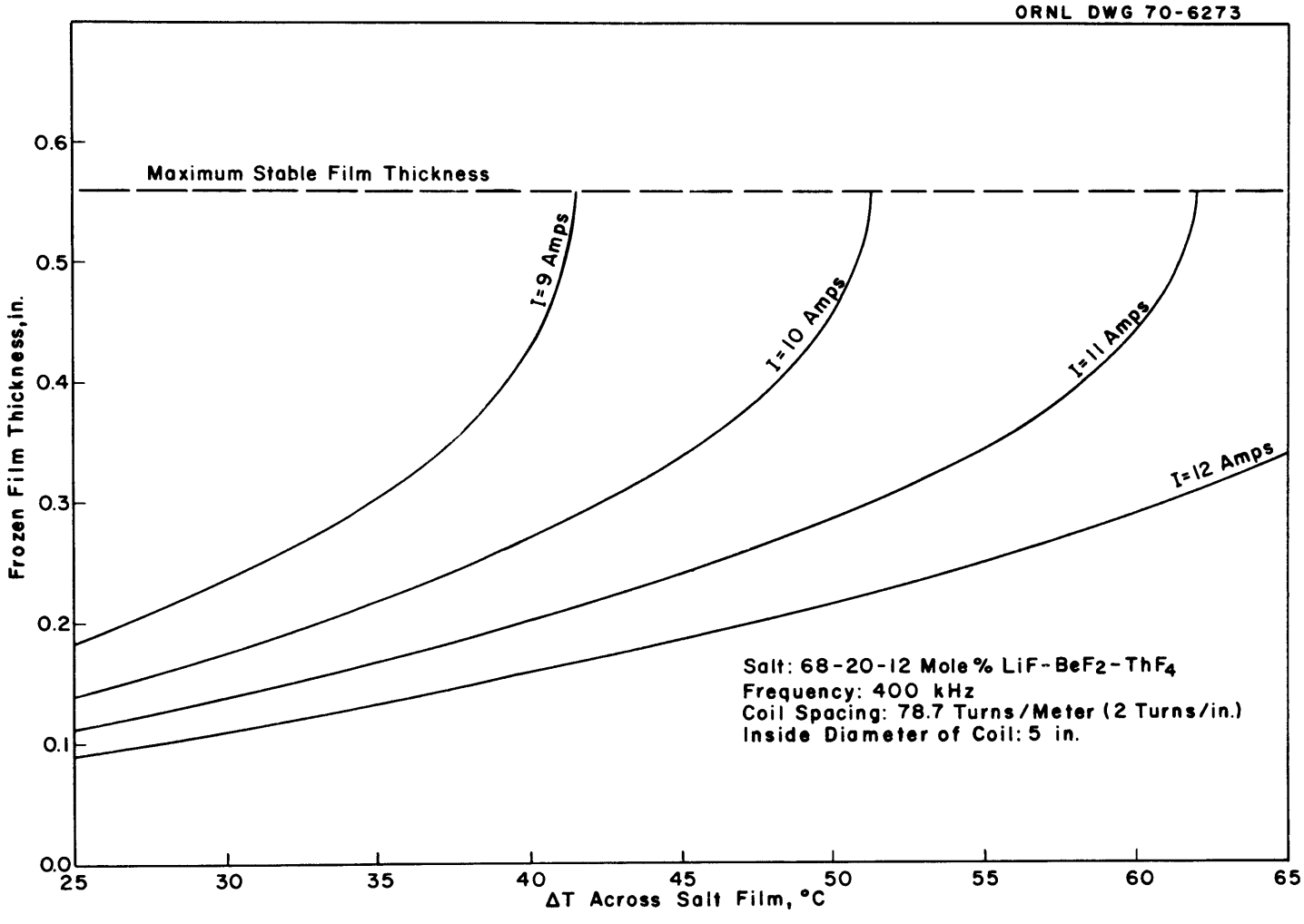

Fig. 7. Effect of Temperature Difference Across Frozen Salt Film on the Film Thickness.

equal to zero and then the resulting equation is solved for the critical frozen film thickness, the following relation results:

$$t_{crit} = \frac{\exp\left(\frac{1}{b}\right) - 1}{2 \exp\left(\frac{1}{b}\right)} D_1, \tag{7}$$

where t_{crit} is the maximum steady-state film thickness that can be maintained in a fluorinator of diameter D_1.

For an rf generator operating at 400 kHz or less, the exponent b is 3.988 and the critical film thickness is given by:

$$t_{crit} = 0.111 D_1. \tag{8}$$

For a 5-in.-ID coil, the critical film thickness is 0.56 in.

For a generator operating at 1000 kHz, Eq. (3) would not be valid; however, the following equation would approximate the heat generation rate:

$$P = 2.387 \times 10^{-4} n^2 I^2 (D_1 - 2t)^{3.146}, \tag{9}$$

in the range 3 in. < $(D_1 - 2t)$ < 5 in. The value of b is seen to be 3.146, and the critical film thickness is given by:

$$t_{crit} = 0.136 D_1. \tag{10}$$

Thus, a larger steady-state film thickness can be obtained in this case.

The following equipment size and coil spacing were chosen somewhat arbitrarily and for convenience for further calculations: a 5-in. coil, which will easily fit inside a 6-in. sched 40 pipe; and a spacing of 2 turns per inch, which is easily obtainable with 1/4- or 3/8-in.-diam conductors. A frequency of 400 kHz is a standard operating frequency for induction heating generators and was used for this reason. The calculations indicated that these choices are acceptable; with a coil current of 11 A, a

frozen film about 0.3 in. thick (which is reasonably insensitive to variations in temperature difference) can be maintained with a temperature difference of 51°C. This temperature difference could be easily measured and controlled. Because of the proportionality between the maximum stable film thickness and the fluorinator diameter, we probably would not use a smaller-diameter vessel for the experimental fluorinator because the frozen film would have to be impractically thin. We would not use a larger-diameter vessel because the effect of axial dispersion would be significant, and would result in a low uranium removal efficiency.

3.2 Control of Frozen Film Thickness, and Approximate Dynamics of Freezing

The existence of a maximum, stable steady-state thickness of the frozen film suggests that controlling the thickness of the film in a fluorinator in which the heat generation rate varies with the diameter of the molten zone may be difficult. The following considerations of the dynamics of the freezing process indicate, however, that this is not the case. The analysis is necessarily approximate since a more realistic formulation results in partial differential equations for a region with a moving boundary; such equations are solved only with great difficulty. In the present analysis, we have neglected the heat capacity of the material in the frozen film and have assumed that the temperature profiles and the heat fluxes are the same as those that would exist at steady state. The effect of this assumption is that the calculated rate of movement of the solid-liquid interface is more rapid than would actually be the case. We conclude that the time required to freeze the fluorinator is sufficiently long to permit corrective action to be taken to prevent salt in the fluorinator from freezing.

As the frozen film interface moves the distance "da" in time "$d\theta$," the heat that must flow through the frozen film consists of the heat being generated in the molten zone of radius a, the latent heat of fusion given up by the material which has changed phase, and the sensible heat contained in this amount of liquid as a result of the change in tempera-

ture between the liquidus and the bulk liquid temperatures. Neglecting the last contribution, the heat passing through the frozen film (per unit length of fluorinator) is given by:

$$Q = - \Delta H_f \rho_s 2\pi a \frac{da}{d\theta} + P(a), \tag{11}$$

where

Q = total heat removed, W/m,
ΔH_f = heat of fusion of the salt, W·sec/g,
ρ_s = density of the solid salt, g/m^3,
a = radius of the molten zone, m,
θ = time, sec,
$P(a)$ = heat generation rate in molten zone of radius a, W/m.

With the assumption that the heat capacity of the frozen film is negligible, Eqs. (2) and (11) can be combined [with $r_1 - t = a$ in Eq. (2)] to obtain the following ordinary differential equation, which approximates the dynamics of the frozen film:

$$\frac{da}{d\theta} = \frac{1}{\Delta H_f \rho_s a} \left[\frac{k(T_i - T_c)}{\ln\left(\frac{a}{r_1}\right)} + \frac{P(a)}{2\pi} \right] . \tag{12}$$

The heat of fusion, ΔH_f, was taken to be 58 cal/g (ref. 7), and the density of the solid salt was taken to be 3.4 g/cm^3. For the operating conditions listed in Fig. 8, the heat generation rate can be expressed as:

$$\frac{P(a)}{2\pi} = 0.00002326\ n^2 I^2 a^{3.988}, \quad \text{cal·sec/cm}, \tag{13}$$

where

n = turns/m,
I = coil current, A,
a = diameter of molten zone, cm.

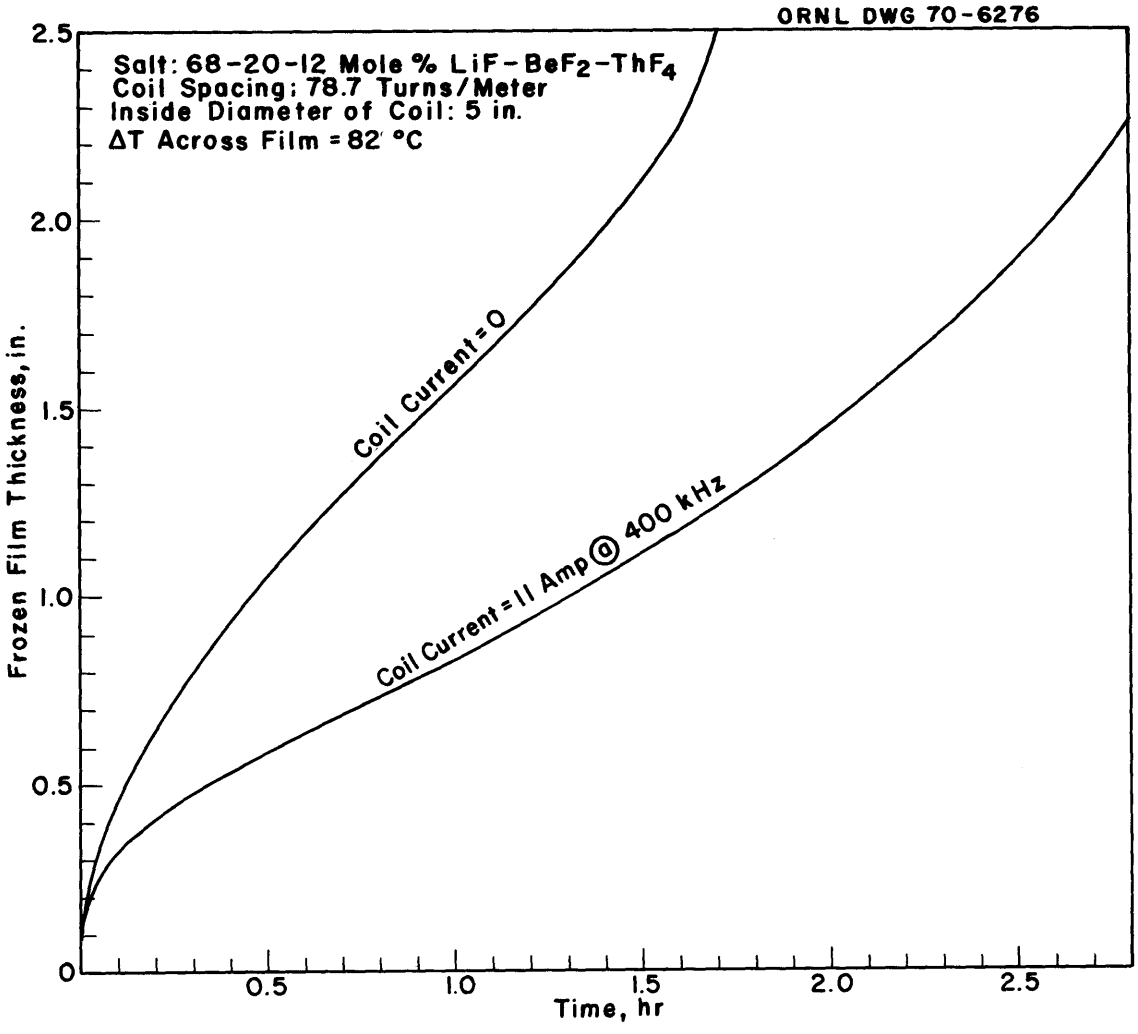

Fig. 8. Rate of Formation of the Frozen Salt Film.

Substitution of the values for the constants into Eq. (12), substitution of Eq. (13) into Eq. (12), and assumption of a 5-in.-ID coil for the fluorinator yield an expression for the time required for the solid-liquid interface to move from the edge of the coil to the position of radius a. The resulting equation is:

$$\theta = 0.05478 \int_{r_1}^{a} \frac{a\,da}{\frac{0.00380\,\Delta T}{\ln\left(\frac{a}{6.35}\right)} + 0.00002326\,n^2 I^2 a^{3.988}} . \qquad (14)$$

As shown in Fig. 7, the maximum stable film thickness with a coil current of 11 A is obtained with a temperature difference of 62°C. Calculations were made with an assumed temperature difference of 82°C (20°C greater than could be allowed for steady-state operation while maintaining a frozen film). Other conditions assumed in the calculation were: a coil spacing of 78.7 turns per meter, and coil currents of 0 A and 11 A. The results of the calculations are shown in Fig. 8, which shows that, with no heat generation in the molten zone, the time required to freeze the fluorinator completely will be greater than 1.5 hr. With the heat generation resulting from an 11-A coil current, the time required for complete freezing will be about 2.9 hr. Equation (12) shows that the freezing process can be reversed by decreasing the temperature difference. We conclude, on the basis of this analysis, that the frozen film thickness in the fluorinator could be controlled, without severe problems, by adjusting the temperature of the wall of the fluorinator. Reliable control of the frozen film thickness could be accomplished most effectively by using a direct measurement of the film thickness in a feedback loop to adjust the wall temperature. We are attempting to devise a convenient method for measuring the thickness of the frozen film.

3.3 Power Requirements for an Experimental Fluorinator

One of the purposes for making the previous analysis was to estimate the size of the high-frequency generator that would be required for a 5-ft-long experimental fluorinator. In the fluorinator considered, the power

supplied by the generator would be dissipated as heat in the molten salt in the fluorinator, in the induction coil, and in the metal walls of the fluorinator. Estimates of the amount of heat generated in the molten salt core and in the induction coil can be made from relationships found in standard textbooks on induction heating (e.g., ref. 8). However, no relationships exist in the literature for estimating the heat generated in a metal cylinder surrounding a cylindrical coil. For our calculations, we have assumed that heat would be generated in the fluorinator vessel at the same rate as in a vessel which has an outside diameter equal to the inside diameter of the fluorinator and which is placed inside a coil having the same spacing and carrying the same current as the coil in the fluorinator.

We have assumed that the fluorinator vessel and the induction coil will be made from nickel since nickel exhibits excellent resistance to fluorine when molten salt is not present and since its specific electrical resistivity is lower than that of other alloys which might be used (providing the coil temperature can be kept above the Curie transition temperature of nickel, which is 358°C). A low specific resistivity for the coil material results in a low heat generation rate in the coil.

Sufficient power can be generated in the molten salt to maintain a salt film 0.3 in. thick inside the coil with a temperature difference of 51°C between the liquid-solid interface and the induction coil when the following conditions are used: a 5-in.-ID coil placed inside a fluorinator vessel made from 6-in. sched 40 pipe, a coil spacing of 2 turns per inch, and a coil current of 11 A at a frequency of 400 kHz. The estimated heat generation rates in the molten salt, the induction coil, and the fluorinator vessel wall are 1661, 133, and 42.7 W/ft, respectively. A total heat generation rate of at least 9180 W would be generated in the case of a 5-ft-long fluorinator.

The reactance of a 5-in.-ID by 5-ft-long coil is very large, and a power factor of 0.15 was estimated from standard expressions[8] for this type of coil. With a power factor this low, a generator that has a

reactive power of 61,200 V-A is required. In order to obtain a coil current of 11 A, more than 5500 V would have to be impressed across the coil. The required voltage can be reduced by dividing the coil into a number of shorter coils that have that same diameter and spacing and are connected in parallel, with adjacent coils wound in opposite directions. If the coil is divided into 10 sections having 12 turns per section, the estimated power factor would be 0.11 and the voltage that must be impressed across each coil would be about 760 V (which is still undesirably high). If the coil were divided into 20 sections having 6 turns per section, the power factor would be 0.093, and the required voltage would be about 450 V.

Although voltages of the magnitude mentioned above would be potentially hazardous and would complicate the removal of molten salt samples from the system during operation, the sampling hazard is decreased by the fact that the induction coil must be electrically insulated from the fluorinator vessel. Use of a higher frequency may result in lower required voltage values; we will investigate this possibility later. Even if high voltages are required, we do not expect to encounter any serious problems in providing the necessary electrical insulation.

In estimating the power requirements for the generator, we have assumed that the coil and pipe are infinitely long and that the voids produced by bubbling fluorine through the molten salt will not affect the heat generation rate; also, we have essentially assumed a value for the heat generation rate in the metal wall, although it is probably not accurate. The effect of these assumptions will probably be to decrease the efficiency of heating the molten salt in the fluorinator to a value lower than that which we have estimated. With a 5-ft-long coil, the magnetic field strength is weaker than that predicted by equations for an infinitely long coil; therefore, the heat generation rate in the salt would be lower than the calculated value. The presence of bubbles will probably cause the heat generation rate to be lower than the rate that would be obtained with no bubbles present. The bubbles would probably reduce the effective conductivity of the salt, and hence the heat generation rate, since the heat generation rate in the salt is directly proportional to the conductivity of the salt.

The importance of the effects mentioned above cannot be easily determined by calculations; hence, we plan to carry out experiments using an aqueous electrolyte solution (probably HNO_3) as a substitute for molten salt.

We conclude that induction heating appears to be a reasonable means for providing a corrosion-free heat source in a molten salt fluorinator and that the operational problems which have been examined appear to be tractable.

4. DEVELOPMENT OF THE METAL TRANSFER PROCESS

E. L. Youngblood L. E. McNeese
E. L. Nicholson W. F. Schaffer, Jr.

An improved rare-earth removal process has been devised, based on the observation that rare earths distribute selectively into molten lithium chloride from bismuth solutions containing rare earths and thorium. Work that will demonstrate all phases of the improved process, which is known as the metal transfer process, is under way. The first engineering experiment (MTE-1) for studying the removal of rare earths from single-fluid MSBR fuel salt by this process was completed during the current reporting period. The main objective of this experiment was to demonstrate the selective removal of rare earths (La and Nd) from a fluoride salt mixture containing thorium fluoride.

4.1 Equipment and Materials Used for Experiment MTE-1

The experiment was performed in a 6-in.-ID carbon-steel vessel (shown in Fig. 9), which has been described previously.[9] The vessel contained two compartments interconnected at the bottom by a pool of molten bismuth that was saturated with thorium. One compartment contained MSBR fuel carrier salt (72-16-12 mole % $LiF-BeF_2-ThF_4$) to which 2 mCi of ^{147}Nd and a sufficient quantity of LaF_3 to produce a lanthanum concentration of 0.38 mole % had been added. The other compartment contained lithium chloride, a cup that contained a lithium-bismuth solution, and a pump for circulating the lithium chloride through the cup. The pump was constructed of quartz and

ORNL DWG 70-4504

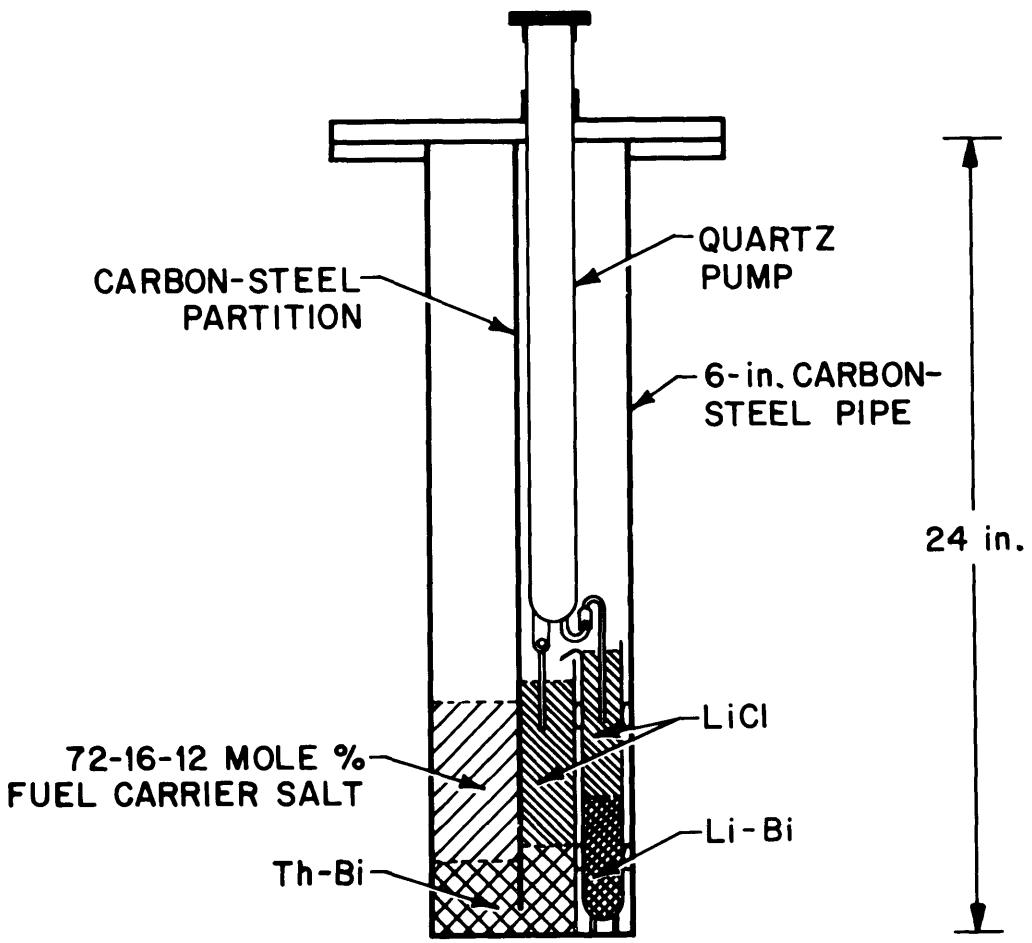

Fig. 9. Carbon-Steel Vessel for Use in the Metal Transfer Experiment.

used sapphire balls as check valves.[9] Lithium chloride was forced in and out of the pump body by varying the argon pressure inside the pump chamber. Electrical probes were used to detect the liquid level in the pump chamber and to actuate solenoid valves in order to change the argon pressure during a given pump cycle. Use of this type of pump permitted accurate control of the flow of lithium chloride through the lithium-bismuth container.

In order to obtain mixing in the main bismuth pool, about 10% of the metal volume was forced to flow back and forth every 7 min through a 1/2-in. slot below the partition between the fluoride and chloride compartments. This flow was effected by reducing the pressure of the argon cover gas in the fluoride compartment relative to that in the chloride compartment. Argon sparge tubes were placed in each side of the vessel as well as in the lithium-bismuth cup in order to promote contact between the salt and metal phases. Lumps of thorium metal (a total of 501 g) measuring approximately 0.5 in. on a side were placed in the bottom of the vessel in order to ensure that the bismuth phase was saturated with thorium. The amount of thorium added in this manner was about 20 times the amount that could dissolve in the bismuth. The exterior of the carbon-steel vessel used for the experiment was spray-coated with nickel aluminide to prevent air oxidation of the carbon steel.

The quantities of materials used in the experiment are shown in Table 5. Most of the materials were purified to remove oxides and other impurities before they were introduced into the system. The lithium chloride was purified by contact with bismuth saturated with thorium at 650°C. The carbon-steel vessel and the bismuth used in the experiment were first treated separately with hydrogen at 650°C for about 12 hr for oxide removal. The bismuth was then added to the carbon-steel vessel and was subsequently treated with hydrogen at 650°C for an additional 10 hr. Purified MSBR fuel carrier salt (72-16-12 mole % $LiF-BeF_2-ThF_4$) was obtained from the Reactor Chemistry Division. The argon used for cover gas and for operation of the lithium chloride pump was purified by passage through a molecular sieve dryer and a bed of uranium turnings operated at 600°C.

Table 5. Materials Used in Metal Transfer Experiment MTE-1

	Volume (cm^3)	g-moles
Fluoride salt 72.0-15.5-12.1-0.4 mole % $LiF-BeF_2-ThF_4-LaF_3$; 2 mCi of $^{147}NdF_3$	709	36.6
Bismuth saturated with thorium (0.35 at. % Th, 0.24 at. % Li)	797	36.7
LiCl	1042	36.6
Li-Bi (35 at. % Li)	192	11.1

The first quartz pump used in the experiment failed to operate properly; when we attempted to operate the pump to begin the experiment, we found that the check valves were stuck. Therefore, the system was cooled to 300°C and the pump was replaced with a second quartz pump of a similar design. The latter pump operated satisfactorily throughout the experiment.

4.2 Experimental Procedure

The sequence of operations carried out during the experiment can be described as follows. The lithium chloride was pumped through the lithium-bismuth container for 3 hr at the flow rate of about 25 cm^3/min. Pumping was then stopped, and the system was allowed to approach equilibrium during a 4-hr period. At the end of this period, filtered samples of the salt and bismuth phases were taken. As shown in Fig. 10, this sequence was repeated for 11 cycles. Three additional cycles were carried out in which the pumping period was increased to 6 hr and the equilibration period was omitted. During the pumping and equilibration periods, a portion of the main bismuth pool was forced back and forth between the fluoride and the chloride compartments at a rate equivalent to 10% of the metal volume every 7 min. The experiment was carried out at 660°C. During the 5-day operating period, the pump was operated 50.5 hr and 81.2 liters of lithium chloride was circulated through the lithium-bismuth container. The filtered samples taken during the experiment were prepared for analysis by cutting off the filter section with tubing cutters and cleaning the external surfaces with emery cloth. The ^{147}Nd activity in each sample was determined by direct counting of the 0.53-MeV gamma rays emitted by the sample. The lanthanum concentration in each sample was determined by neutron activation.

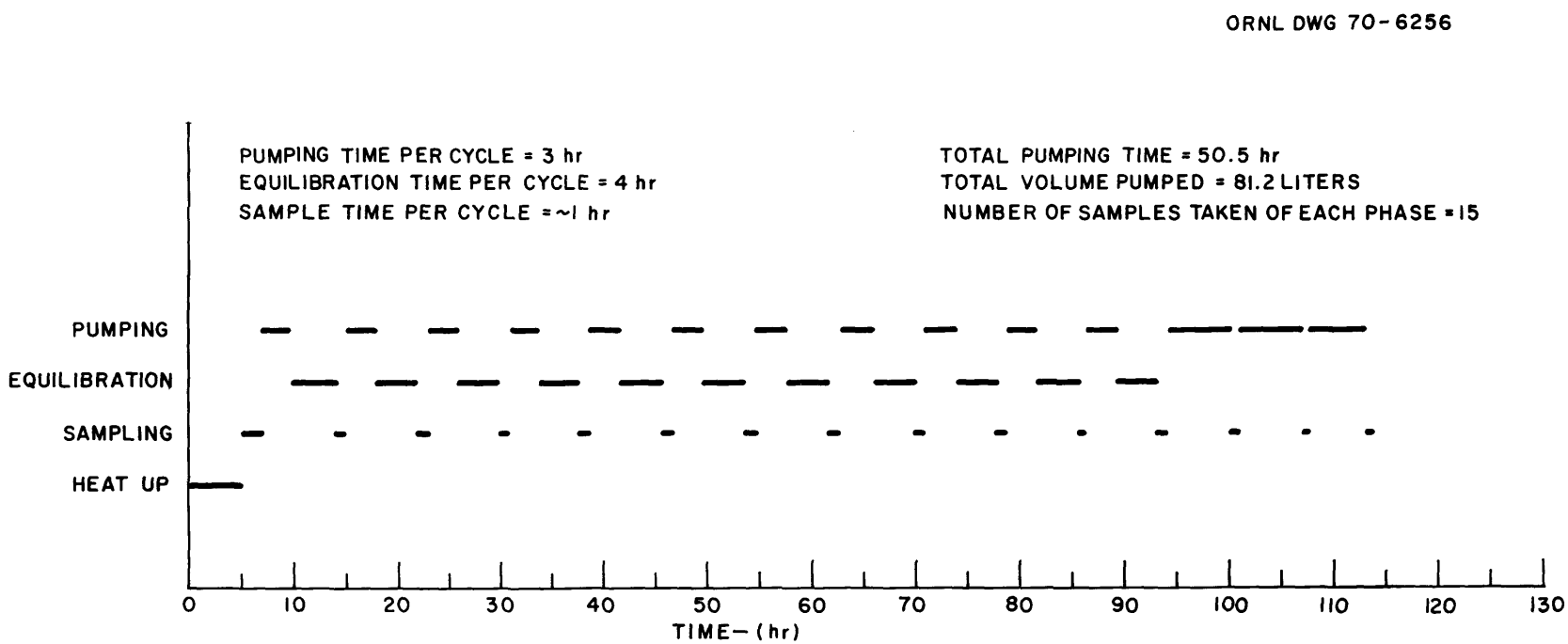

Fig. 10. Operating Schedule for Metal Transfer Experiment MTE-1.

4.3 Experimental Results

During the experiment the rare earths should have distributed between the salt and metal phases in a manner depending on the concentration of reductant in the metal phase. The relative amount of rare earth in a salt and metal phase at equilibrium can be expressed by the distribution coefficient, which is defined as:

$$D_M = \frac{\text{mole fraction of M in the bismuth phase}}{\text{mole fraction of M in the salt phase}} .$$

At equilibrium, a portion of the rare earths originally present in the fluoride salt would have been extracted into the bismuth phase, from which it should have distributed into the lithium chloride. The lithium concentration in the lithium-bismuth solution (35 at. % lithium) was sufficiently high that, at equilibrium, essentially all of the neodymium and lanthanum would be removed from lithium chloride in contact with this metal phase. Therefore, continued circulation of the lithium chloride through the lithium-bismuth cup should have gradually removed the neodymium and lanthanum from the fluoride salt and deposited these materials in the lithium-bismuth solution.

The concentrations of lanthanum, neodymium, and ^{228}Ra, a decay product of ^{232}Th, were determined in the salt and bismuth phases periodically throughout the experiment. These data are summarized in Table 6. Values for the distribution coefficients thus obtained were relatively constant during the run. As shown in Figs. 11 and 12, the average values for the distribution coefficients between the fluoride salt and bismuth for lanthanum and neodymium were 0.044 and 0.073, respectively. The distribution coefficient values are in good agreement with values obtained in previous studies.[10] Distribution coefficient values for lanthanum and neodymium between the bismuth and lithium chloride are shown in Figs. 13 and 14. These data show considerable scatter during the first two-thirds of the experiment because of the low concentrations of rare earths in the lithium chloride. The neodymium concentration in the lithium chloride was too low to be determined accurately, and the lanthanum concentration was lower than

Table 6. Concentration of Rare Earths, Lithium, and Thorium in the Salt and Bismuth Phases During Metal Transfer Experiment MTE-1

Pumping Time (hr)	Volume of LiCl Pumped (liters)	Fluoride Salt			Bismuth-Thorium					Lithium Chloride			Lithium-Bismuth			
		La (mg/g)	^{147}Nd[a] (dis $min^{-1}g^{-1}$ x 10^{-6})	^{228}Ra[b] (counts $min^{-1}g^{-1}$)	La (mg/g)	^{147}Nd[a] (dis $min^{-1}g^{-1}$ x 10^{-6})	^{228}Ra[b] (counts $min^{-1}g^{-1}$)	Li (ppm)	Th (wt %)	La (mg/g)	^{147}Nd[a] (dis $min^{-1}g^{-1}$) x 10^{-4}	^{228}Ra[b] (counts $min^{-1}g^{-1}$)	La (mg/g)	^{228}Ra[a] (counts $min^{-1}g^{-1}$)	Li (wt %)	Th (ppm)
0	0	8.21	1.56	1429	0.049	0.36	10	92	0.44	0.013	c	1414	0.0003	6.6	1.63	3.4
3	5.4	7.51	1.55		0.099	0.37		93	0.37	0.017	c		0.021		1.56	4.2
6	10.4		1.61	1183		0.37	10					1403		453		
9	15.1	7.22	1.49		0.098	0.41		78	0.38	0.022	c		0.031		1.58	3.0
12	20.0		1.50	947		0.37	9					2044		477		
15	25.0	6.58	1.46		0.068	0.36		270	0.42	0.013	c		0.029		1.63	22.5
18	29.9		1.36	744		0.29	7					2748		442		
21	34.9	5.87	1.41		0.090	0.33		420	0.45	0.021	c		0.027		1.54	18.4
24	39.7		1.17	514		0.25	5	74				2980		481		
27	44.0	5.42	1.30		0.979	0.26		80	0.43	0.162	c		0.028		1.54	10.0
30	48.8		1.16	443	0.060	0.22	3	78			2.85	3230		475		
33	54.2	4.45	1.11		0.228	0.18		80	0.28	0.323	3.23		0.024		1.60	4.5
39	64.0	3.89	1.04	340		0.22	3				1.61	2650		434		
45	65.5	3.72	0.99	456		0.24	2	76			1.23	2900		433		
50.5	81.2	3.92	0.94		0.058	0.18		120	0.32	0.131	2.46		0.114		1.53	7.0

ations per minute per gram, corrected for decay.

r minute per gram.

cted.

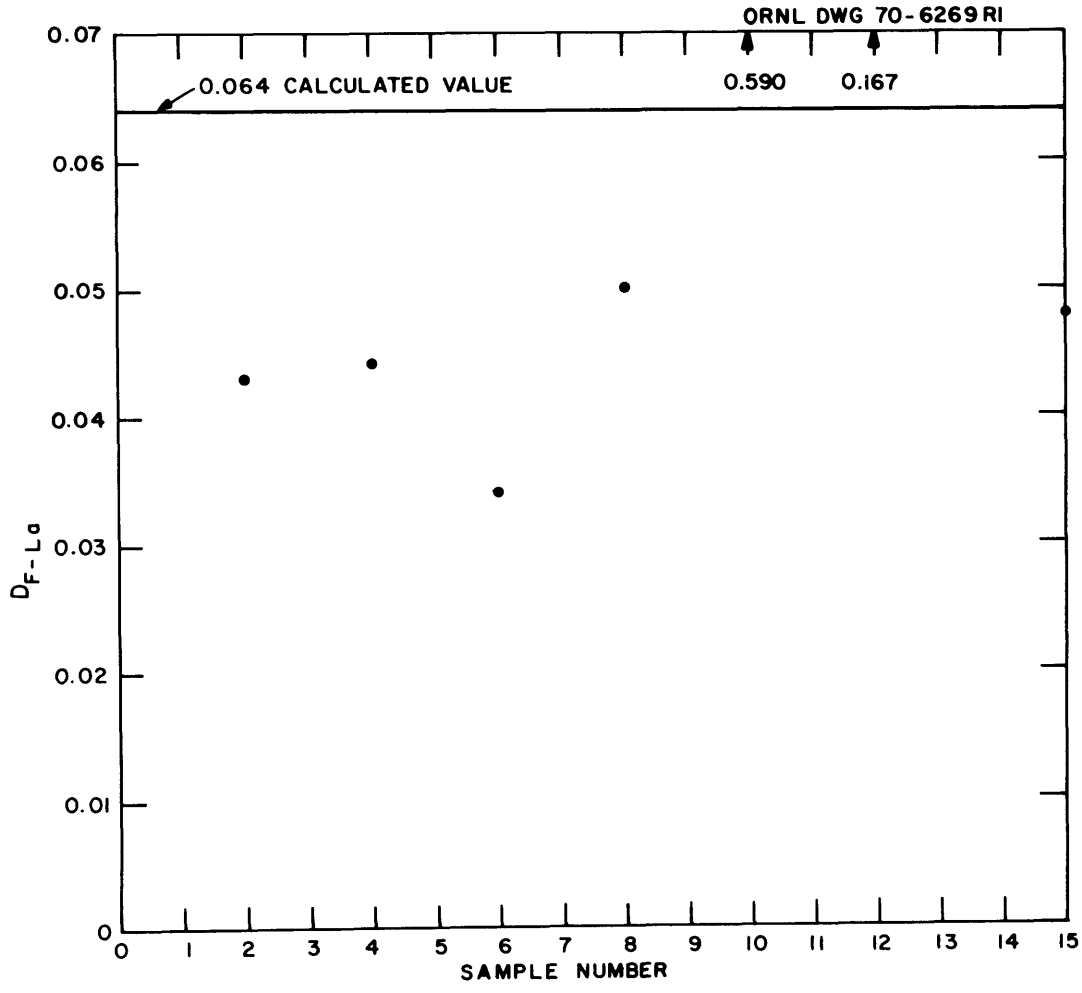

Fig. 11. Distribution Coefficient for Lanthanum Between Fluoride Salt and Bismuth Saturated with Thorium During Metal Transfer Experiment MTE-1.

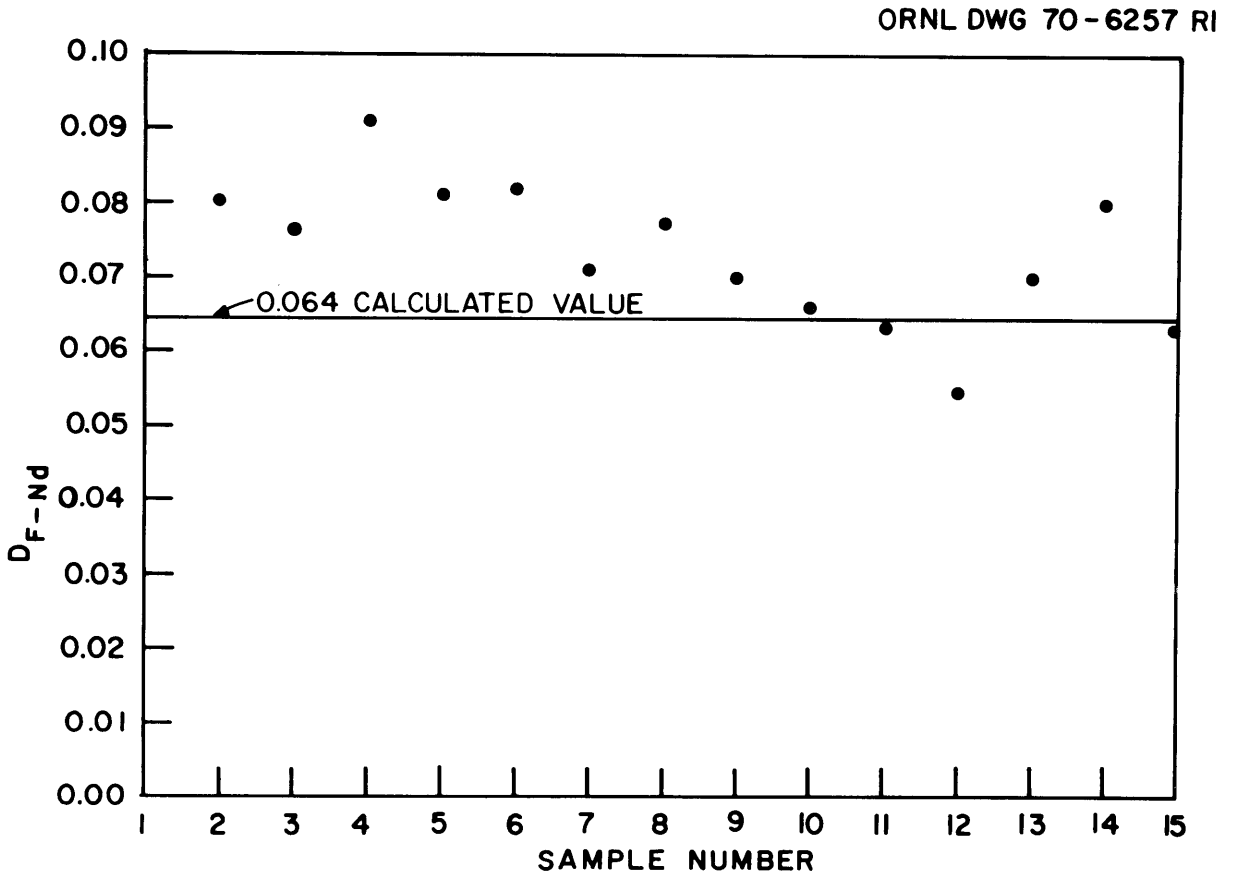

Fig. 12. Distribution Coefficient for Neodymium Between Fluoride Salt and Bismuth Saturated with Thorium During Metal Transfer Experiment MTE-1.

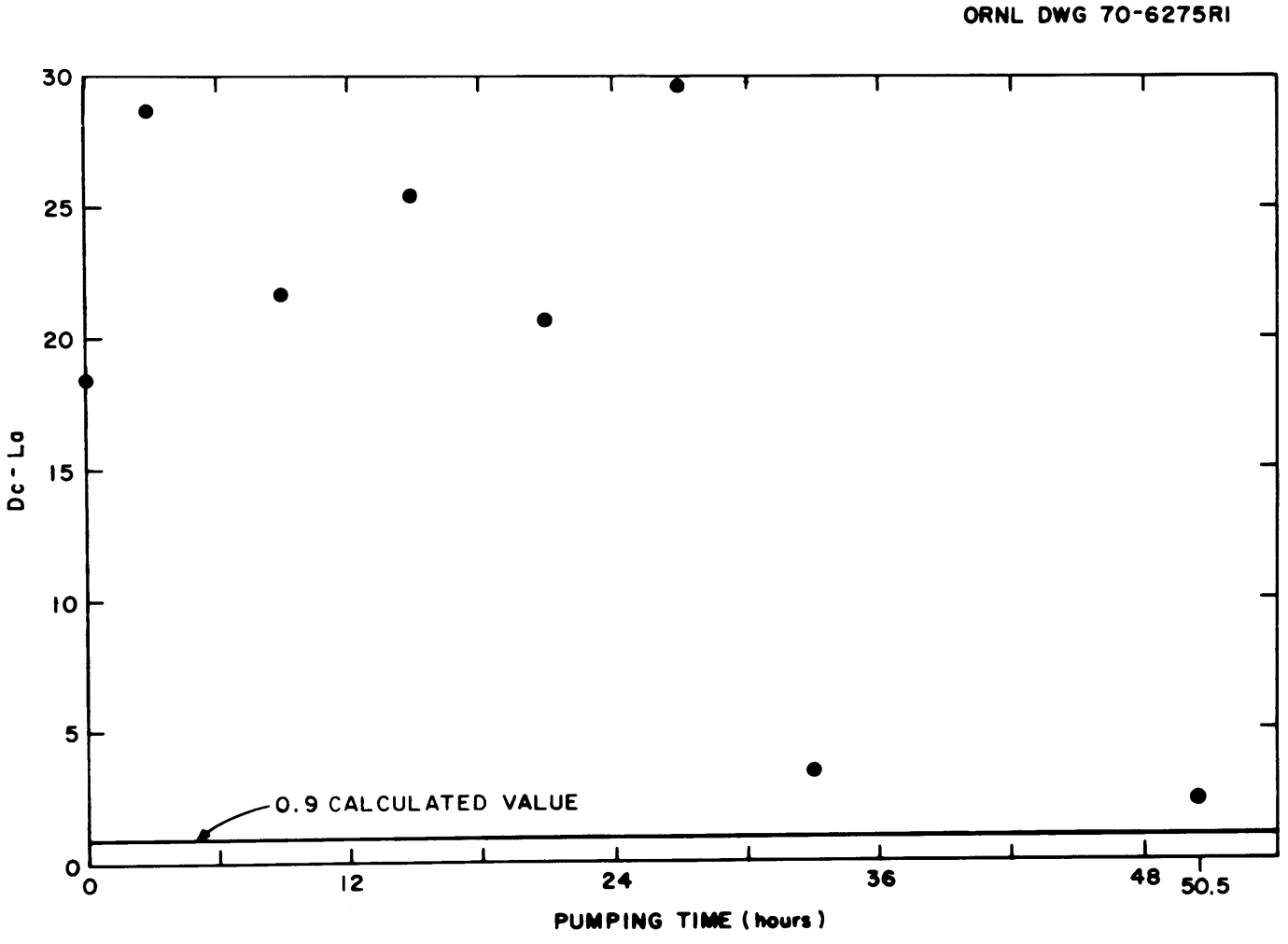

Fig. 13. Distribution Coefficient for Lanthanum Between LiCl and Bismuth Saturated with Thorium During Metal Transfer Experiment MTE-1.

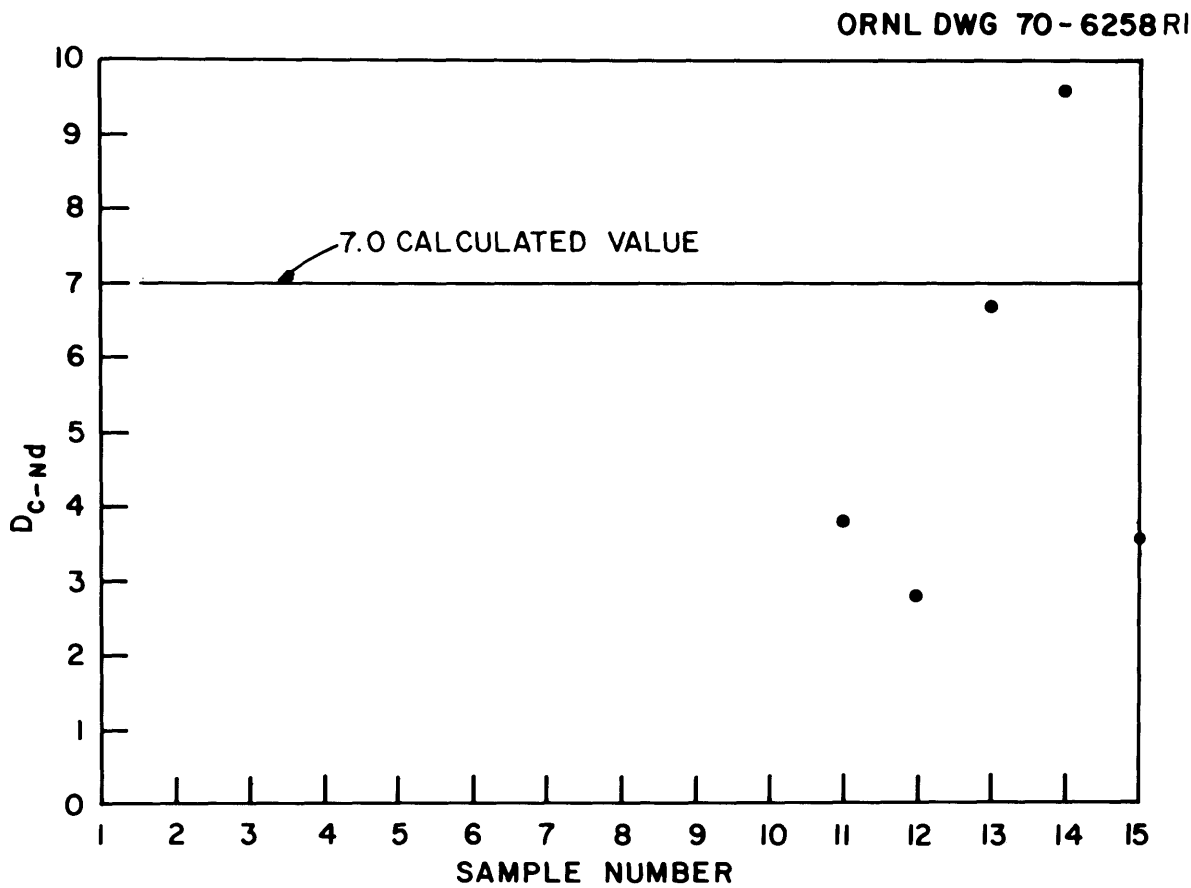

Fig. 14. Distribution Coefficient for Neodymium Between LiCl and Bismuth Saturated with Thorium During Metal Transfer Experiment MTE-1.

expected. These results probably indicate that the contact between the bismuth and lithium chloride phases was not sufficient to maintain equilibrium during this period. An argon sparge tube was inserted into the lithium chloride about midway through the run, and during the last third of the experiment the average distribution coefficients for lanthanum (2.8) and neodymium (5) between the bismuth and lithium chloride phases were reasonably close to expected values[11] (0.9 for La and 7.0 for Nd).

The distribution of radium was also followed during the experiment. Most of the radium was introduced with the fluoride salt; a small amount was introduced with the thorium metal that dissolved in the bismuth phase. During the experiment, the radium slowly transferred from the fluoride salt to the lithium chloride and lithium-bismuth phases, as shown in Fig. 15. At the end of the experiment, 72% of the radium was in the lithium chloride, 15% was in the fluoride salt, 12% was in the lithium-bismuth solution, and less than 1% was in the bismuth-thorium solution.

Approximately 50% of the lanthanum and 25% of the neodymium (after correcting for ^{147}Nd decay) originally present in the fluoride salt were removed during the experiment. Figure 16 shows the decrease in the lanthanum and neodymium concentrations in the fluoride salt as a function of pumping time and run time. The rates at which the rare earths were removed are in agreement with the expected removal rates. However, the lanthanum and neodymium removed from the fluoride salt did not collect in the lithium-bismuth as expected. No neodymium was detected in the lithium-bismuth solution during the run, and only a small fraction of the lanthanum (<1%) was collected in the lithium-bismuth. The concentration of lanthanum in the lithium-bismuth solution during the experiment is shown in Fig. 17. At the conclusion of the experiment most of the rare earths that had been removed from the fluoride salt were found in a layer of material located at the interface between the LiCl and the thorium-saturated bismuth. Reaction of oxide impurities in the system with the rare earths is thought to have caused the rare earths to deposit at the lithium chloride--bismuth-thorium interface rather than in the lithium-bismuth solution. Details are given in the following section.

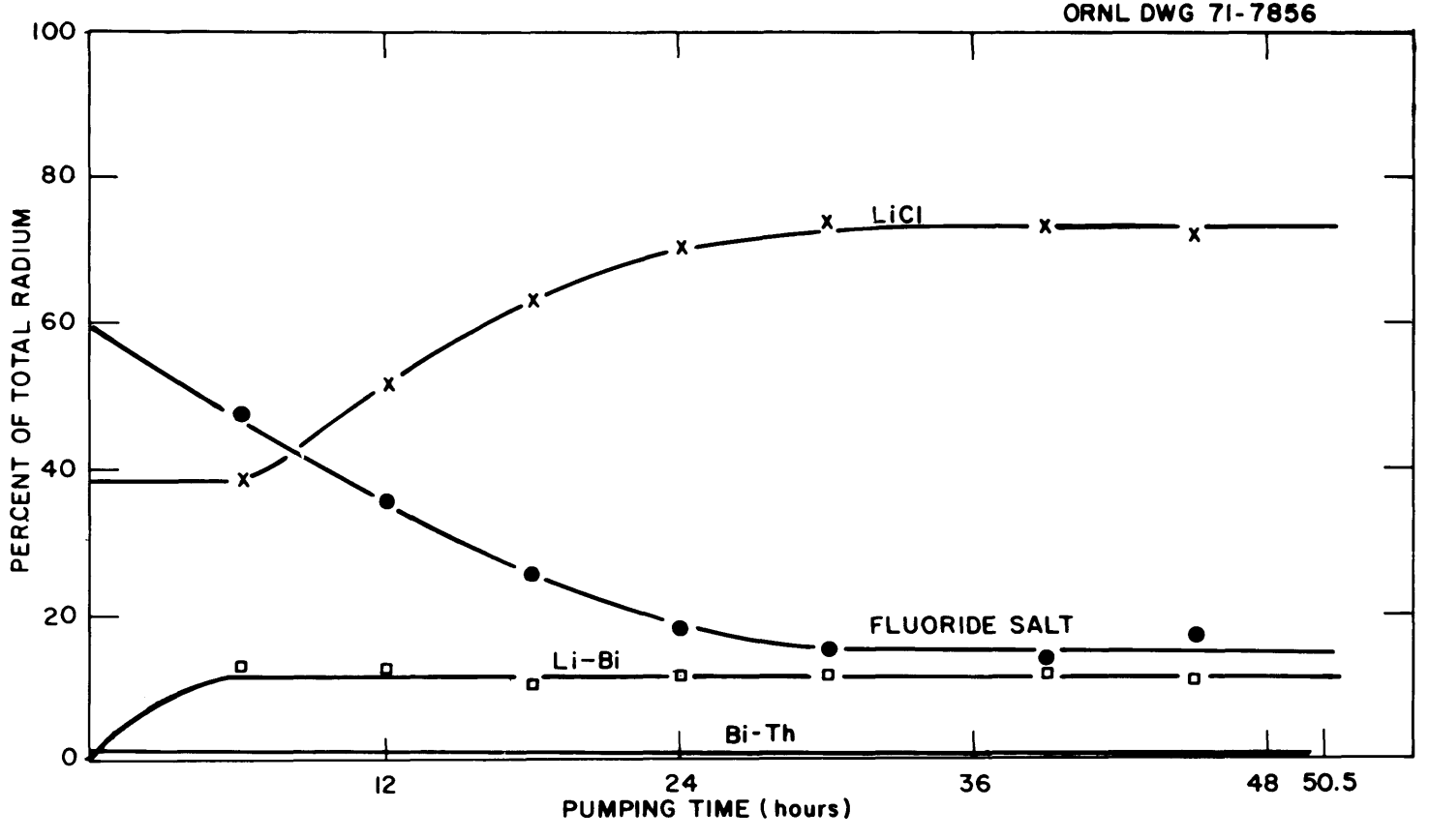

Fig. 15. Distribution of Radium Between Fluoride Salt, Bismuth Saturated with Thorium, and LiCl During Metal Transfer Experiment MTE-1.

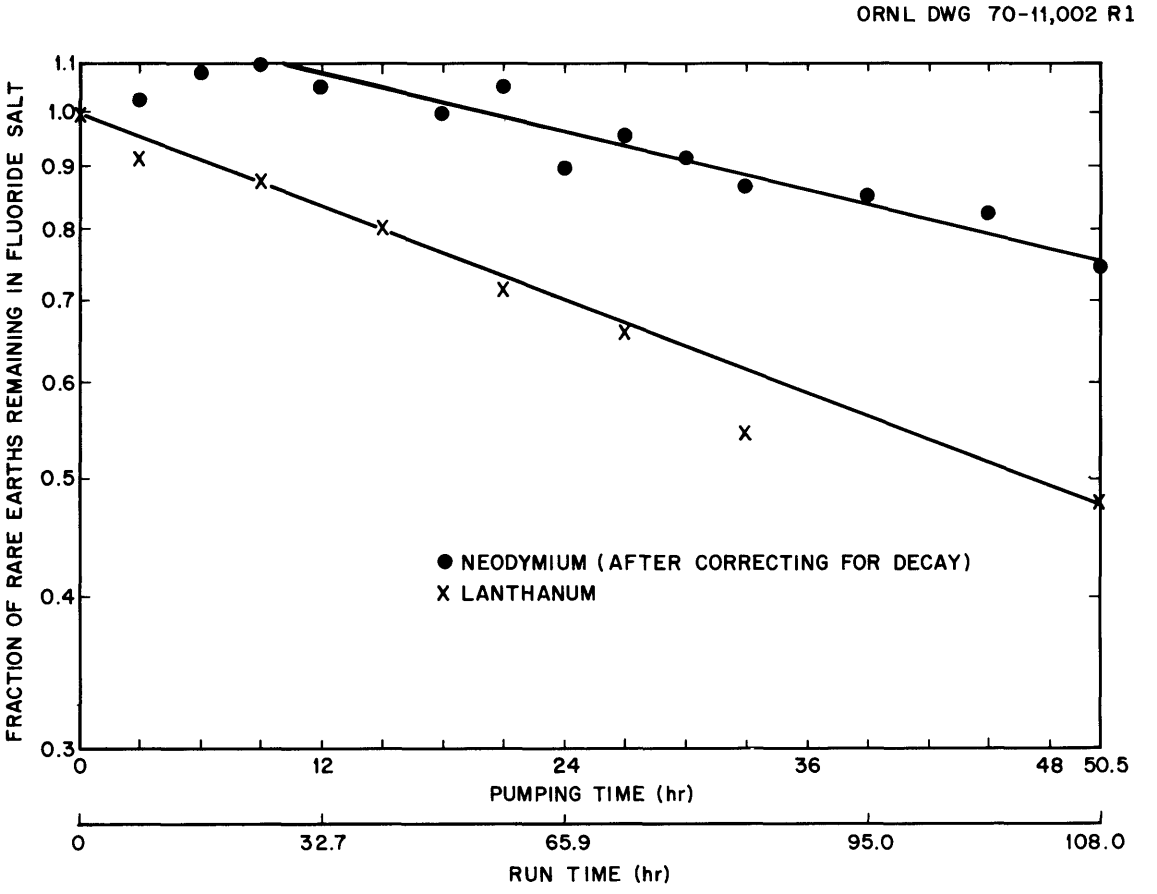

Fig. 16. Rate of Removal of Neodymium and Lanthanum from the Fluoride Salt in Metal Transfer Experiment MTE-1.

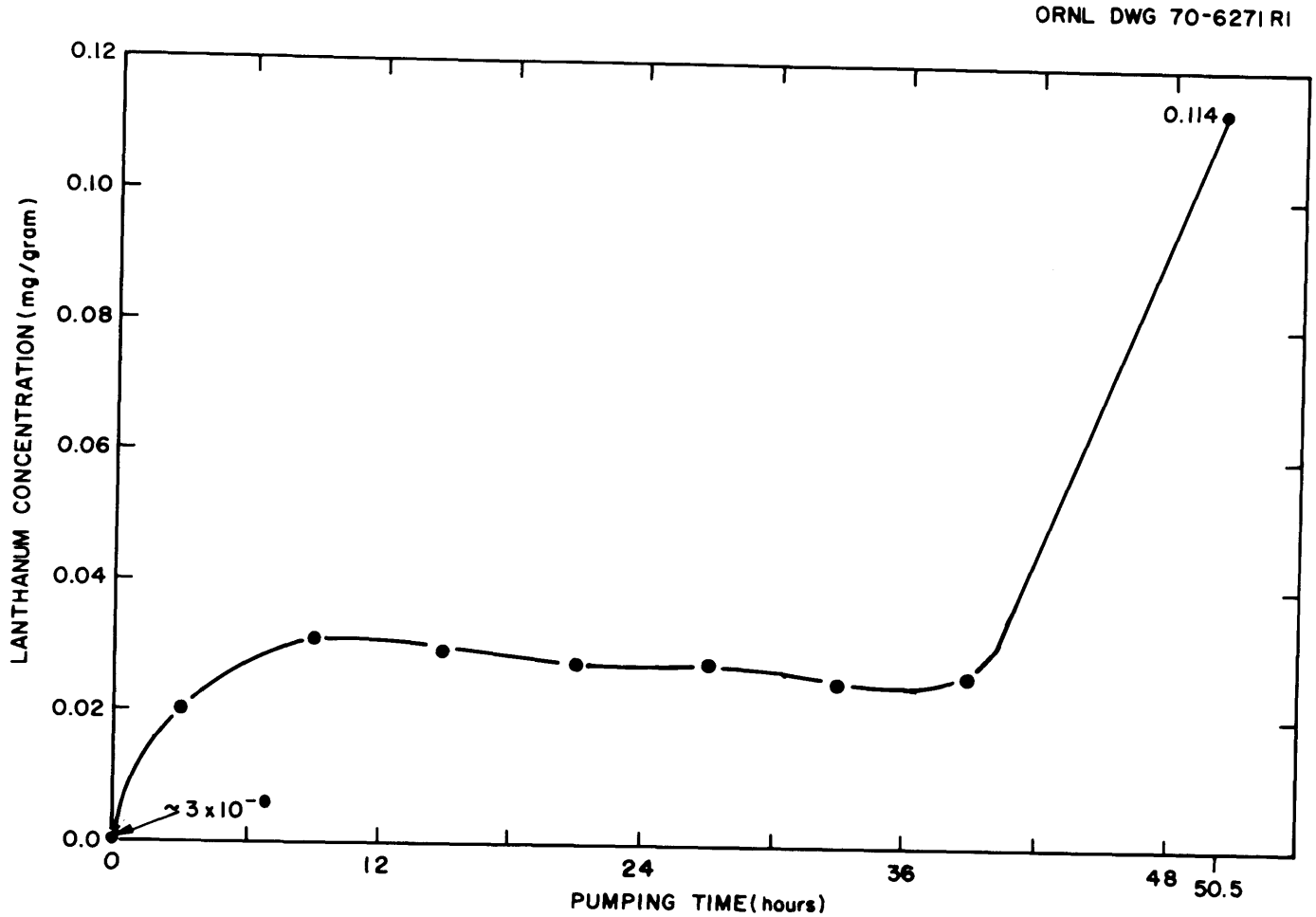

Fig. 17. Concentration of Lanthanum in the Lithium-Bismuth Solution During Metal Transfer Experiment MTE-1.

4.4 Postoperational Equipment Examination

At the end of the experiment, the carbon-steel vessel was cut apart for inspection. Most of the La and Nd that had been removed from the fluoride salt during the experiment was found in a 1/8-in.-thick layer of black material located at the interface between the lithium chloride and the bismuth that was saturated with thorium. Chemical analysis showed the black layer to contain 3.6 wt % La, 7.7 wt % Th, 12 wt % Li, 0.95 wt % Si, 0.54 wt % Fe, 59 wt % Cl, 4.4 wt % O, with the remaining material being bismuth. Thorium oxide and lithium chloride were the only compounds that could be positively identified by X-ray diffraction. Thorium oxide was expected to be present at the point where the black material was found, as the result of reaction of thorium with oxide impurities in the system. The chemical form of the rare earths in the black material was not determinded; however, it is believed that the presence of oxide in the system is responsible for the accumulation of rare earths at the interface between the lithium chloride and the thorium-saturated bismuth rather than in the lithium-bismuth solution. Oxide impurities were probably introduced into the system in two ways: (1) by deterioration of the quartz pumps, and (2) by exposure of the salt to air during installation of the second quartz pump.

Other areas in the system were also checked for accumulation of rare earths. A layer of material approximately 1/8 in. thick was noted at the bottom of the bismuth that was saturated with thorium. The appearance of this layer was different from that of the remainder of the metal phase. The material was pyrophoric, and sparks and yellow smoke could be produced by scratching its surface. It contained 20 wt % thorium and is assumed to be composed of a mixture of thorium bismuthide particles and bismuth. Although the Nd and La concentrations in this layer were about ten times the concentrations of the rare earths in filtered samples of the bismuth-thorium solution taken during the run, the actual rare-earth inventory amounted to only about 3% of the total rare earths in the system. Lumps of undissolved thorium metal could also be seen in the thorium-bismuth phase, which indicates that sufficient thorium was present to maintain the thorium con-

centration in the bismuth at its solubility during the run. The carbon-steel dip tubes and portions of the quartz pump were examined for ^{147}Nd activity. No significant amounts of ^{147}Nd were found on these components or in the lithium chloride that had condensed in the upper portion of the vessel. The carbon-steel vessel and other steel components showed no evidence of corrosion. The quartz pump was also in reasonably good condition. The surfaces of the quartz that had been in contact with the lithium chloride were white in appearance, and the quartz was somewhat weaker than initially as the result of devitrification.

4.5 Design and Testing of a Carbon-Steel Pump Having Molten-Bismuth Check Valves

Because of the difficulties encountered with the operation of quartz pumps for circulating the lithium chloride in metal transfer experiments, a carbon-steel pump having molten-bismuth check valves was designed and tested. The pump, shown schematically in Fig. 18, was operated with lithium chloride at a flow rate of about 25 cm^3/min at 650°C for about 2 weeks. The pump operated satisfactorily and appears to be suitable for use in future metal transfer process experiments.

5. STUDY OF THE PURIFICATION OF SALT BY CONTINUOUS METHODS

R. B. Lindauer L. E. McNeese

To date, the molten salt required for development work, as well as for the MSRE, has been purified from harmful contaminants (mainly sulfur, oxygen, and iron fluoride) by batch processes. It is believed that the labor costs associated with salt purification can be reduced considerably by the use of a continuous process for the most time-consuming operation, which is the hydrogen reduction of iron fluoride. Equipment[12] has been installed in which molten salt and gas can be countercurrently contacted in a packed column to obtain data for design of a full-scale continuous salt purification facility.

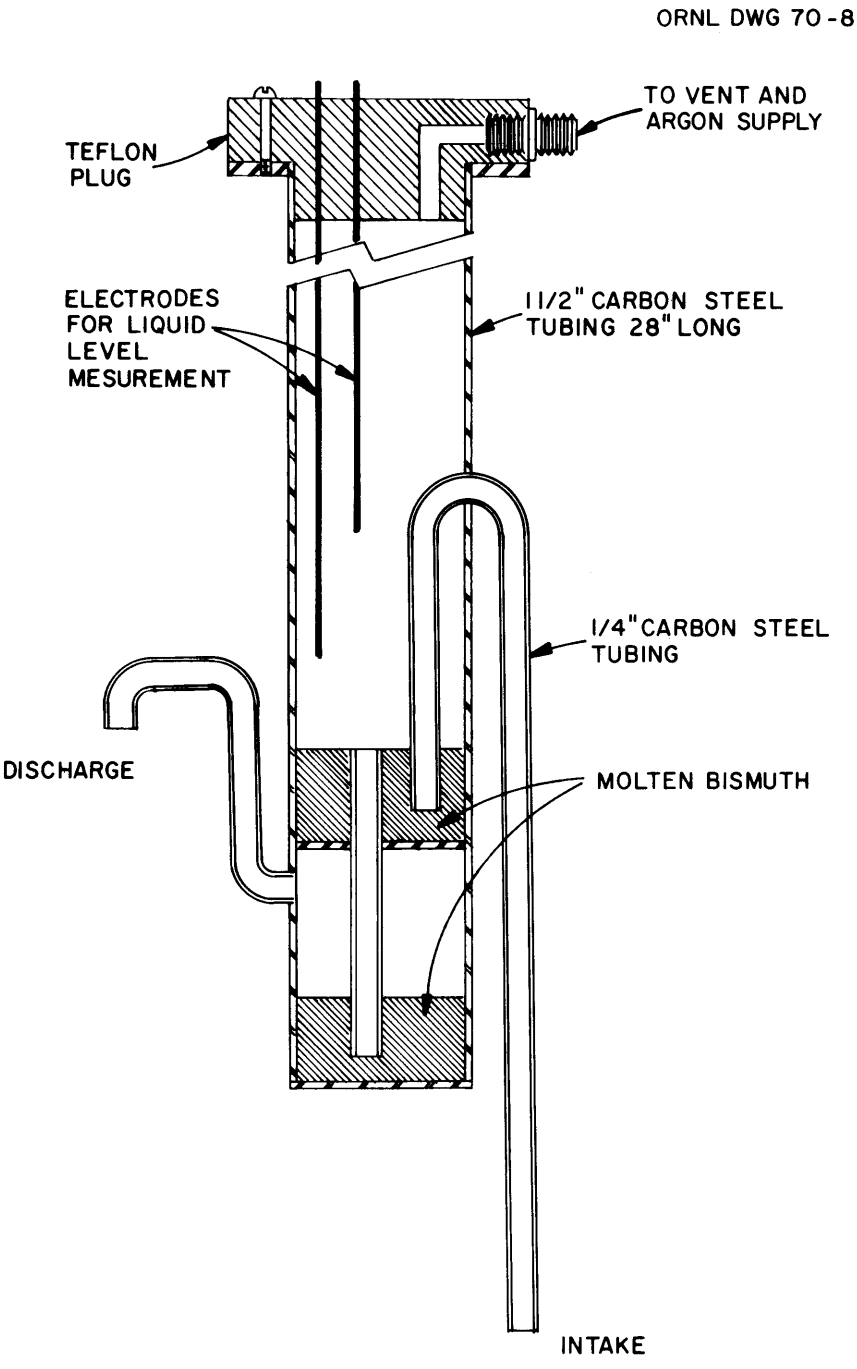

Fig. 18. Carbon-Steel Pump with Molten-Bismuth Check Valves for Metal Transfer Experiments.

During this reporting period, the system was charged with 28 kg of $LiF-BeF_2$ (66-34 mole %), and ten flooding runs were carried out using hydrogen and argon. After the first flooding run with hydrogen had been completed, the feed line to the column became plugged. Since oxide in the salt was believed to be causing the restriction, the salt was treated with a H_2-HF mixture. Oxide exceeding the amount that is soluble in the salt was removed, as indicated by analysis of the off-gas stream for water; however, the plugging recurred after salt was again fed through the column. The difficulty was apparently caused by plugging of the 1/16-in.-diam holes at the bottom of the inlet salt distribution ring. Since no restriction was found in the 1/4-in.-OD feed line, a 3/16-in.-diam hole was drilled through the inner wall of the distributor ring to provide an alternate salt inlet and the feed line was replaced with a 3/8-in.-diam line. After this modification, satisfactory salt flow to the column was obtained. Details of the operations carried out for the removal of oxide from the salt and of the flooding runs are given in the remainder of this section.

5.1 Batch Treatment of Salt for Oxide Removal

After the first run, most of the salt in the system (13.3 liters) was treated with a 4% $HF-H_2$ mixture in the feed tank for 9 hr. At the beginning of the treatment period, the salt was heated to 650°C to dissolve as much of the oxide as possible. As oxide was removed from the salt, the temperature of the salt was slowly decreased to a final value of 535°C in order to increase the solubility of HF in the salt and thereby increase the rate of reaction between HF and the oxide.

The off-gas stream from the oxide removal operation was continuously analyzed for water by use of a electrolytic hygrometer, which was preceded by a NaF bed for removing HF.[13] A total of 580 ppm of oxide was removed; this is slightly more than twice the solubility of BeO in the salt at 650°C. The average HF utilization was 30%.

5.2 Measured Flooding Rates During Countercurrent Flow of Molten Salt and Hydrogen or Argon

During the flooding runs, salt flow rates of approximately 50 to 400 cm^3/min were used with argon and hydrogen flow rates of up to 7.5 and about 30 liters/min, respectively, as shown in Table 7. The temperature of the column was 700°C in each case. The pressure drop across the column increased linearly with increases in gas flow rate as shown in Fig. 19, which summarizes the best data from the ten runs. At the flow rates studied thus far, the salt flow rate had only a minor effect on pressure drop. In the figure, points obtained with the higher salt flow rates usually lie near the upper side of the band, although some data scatter was observed. Five of the ten runs were terminated when the salt-gas interface was depressed below the seal loop in the exit line in the column by the combined pressure drop in the off-gas line and in the column. The maximum flow rate possible with the present system is about 19% of the calculated flooding rate, although smooth operation is observed only up to about 12% of the calculated flooding rate. At the higher flow rates, operation was erratic and the pressure drop across the column fluctuated over a range of 2 to 3 in. of salt. The variation in pressure drop was possibly the result of poor salt distribution at the top of the column. One run was carried out in which the system was operated with a high salt-gas flow ratio (using an argon flow rate of about 1 liter/min). The salt flow rate was increased stepwise to 280 cc/min; then, after 15 min at this condition, the salt flow rate was increased to 400 cm^3/min for 5 min. No indication of flooding was observed. The pressure drop across the column was about 30 in. H_2O. These observations indicate that a column of this type should have a much higher capacity for an operation, such as removal of oxide from salt by treatment with H_2-HF, in which the HF utilization is high and low gas-to-salt flow ratios can be used.

In the final flooding run, stable operation was obtained with a salt flow rate of 100 cm^3/min and hydrogen flow rates up to 20 liters/min. This hydrogen flow rate is sufficient to reduce 400 ppm of iron (as Fe^{2+}) from

Table 7. Summary of Countercurrent Runs Made with $LiF-BeF_2$

Run No.	Average Salt Flow Rate (cm^3/min)	Maximum Gas Flow Rate (liters/min)	Gas Used	Duration of Contacting (min)	Percent of Calculated Flooding Rate	Maximum Salt Holdup (%)
1	53	30.5	H_2	115	12	13
2	173	7.5	Ar	45	23	>15
3	140	6.3	Ar	130	16	15
4	120	23.5	H_2	45	15	24
5	90	25.5	H_2	35	14	15
6	282[a]	~1	Ar	40	6	18
7	175	24.0	H_2	58	19	21
8	183	6.2	Ar	60	19	24
9	122	6.8	Ar	80	17	11
10	104	24.3	H_2	95	15	18

[a]Rate was increased to 400 cm^3/min toward the end of the run without flooding the column.

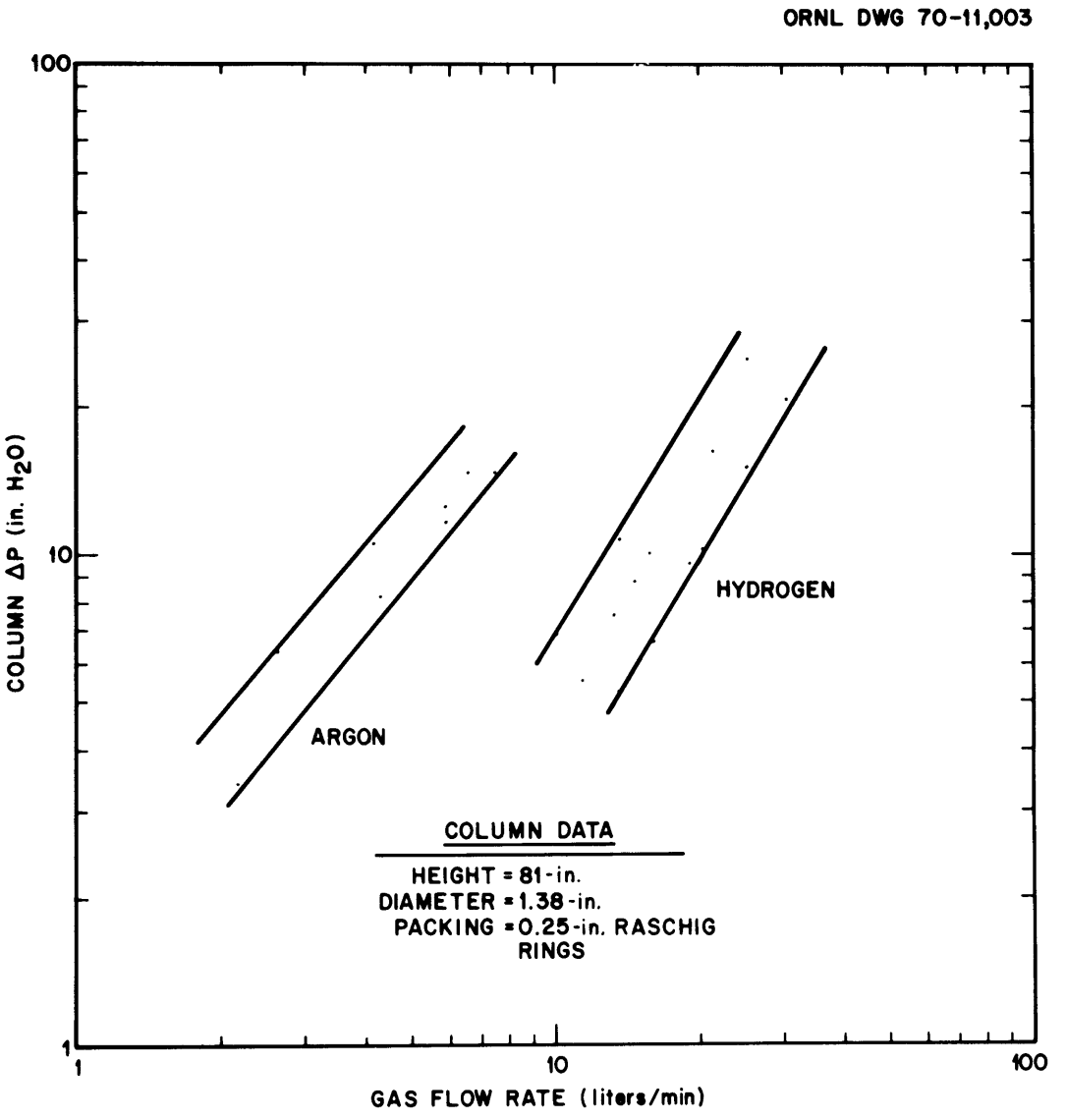

Fig. 19. Column Pressure Drop During Countercurrent Flow of Molten Salt (66-34 mole % $LiF-BeF_2$) and Either Argon or Hydrogen.

a 100 cm^3/min salt stream, assuming that the gas and salt reach equilibrium at 700°C; however, the mass transfer coefficient is probably not sufficiently high to allow equilibrium to be reached with the present column height (81 in.).

6. SEMICONTINUOUS REDUCTIVE EXTRACTION EXPERIMENTS IN A MILD-STEEL FACILITY

B. A. Hannaford C. W. Kee
L. E. McNeese

Following routine H_2-HF treatment of the bismuth and salt in the system, the phases were transferred to their respective feed tanks. Then 90 g of purified LiF-UF_4 eutectic salt was added to the salt phase to produce a UF_4 concentration of about 0.0003 mole fraction for the first mass transfer run (UTR-1). Hydrodynamic performance during the 140-min run was excellent, and ten pairs of bismuth and salt samples were taken. The column was operated at 63% and 82% of flooding (at a bismuth-to-salt volumetric flow rate ratio of unity); nevertheless, virtually none of the uranium was extracted from the salt due to an operational difficulty that prevented reductant from being added to the bismuth.

Dissolution of thorium in the bismuth feed tank in preparation for the second mass transfer experiment proceeded slowly as the result of poor mixing in the tank. In run UTR-2, 95% of the uranium was extracted from the salt. The run was made with a 200% excess of reductant over the stoichiometric requirement and with bismuth and salt flow rates of 247 ml/min and 52 ml/min, respectively. These flow rates are equivalent to about 83% of flooding.

6.1 Preparation for Mass Transfer Experiments

In preparation for the first mass transfer experiment with uranium, the salt and bismuth were treated with H_2-HF to remove traces of oxides. The procedure was essentially the same as described earlier,[14] except that the gas flow rate (30% HF-H_2) was only 15 scfh. The utilization of

HF decreased from an initial value of about 30% to 5 to 10% during most of the 15-hr treatment period. At the end of the period, it decreased rapidly to about 1%. Following periods of hydrogen sparging to reduce iron fluoride, and argon sparging to remove HF, a 400-g charge of thorium metal was added to the treatment vessel in order to transfer zirconium from the salt phase to the bismuth phase and to supply the necessary reductant in the bismuth for the first mass transfer experiment. About 24 hr after the thorium metal had been added to the treatment vessel, the salt and bismuth phases were sampled and transferred to the respective feed tanks.

A 270-g batch of $LiF-UF_4$ eutectic salt was prepared by placing 51.6 g of LiF and 231 g of UF_4 in a small graphite crucible in which the materials were melted and sparged with a $HF-H_2$ mixture for about 6 hr at 650°C. The H_2-HF gas flow rate was too low during this period to obtain meaningful gas samples without upsetting the off-gas pressure, and in turn, the gas flow rate and the composition of the gas. Following the treatment period, the eutectic mixture was solidified and divided into two parts. A 90-g portion was added to the salt feed tank in preparation for the first mass transfer experiment (UTR-1).

6.2 Mass Transfer Experiment UTR-1

The first uranium mass transfer run (UTR-1) was very successful from the standpoint of hydrodynamics and demonstrated that simultaneous samples of the bismuth and salt leaving the extraction column can be taken easily. However, the run failed to provide mass transfer data for reasons described below.

During the run, a uniform flow rate of each phase was maintained at 100 ml/min (about 63% of flooding) for 90 min, during which seven sets of simultaneous samples of the salt and bismuth streams leaving the column were taken. Three additional sets of samples were taken during the 25-min period in which the salt and bismuth flow rates were increased to 130 ml/min (about 82% of flooding). The flow rates were determined from the changes in the

bismuth and salt volumes in the feed tanks during the run, as shown in Fig. 20. Analyses of the flowing bismuth samples for uranium and thorium showed little, if any, of these materials (<2 ppm of U and <4 ppm of Th). A review of the procedure followed during the earlier addition of thorium metal to the treatment vessel showed that most of the thorium had failed to enter the crucible containing the bismuth and salt because a cube of thorium had blocked the hole in the graphite crucible cover, causing the thorium cubes that were subsequently added to come to rest on the crucible cover.

Uranium analyses of salt from the salt feed tank and from the salt receiver vessel were identical (1200 ppm), which indicates that there was no transfer of uranium from the salt. This confirmed analytical results for the bismuth samples, which also showed that no transfer of uranium to the bismuth phase occurred during the experiment; however, the uranium concentrations reported for the set of nine flowing salt samples averaged 1092 ppm; each value in this set was less than the expected value of 1200 ppm.

A possible explanation for the low uranium concentrations in the flowing salt samples was considered and discarded. If the salt contained as much as 3 vol % entrained bismuth, the effect would be a decrease in the uranium concentration in the sample to about the average value observed since the bismuth contained no uranium. However, the analysis of random salt samples indicated bismuth concentrations of less than 80 ppm, or less than approximately 0.003 vol %. Similarly, there was no inverse correlation of reported sample weights with indicated uranium concentrations. The entrainment detector (located between the salt outlet from the column and the salt sampler) also provided evidence that bismuth entrainment in salt leaving the column was less than (probably much less than) 1.5 vol %, the entrainment rate that would be required in order for the bismuth level in the detector to reach the lower probe. The bismuth entrainment measurements were made while the column was operating at 82% of flooding; the salt in the drain line below the entrainment detector was frozen during this period.

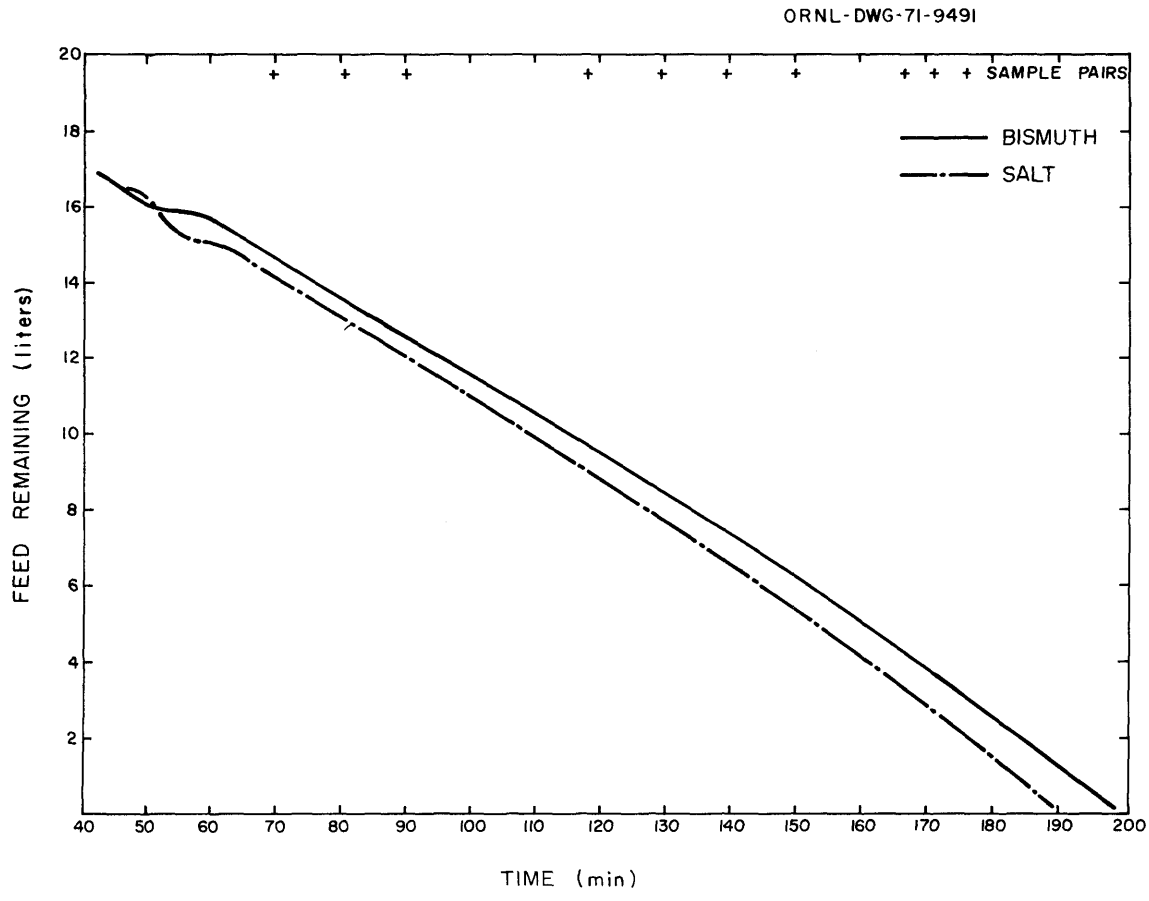

Fig. 20. Volumes of Bismuth and Salt Remaining in Feed Tanks vs Run Time for Run UTR-1. The bismuth and salt flow rates were approximately equal and had the values of 100 ml/min for the period 60 to 150 min and 130 ml/min for the period 150 to 175 min.

Following experiment UTR-1, the salt and bismuth were returned to their respective feed tanks in preparation for experiment UTR-2.

6.3 Mass Transfer Experiment UTR-2

Because of the difficulty encountered in adding thorium metal to the treatment vessel prior to run UTR-1, the thorium reductant for experiment UTR-2 was added directly to the bismuth feed tank. The 192.5-g charge dissolved very slowly in the bismuth, possibly because of inadequate agitation of the metal phase by the argon sparge. Periodic samples of the metal phase (taken with a standard fritted sampler and with a graphite ladle) showed that the thorium concentration was increasing at the rate of only about 2 ppm/hr. After 200 hr at 540°C and 120 hr at 630°C, a filtered sample and a ladle sample indicated thorium concentrations of 750 ppm and 1100 ppm, respectively. These values should be compared with the thorium solubility in bismuth at 540°C (i.e., 880 ppm) and a material balance value of 1165 ppm, assuming complete dissolution of the thorium.

The balance of the $LiF-UF_4$ eutectic (180 g) was added to the salt feed tank to bring the uranium concentration to about 3000 ppm. Because of uncertainty in the value for the thorium concentration in the bismuth, a bismuth-to-salt flow rate ratio of 5 was used for experiment UTR-2.

The first attempt to begin run UTR-2 was halted by the failure of bismuth to transfer from the bismuth feed tank. The site of the obstruction was apparently the open end of the feed tank dip tube since the line was cleared by back-flowing argon through the line. After bismuth and salt flow to the column had been initiated, the bismuth flow rate was increased to about five times the salt flow rate in order to achieve the desired run conditions. The flow rates of both bismuth and salt were steady over a period of about 40 min, as shown in Fig. 21. During this period, seven pairs of samples were taken of bismuth and salt streams leaving the column; the bismuth and salt flow rates were 247 and 52 ml/min, respectively, corresponding to operation at about 83% of the column flooding rate. The small variations in the flow rates during this period are indicated by the close approximation to straight lines shown by the liquid-level curves in Fig. 21.

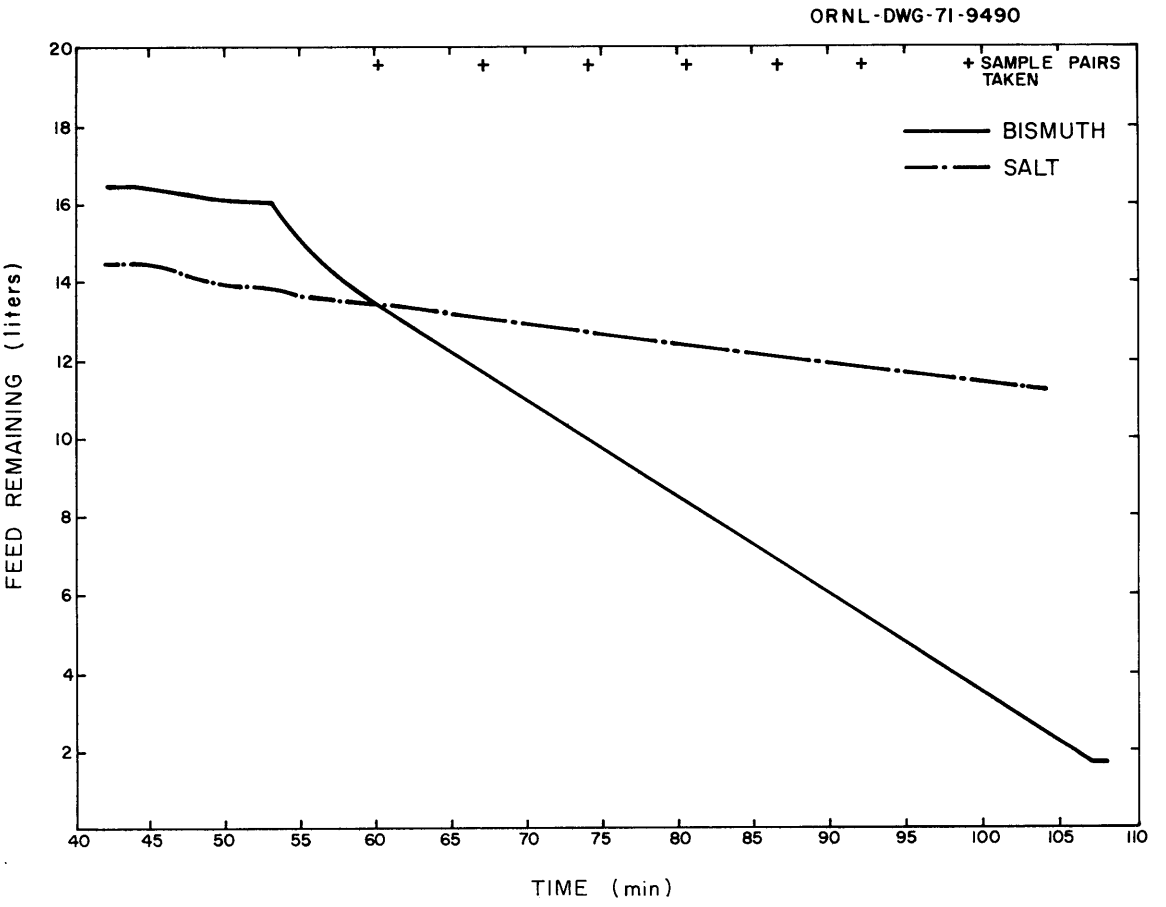

Fig. 21. Volumes of Bismuth and Salt Remaining in Feed Tanks vs Run Time for Run UTR-2. Flow rates inferred from slopes; bismuth, 247 ml/min; salt, 52 ml/min. Fraction of flooding, 83%.

In addition to samples of the salt and bismuth streams leaving the column, samples were also taken from bismuth and salt feed and receiver tanks. The resulting data are tabulated in Table 8. The fraction of uranium extracted, based on the data from the salt samples, was 95%. The scatter in the uranium analyses of the salt and bismuth streams leaving the column was larger than expected. A uranium material balance based on the average uranium concentration in salt leaving the column would require an average uranium concentration of about 230 ppm (as compared with the observed value of 174 ppm) in bismuth leaving the column. Zirconium concentrations in the bismuth samples were within about 25% of the expected values. Excellent agreement was observed between thorium and lithium concentrations in the bismuth stream leaving the column and in the bismuth receiver vessel. The thorium concentration in the bismuth fed to the column is believed to have been 659 ppm, as indicated by the amount of dissolved metals in the bismuth after the experiment. The quantity of reductant present in the bismuth during the experiment (thorium and lithium) amounted to a stoichiometric excess of about 200% over that required to reduce the uranium and zirconium in the feed salt.

This experiment is important because it represents the first known demonstration of the continuous extraction of uranium from molten salt into bismuth containing reductant. The results indicate that high uranium removal efficiencies can be obtained in a packed column having a reasonable length. Additional experiments will be carried out in order to determine more exactly the mass transfer performance of packed column extractors over a range of operating conditions.

7. MEASUREMENT OF AXIAL DISPERSION COEFFICIENTS IN PACKED COLUMNS

J. S. Watson L. E. McNeese

Axial dispersion in the continuous (salt) phase can reduce the performance of packed column contactors that are proposed for the MSBR fuel processing system. Effects of axial dispersion will be most severe where

Table 8. Summary of Mass Transfer Data Obtained in Run UTR-2

Bismuth flow rate, 247 ml/min; salt flow rate, 52 ml/min

Fraction of uranium transferred = $\frac{3000 - 150}{3000}$ = 0.95.

U balance, flowing stream samples =

$$\frac{\text{U entering Bi}}{\text{U leaving salt}} = \frac{1.53 \text{ millimoles/min}}{2.10 \text{ millimoles/min}} = 0.73.$$

Origin of Sample	U Conc. in Salt Phase (ppm)	Bismuth Phase								
		U		Zr		Th		Li		Total Dissolved Metals (meq/liter)
		(ppm)	(meq/liter)	(ppm)	(meq/liter)	(ppm)	(meq/liter)	(ppm)	(meq/liter)	
Feed tanks	3000	21	3.4	∿0	∿0	1110[a] 617[b]	109	20	27.6	140[c]
Flowing stream 1	426[d]	224	36.3	22	9.3	330	55	47	65	166
Flowing stream 2	144	223	36.3	24	10	390	64.9	39	54	165
Flowing stream 3	114	138	22.4	22	9.3	320	53.3	45	62	147
Flowing stream 4	137	140	22.7	21	8.9	300	50	33	46	128
Flowing stream 5	163	197	31.9	18	7.6	270	45	33	46	131
Flowing stream 6	161	140	22.7	25	11	420	70	34	47	151
Flowing stream 7	181	155	25.1	16	6.8	140	23.3	28	39	94
Flowing stream ave.	150	174	28.2	21	8.9	310	51.6	37	51	140
Receiver tanks	146	737[a]	--	--	--	308	51.3	34	47	

[a] Questionable value.

[b] Calculated as the difference: 144 meq/liter minus the sum of the concentrations of U, Zr, and Li.

[c] Most probable value, based on average for flowing bismuth samples.

[d] Questionable value; not included in calculated average value.

high flow rate ratios are required. An experimental program is in progress in which axial dispersion coefficients in packed columns are measured under conditions similar to those in the proposed reductive extraction processes; in this program, mercury and water are used to simulate bismuth and molten salt. The measured axial dispersion coefficients will be used to estimate column performance in the proposed system. Devices for reducing axial dispersion in packed columns are also under development.

The equipment and experimental technique used for these studies have been described previously.[15] The technique consists of injecting a tracer solution at a constant rate near the top of a packed column in which water and mercury are in countercurrent flow. The tracer tends to diffuse upstream in the continuous (water) phase as a result of axial dispersion caused by the downflowing mercury droplets. The system is allowed to reach steady state, and then the concentration profile of the tracer in the continuous phase is determined. As indicated previously, a semilogarithmic plot of relative tracer concentration vs distance down the column produces a straight line having a slope that is inversely proportional to the axial dispersion coefficient. During this reporting period, measurements were carried out in a 2-in.-ID column having a length of approximately 4 ft. The column was packed with 1/4-in.-diam solid cylinders or Raschig rings or 1/2-in.-diam Raschig rings. The packing, which was made of either polyethylene or Teflon, is not wet by either mercury or water.

7.1 Experimental Results

The results of six runs made with 1/4-in. Raschig rings are shown in Figs. 22 through 27. Data for five runs with 1/4-in. solid cylindrical packing are shown in Figs. 28 through 32, and data obtained during 13 runs with 1/2-in.-diam Raschig rings are shown in Figs. 33 through 45. The data from all these runs are summarized in Tables 9-11, and are shown along with previous data from seven runs with 3/8-in.-diam Raschig ring packing in Fig. 46. In each case, the axial dispersion coefficient was independent of the dispersed-phase (mercury) flow rate. Dispersion coefficients for 3/8- and 1/2-in. packing were also independent of the continuous-phase (water) flow rate; their values were 3.5 and 4.8 cm^3/sec, respectively. Data for

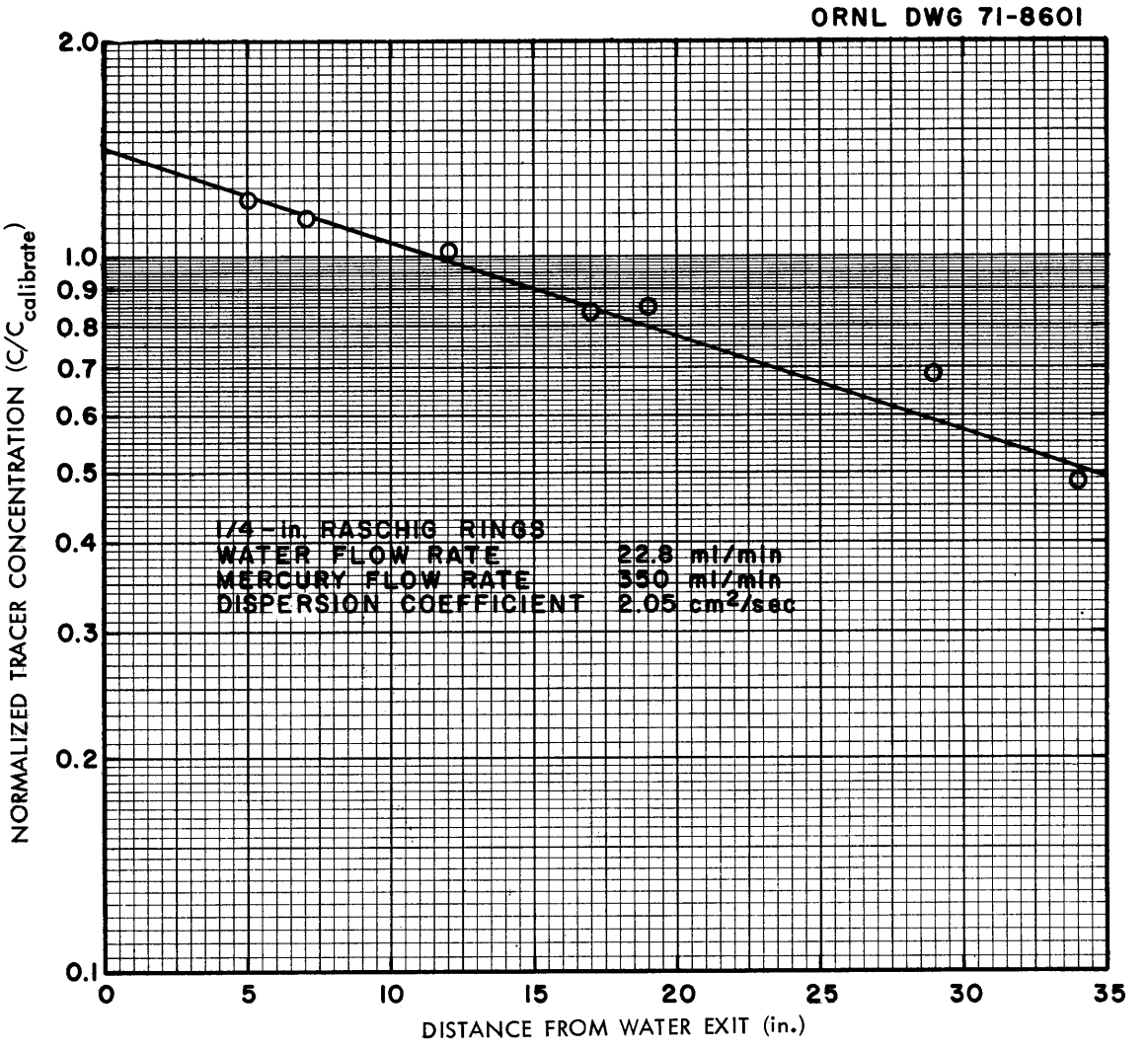

Fig. 22. Variation of Normalized Tracer Concentration with Distance Along a 2-in.-diam Column Packed with 1/4-in. Raschig Ring Packing During Run 1.

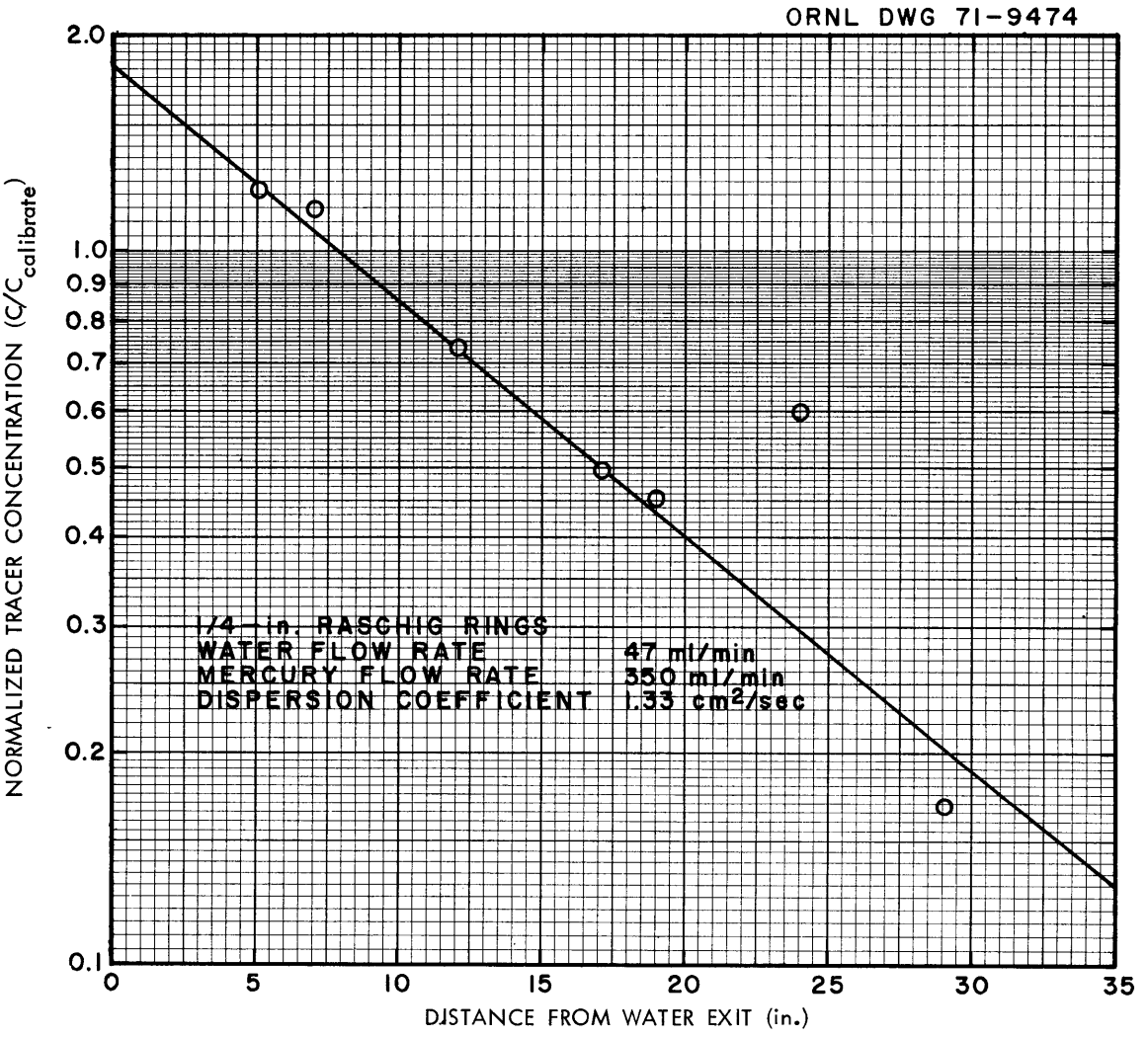

Fig. 23. Variation of Normalized Tracer Concentration with Distance Along 2-in.-diam Column Packed with 1/4-in. Raschig Ring Packing During Run 2.

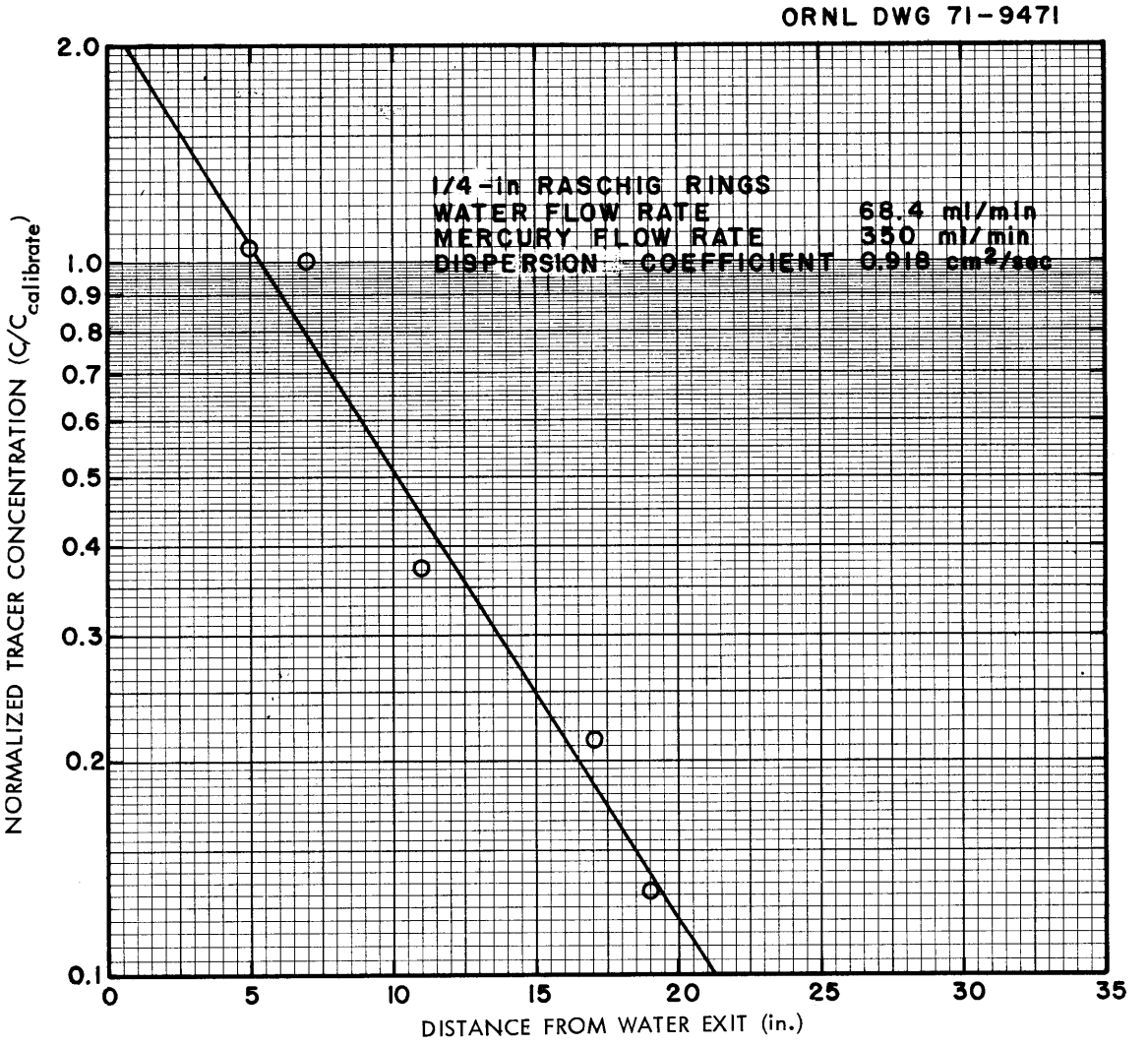

Fig. 24. Variation of Normalized Tracer Concentration with Distance Along 2-in.-diam Column Packed with 1/4-in. Raschig Ring Packing During Run 3.

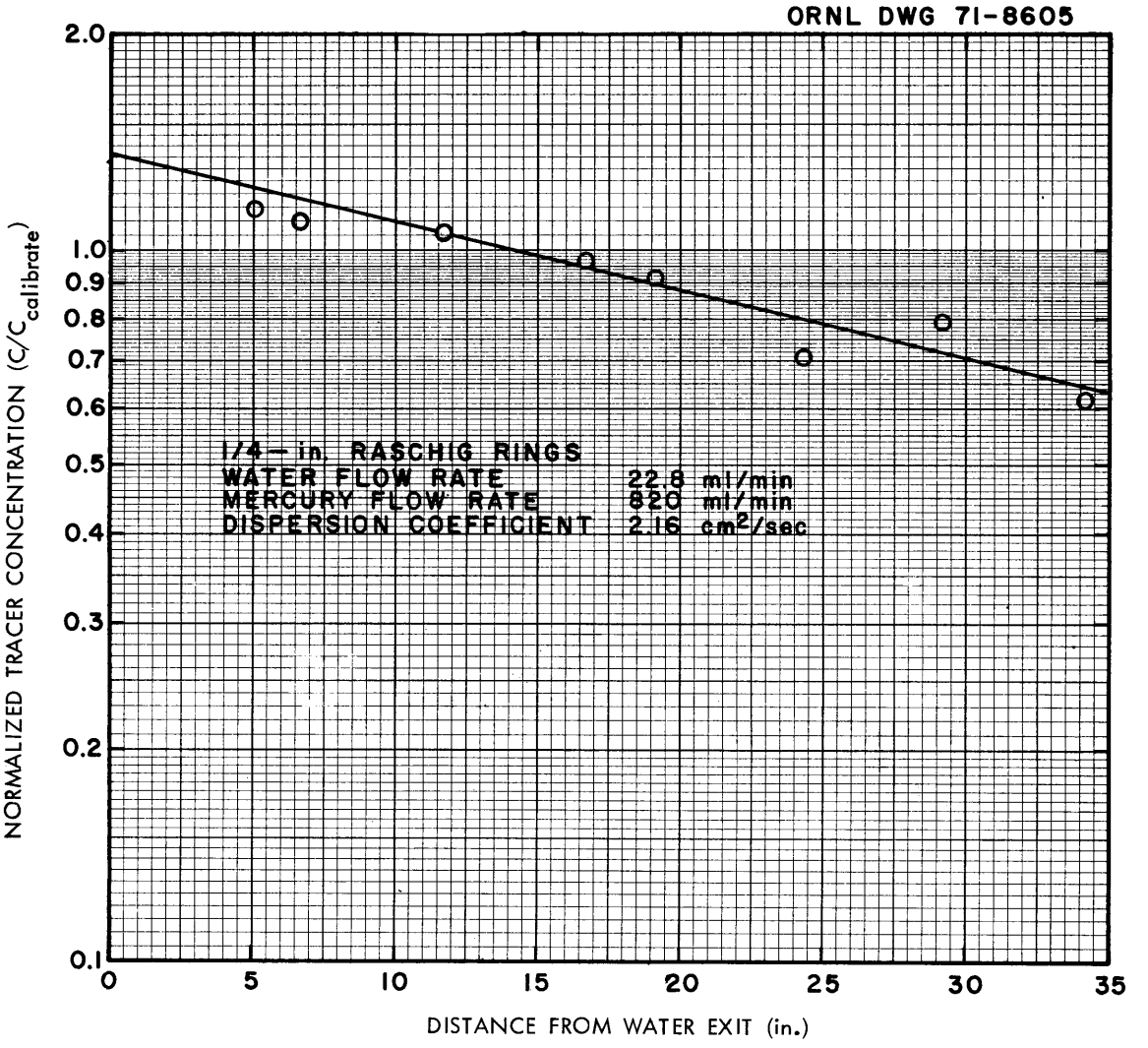

Fig. 25. Variation of Normalized Tracer Concentration with Distance Along 2-in.-diam Column Packed with 1/4-in. Raschig Ring Packing During Run 4.

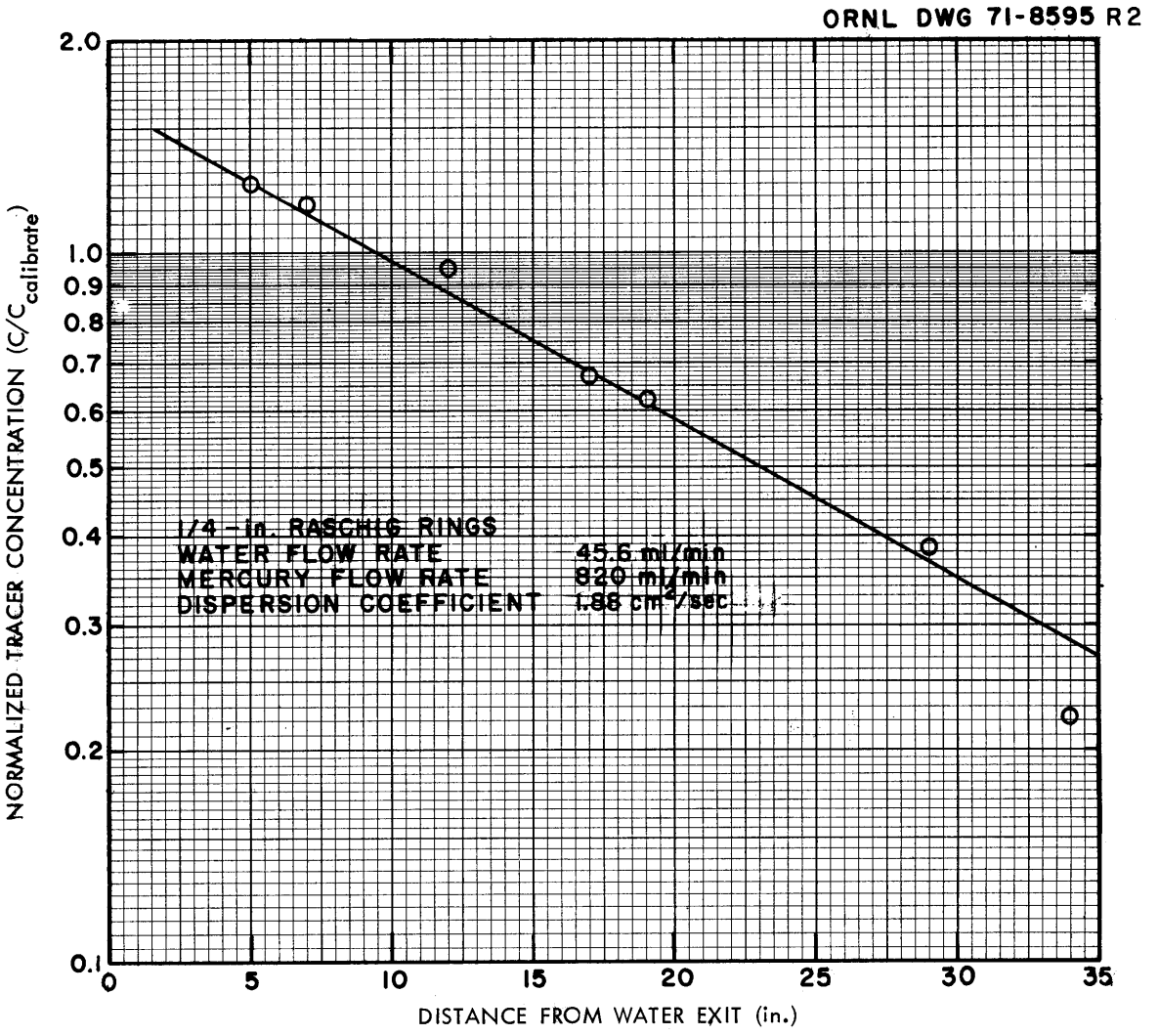

Fig. 26. Variation of Normalized Tracer Concentration with Distance Along 2-in.-diam Column Packed with 1/4-in. Raschig Ring Packing During Run 5.

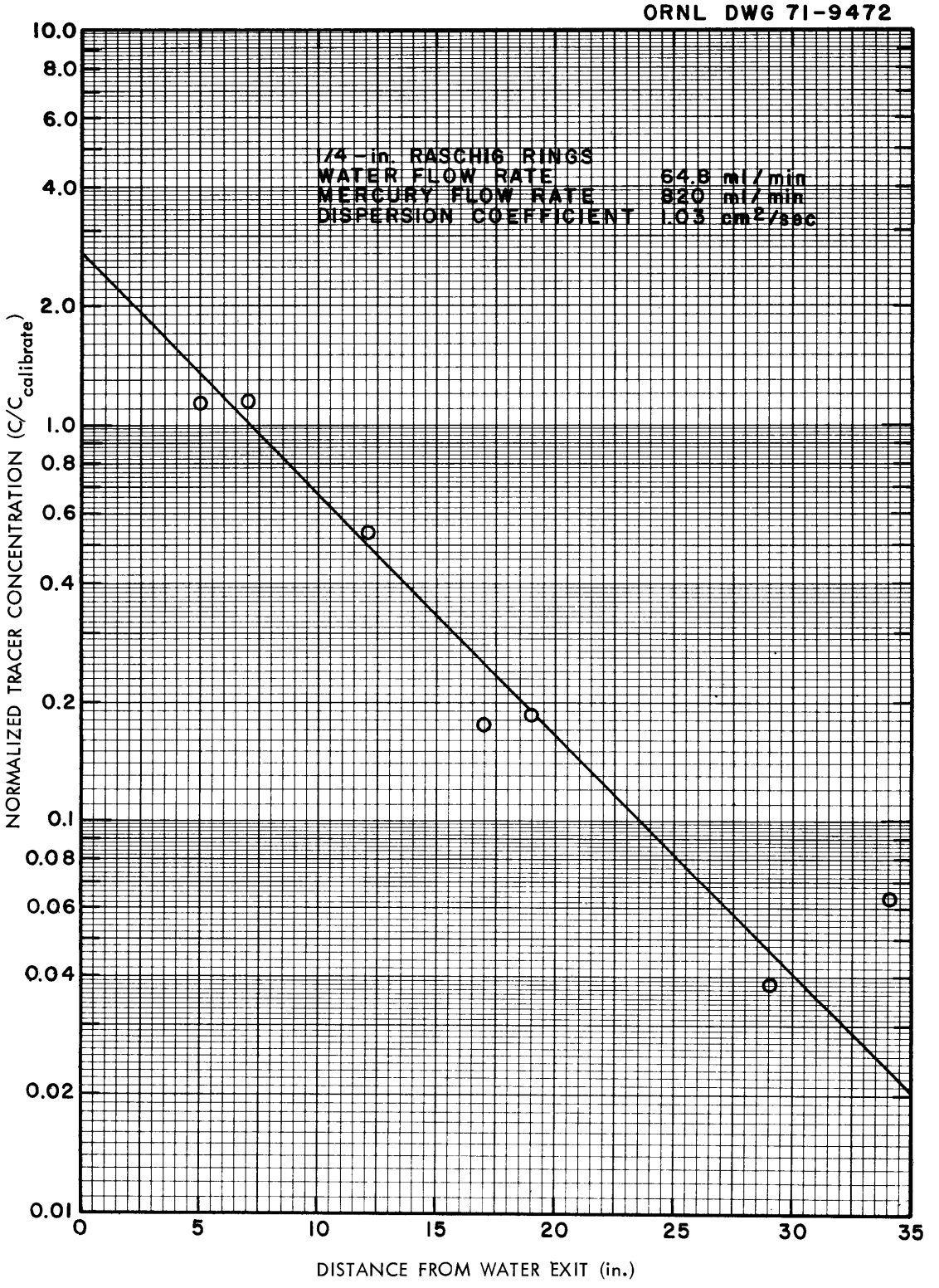

Fig. 27. Variation of Normalized Tracer Concentration with Distance Along 2-in.-diam Column Packed with 1/4-in. Raschig Ring Packing During Run 6.

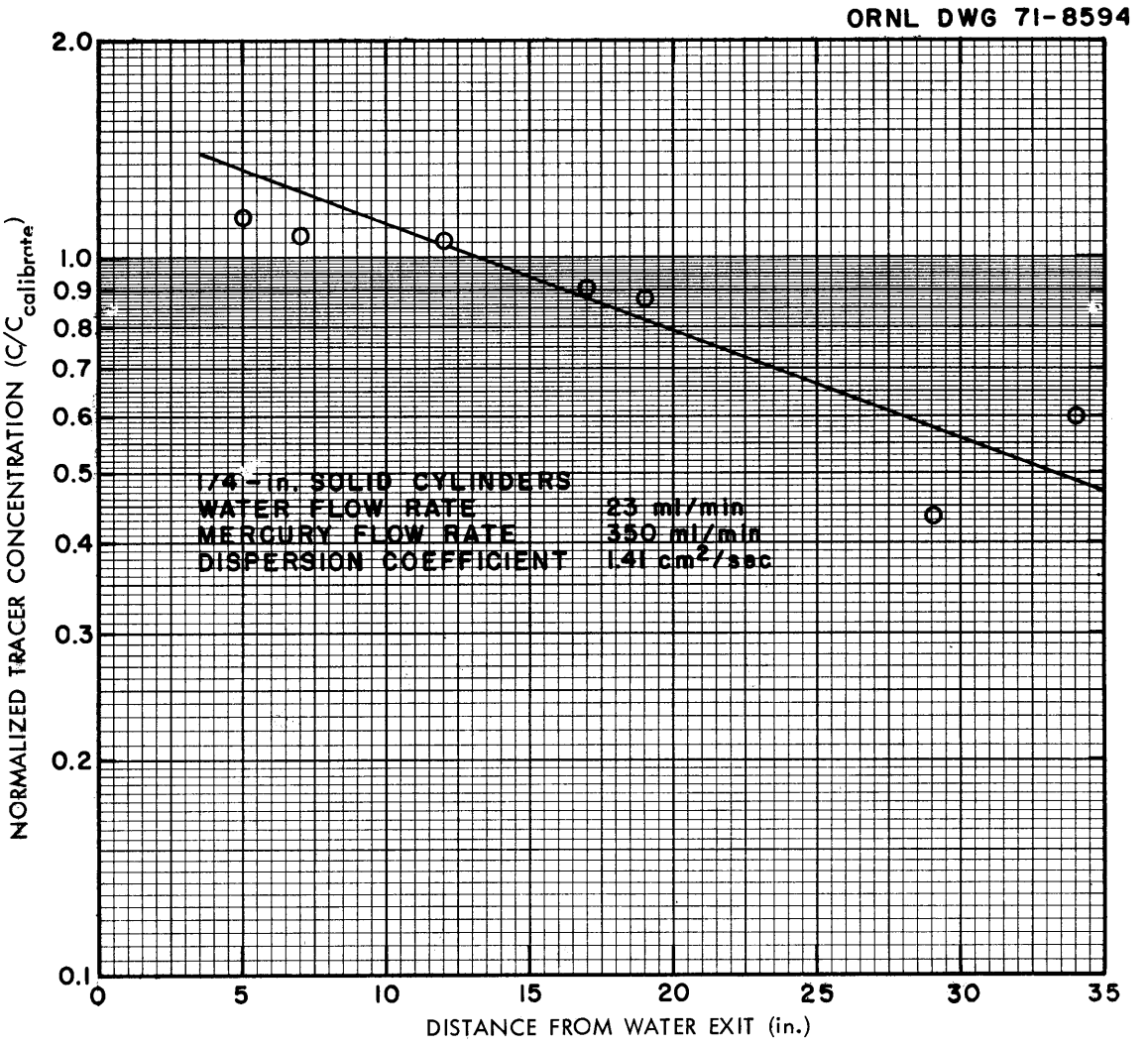

Fig. 28. Variation of Normalized Tracer Concentration with Distance Along 2-in.-diam Column Packed with 1/4-in. Solid Cylindrical Packing During Run 1.

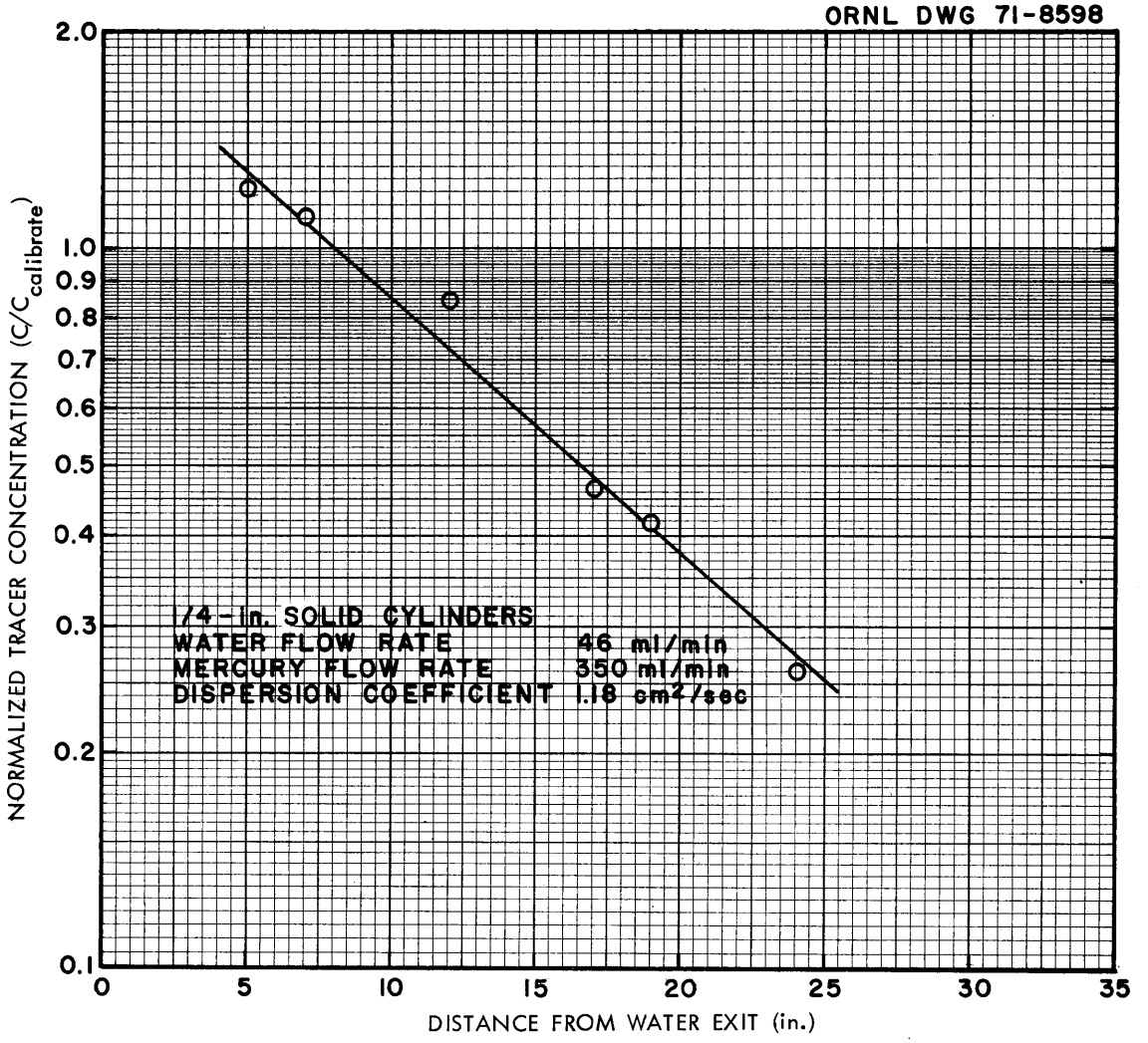

Fig. 29. Variation of Normalized Tracer Concentration with Distance Along 2-in.-diam Column Packed with 1/4-in. Solid Cylindrical Packing During Run 2.

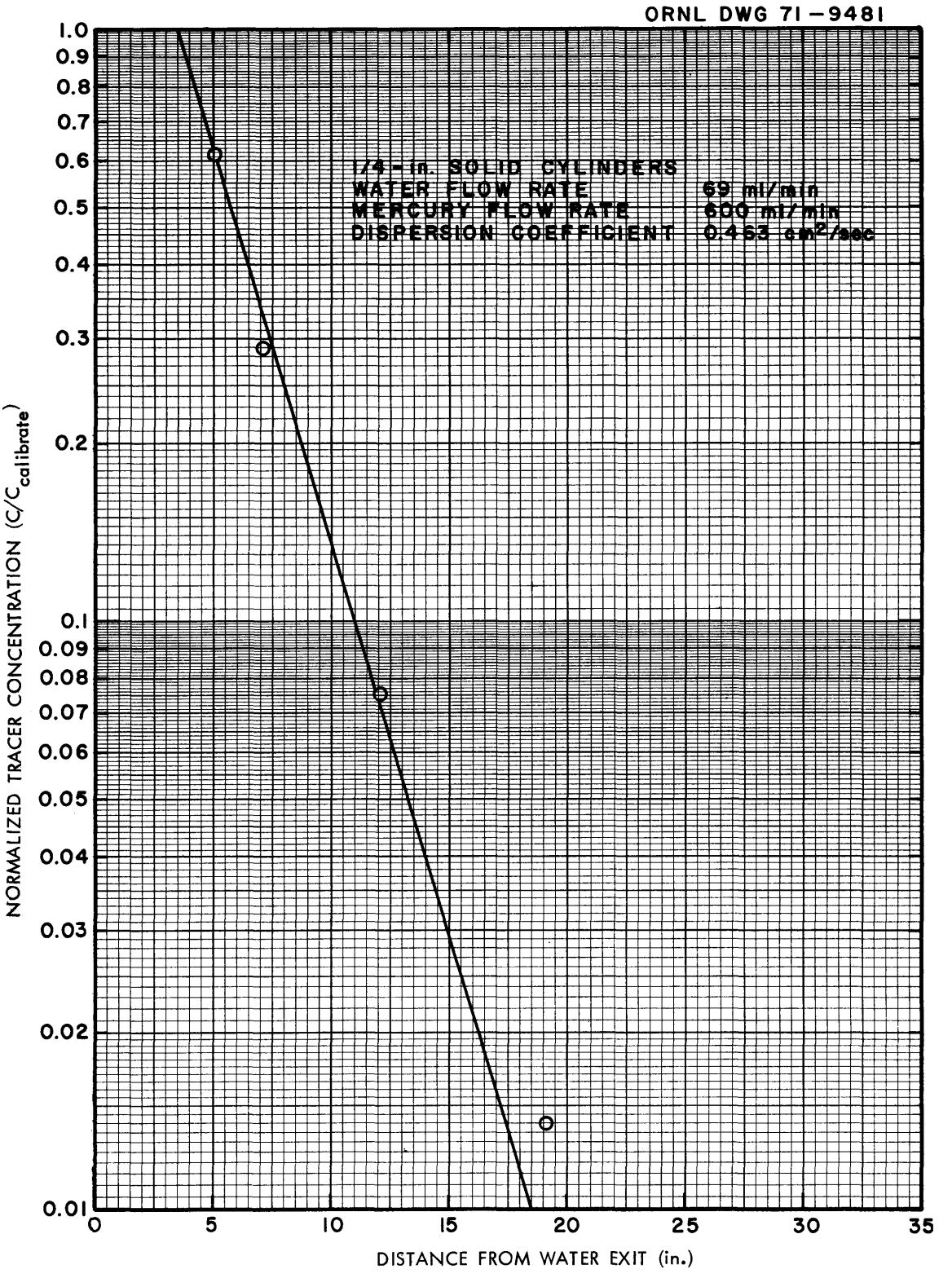

Fig. 30. Variation of Normalized Tracer Concentration with Distance Along 2-in.-diam Column Packed with 1/4-in. Solid Cylindrical Packing During Run 3.

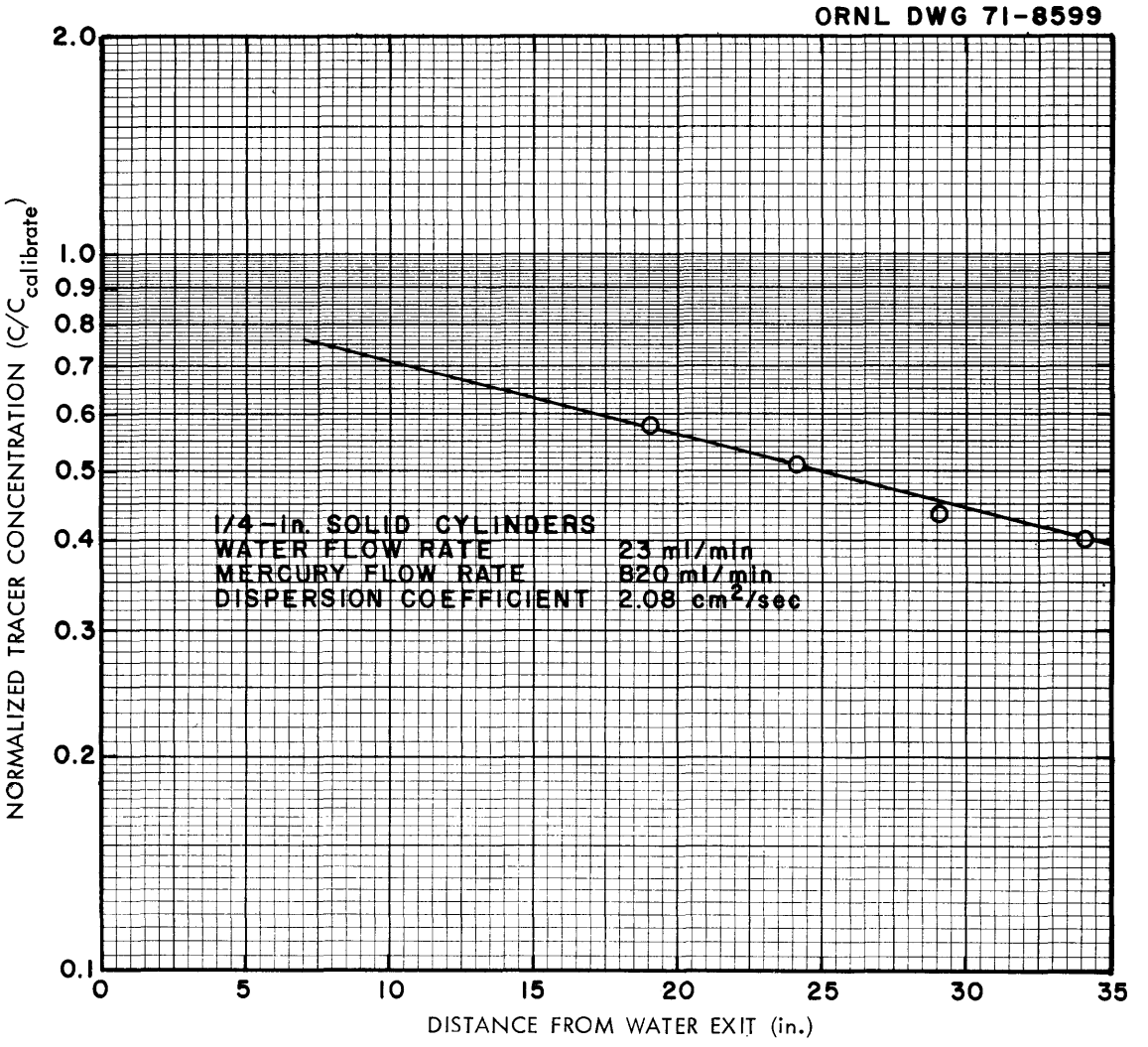

Fig. 31. Variation of Normalized Tracer Concentration with Distance Along 2-in.-diam Column Packed with 1/4-in. Solid Cylindrical Packing During Run 4.

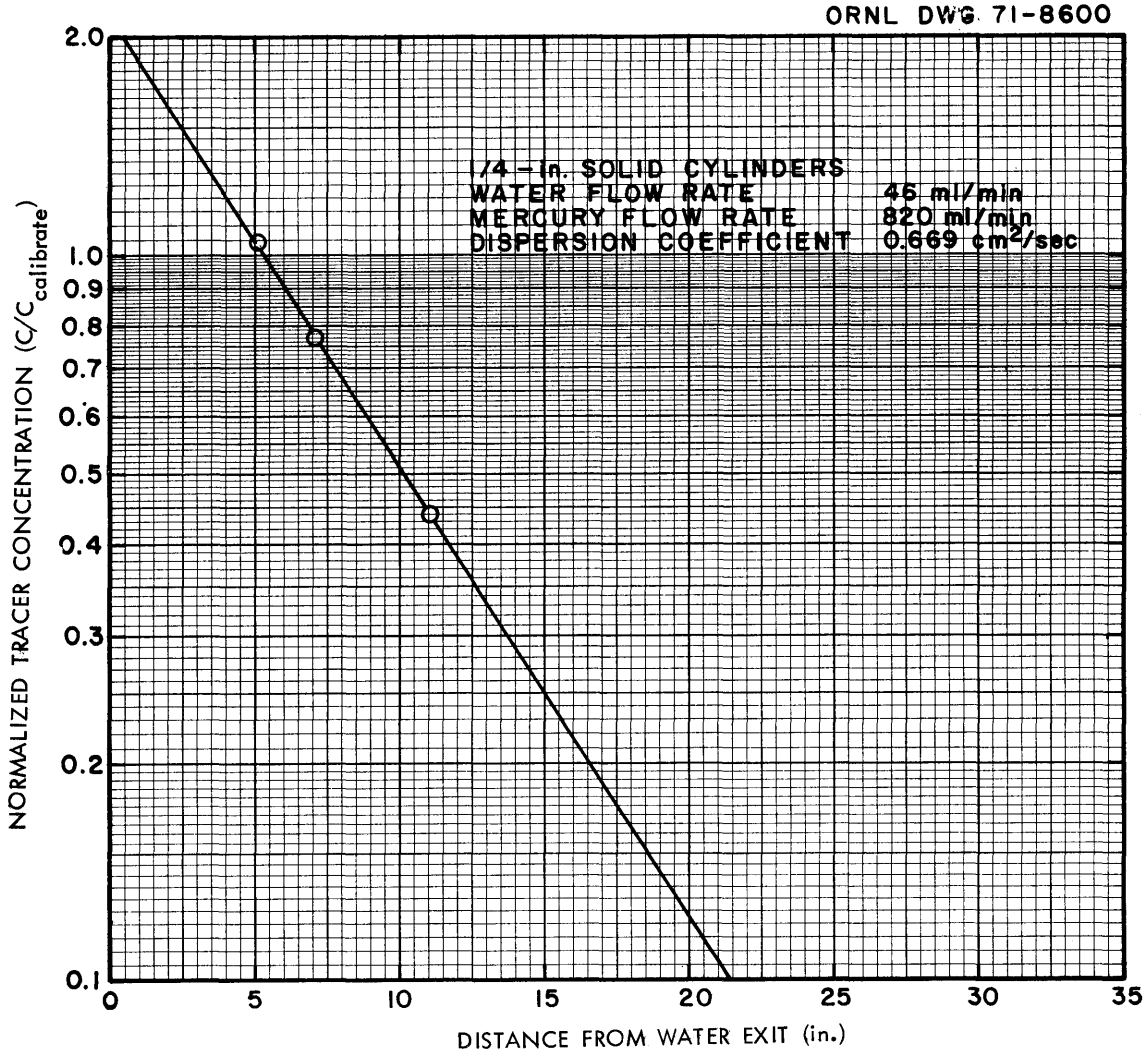

Fig. 32. Variation of Normalized Tracer Concentration with Distance Along 2-in.-diam Column Packed with 1/4-in. Solid Cylindrical Packing During Run 5.

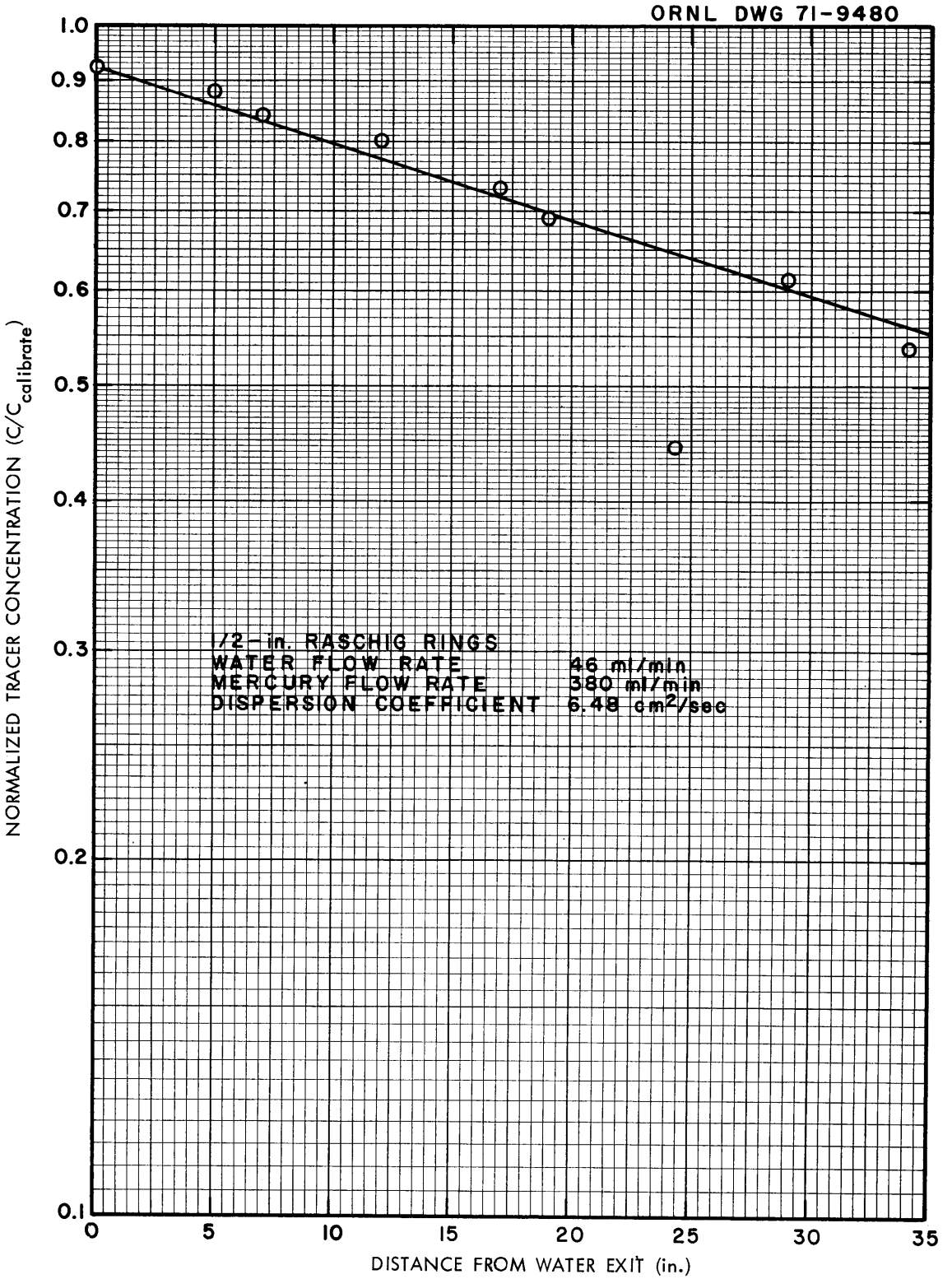

Fig. 33. Variation of Normalized Tracer Concentration with Distance Along 2-in.-diam Column Packed with 1/2-in. Raschig Ring Packing During Run 1.

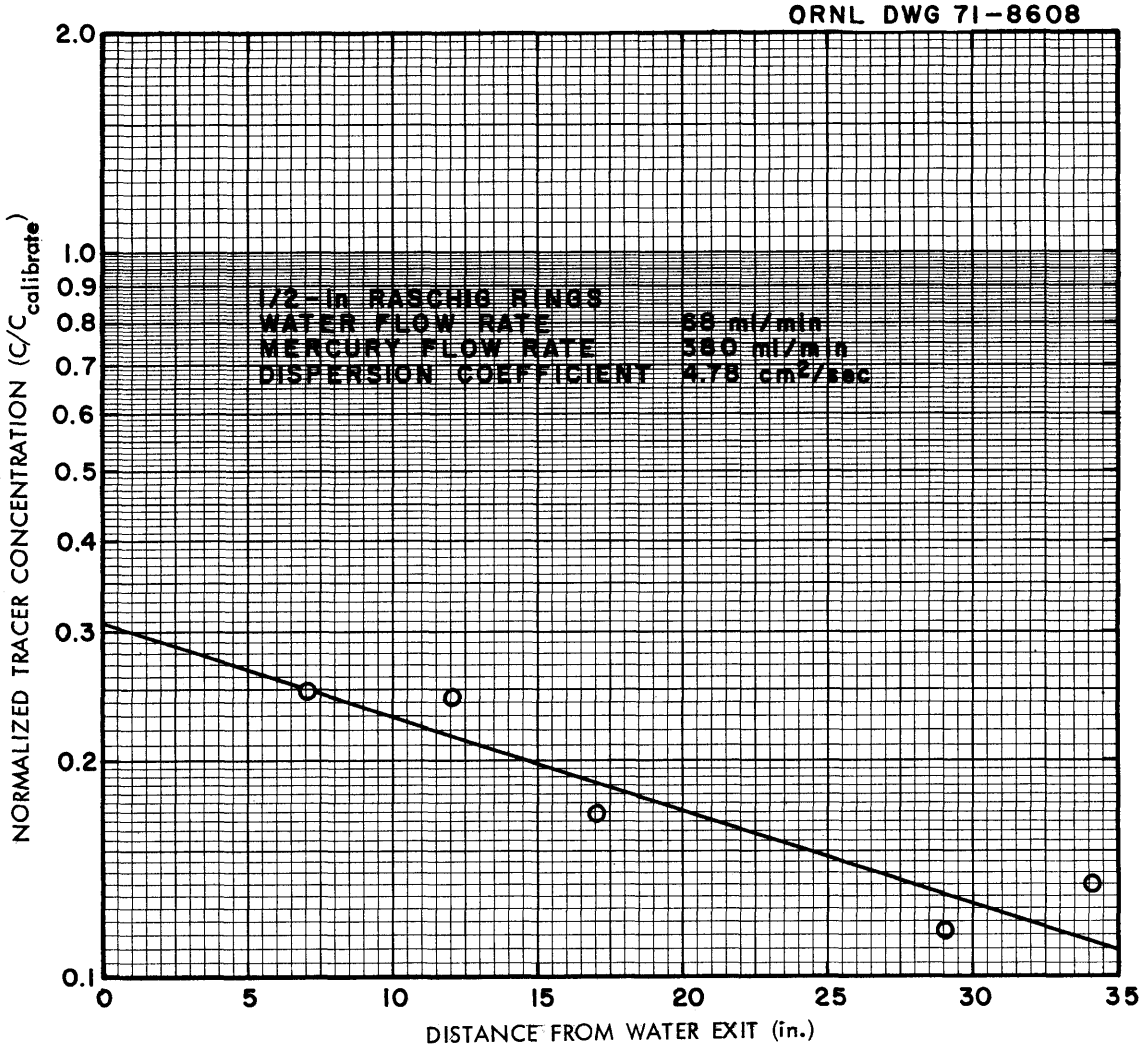

Fig. 34. Variation of Normalized Tracer Concentration with Distance Along 2-in.-diam Column Packed with 1/2-in. Raschig Ring Packing During Run 2.

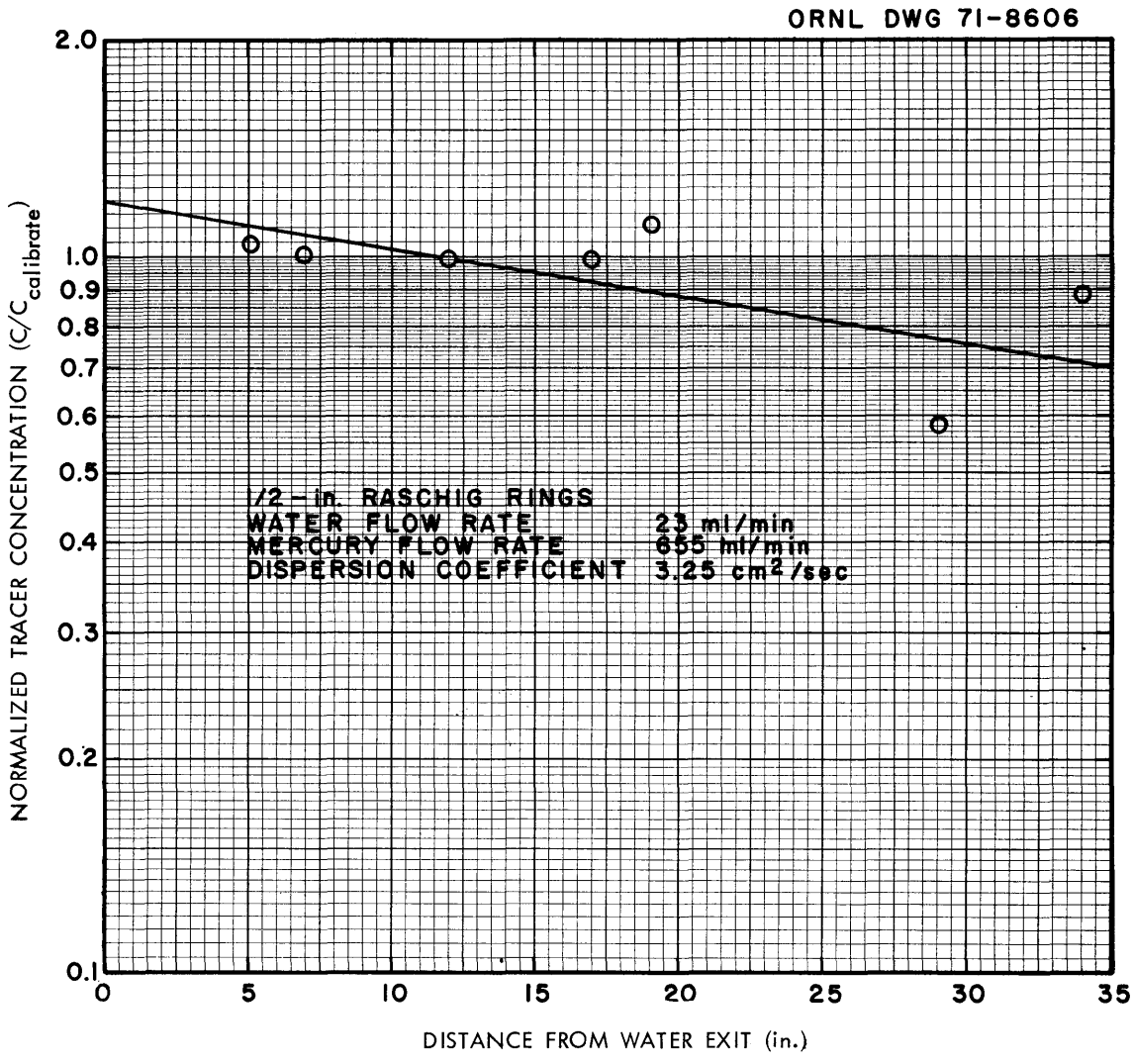

Fig. 35. Variation of Normalized Tracer Concentration with Distance Along 2-in.-diam Column Packed with 1/2-in. Raschig Ring Packing During Run 3.

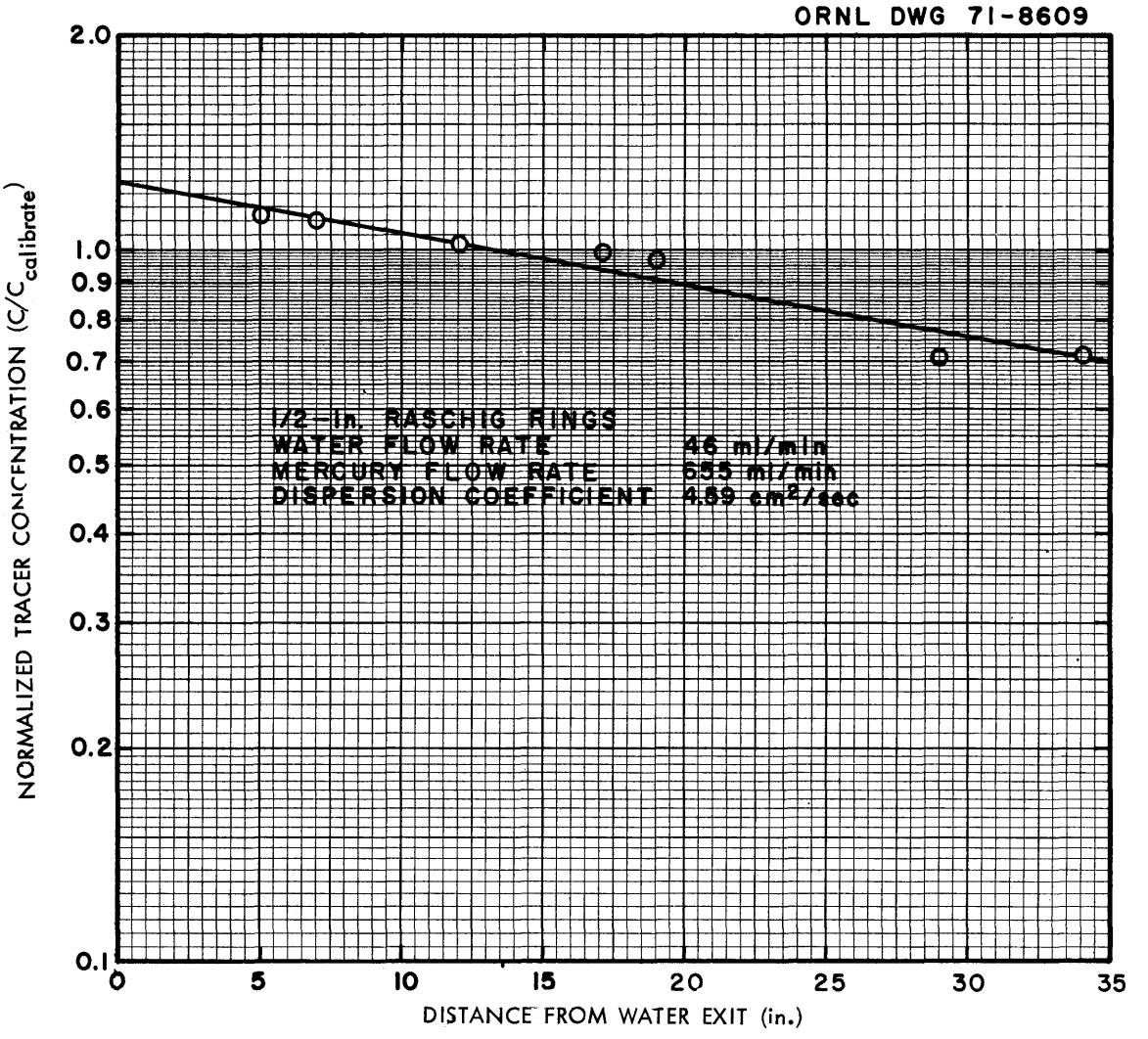

Fig. 36. Variation of Normalized Tracer Concentration with Distance Along 2-in.-diam Column Packed with 1/2-in. Raschig Ring Packing During Run 4.

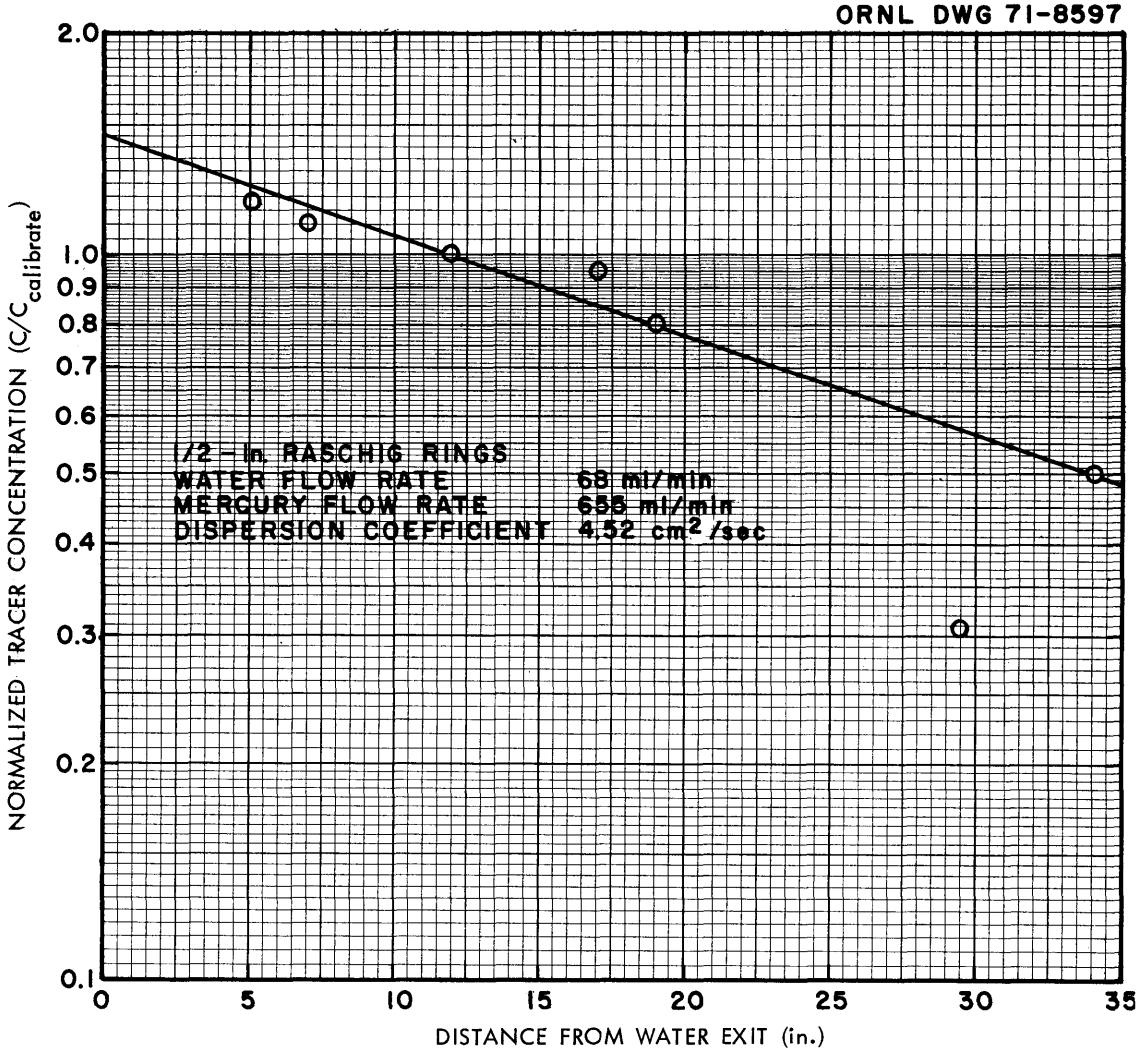

Fig. 37. Variation of Normalized Tracer Concentration with Distance Along 2-in.-diam Column Packed with 1/2-in. Raschig Ring Packing During Run 5.

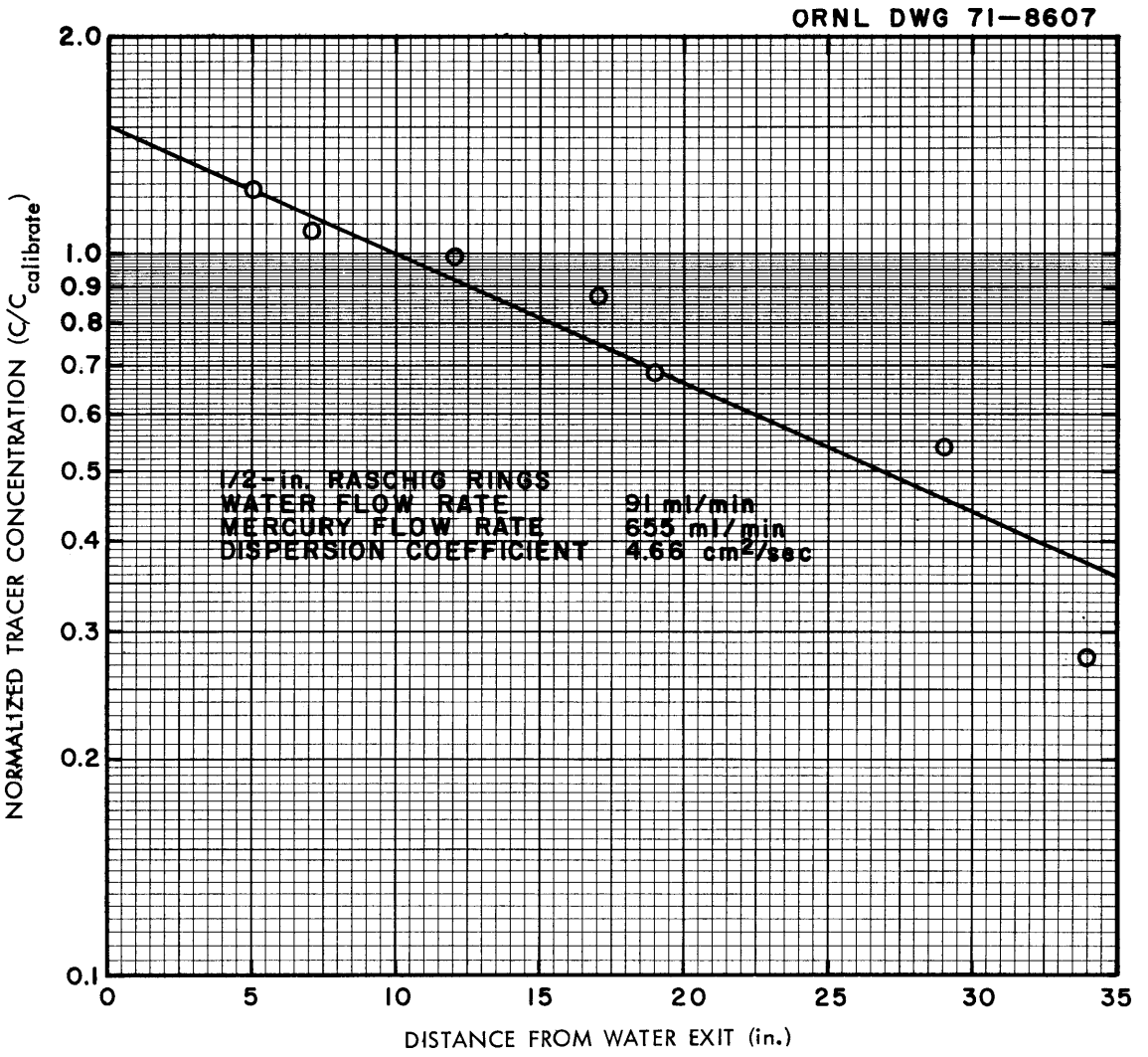

Fig. 38. Variation of Normalized Tracer Concentration with Distance Along 2-in.-diam Column Packed with 1/2-in. Raschig Ring Packing During Run 6.

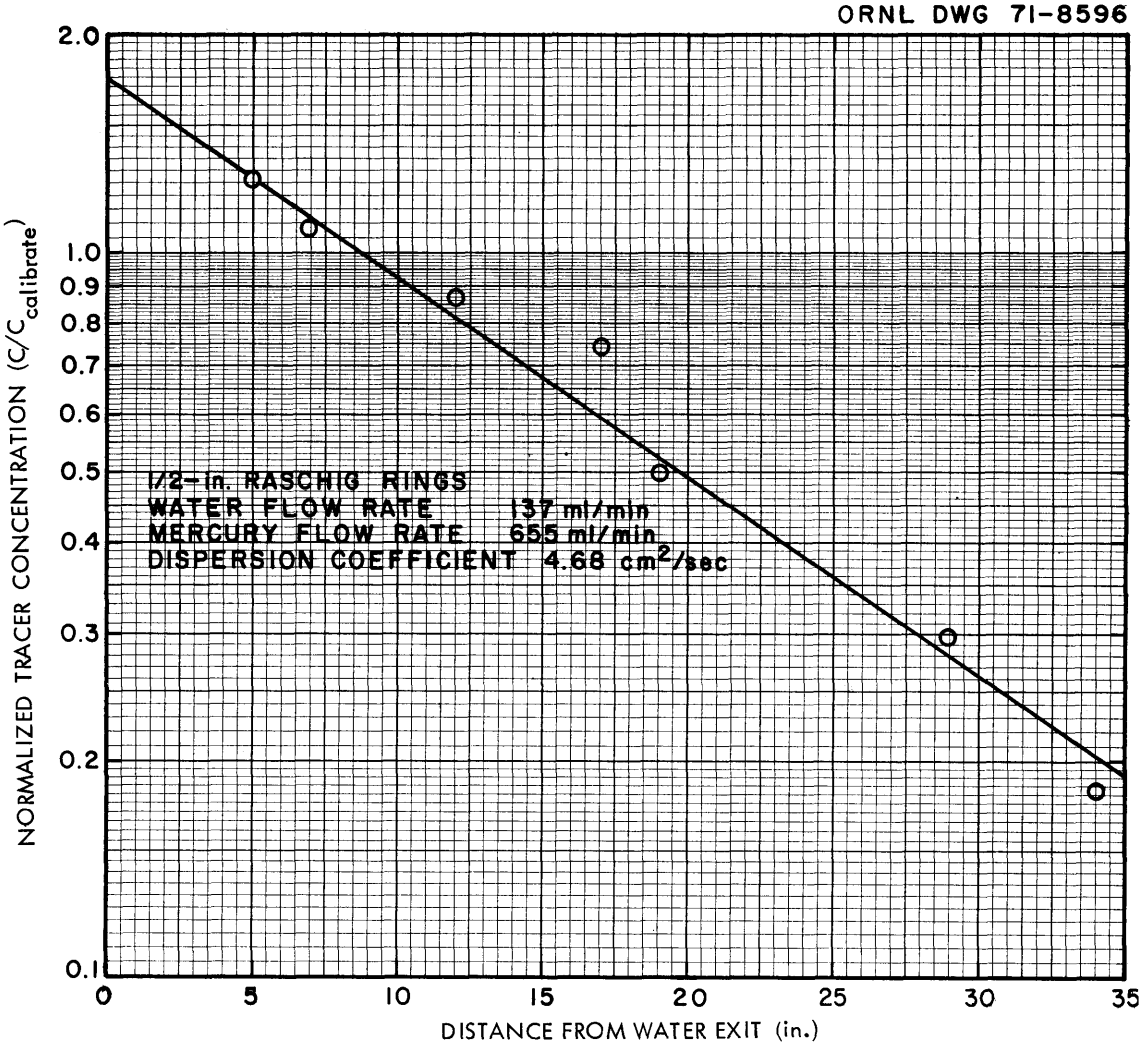

Fig. 39. Variation of Normalized Tracer Concentration with Distance Along 2-in.-diam Column Packed with 1/2-in. Raschig Ring Packing During Run 7.

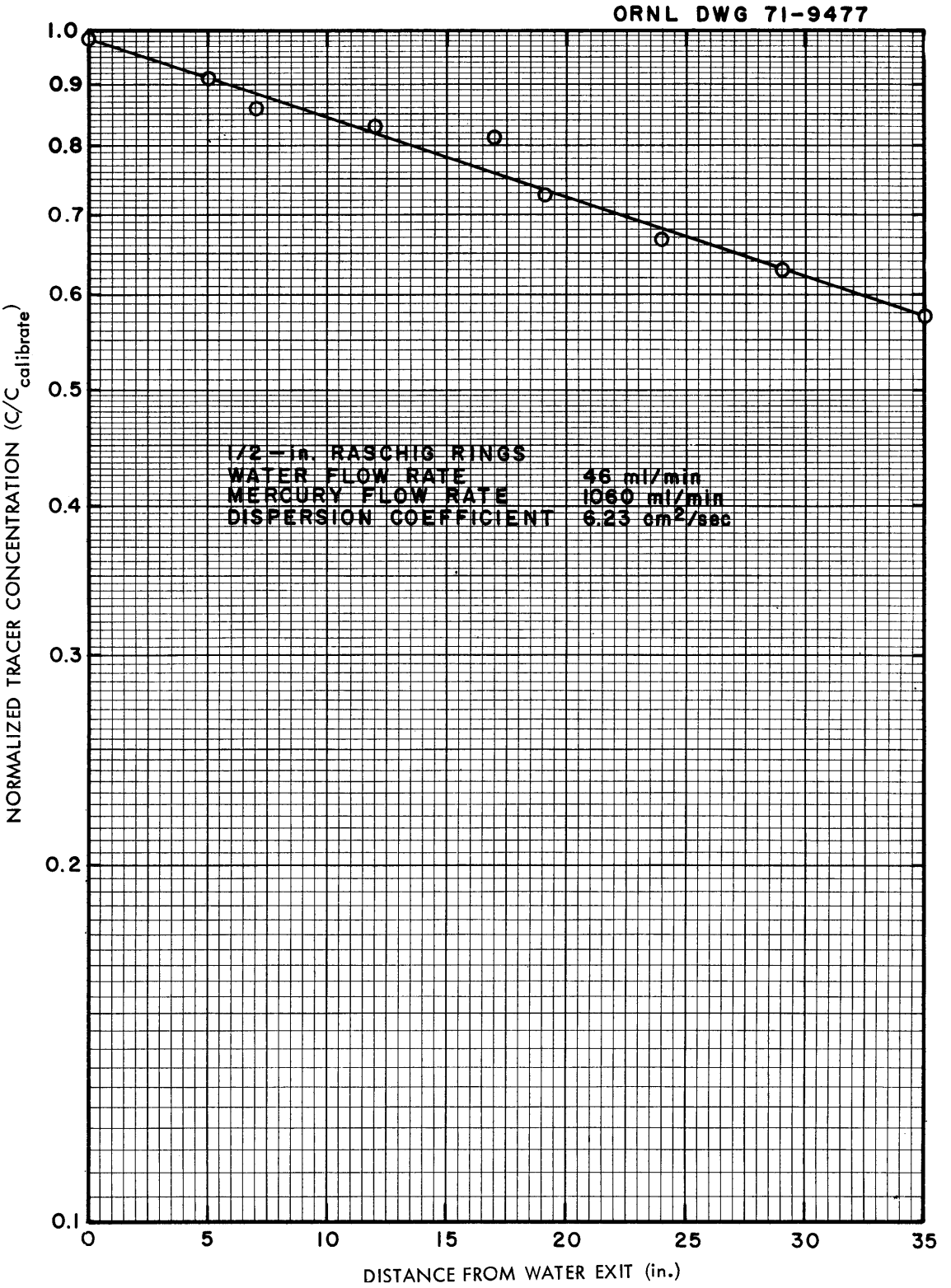

Fig. 40. Variation of Normalized Tracer Concentration with Distance Along 2-in.-diam Column Packed with 1/2-in. Raschig Ring Packing During Run 8.

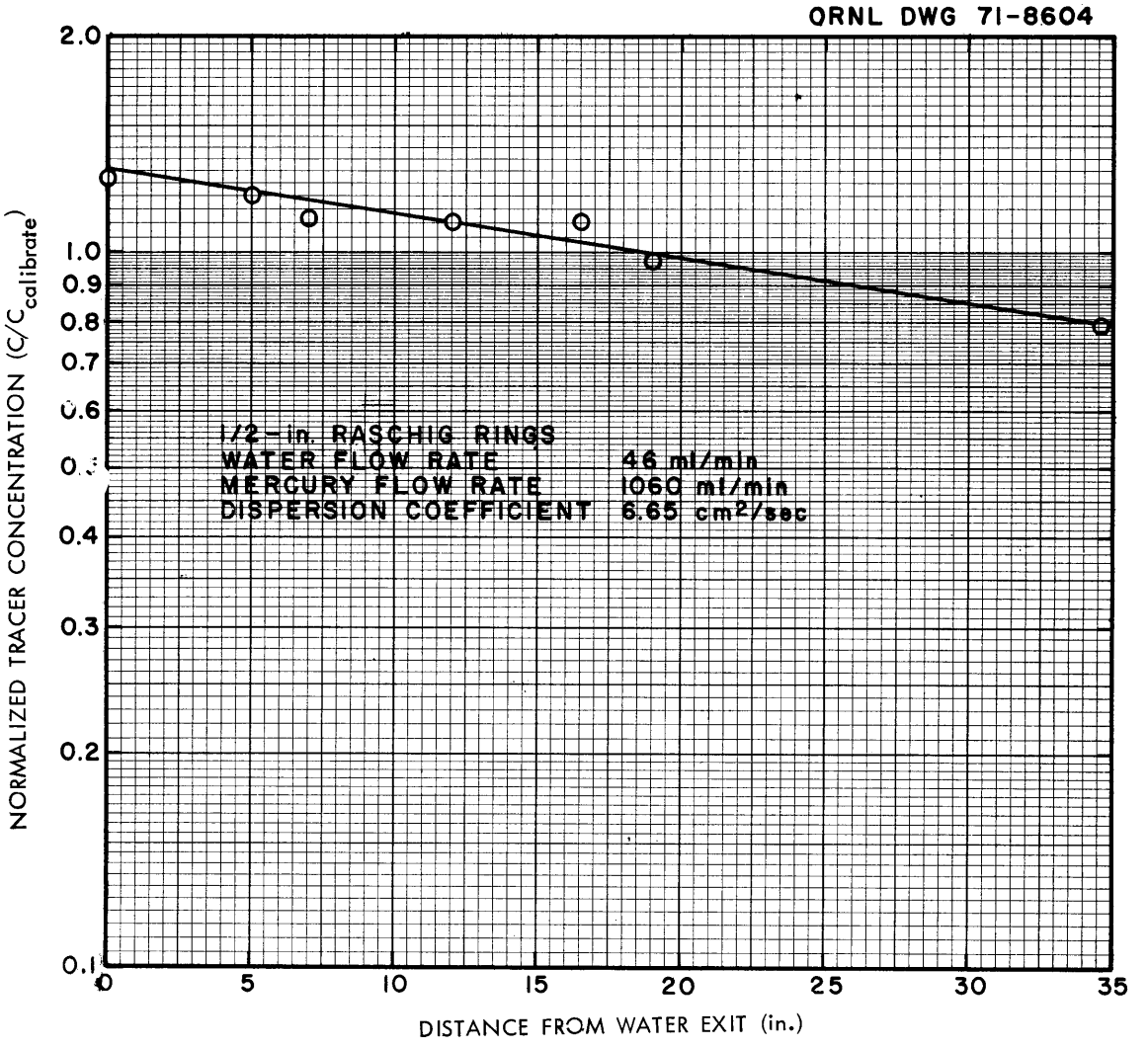

Fig. 41. Variation of Normalized Tracer Concentration with Distance Along 2-in.-diam Column Packed with 1/2-in. Raschig Ring Packing During Run 9.

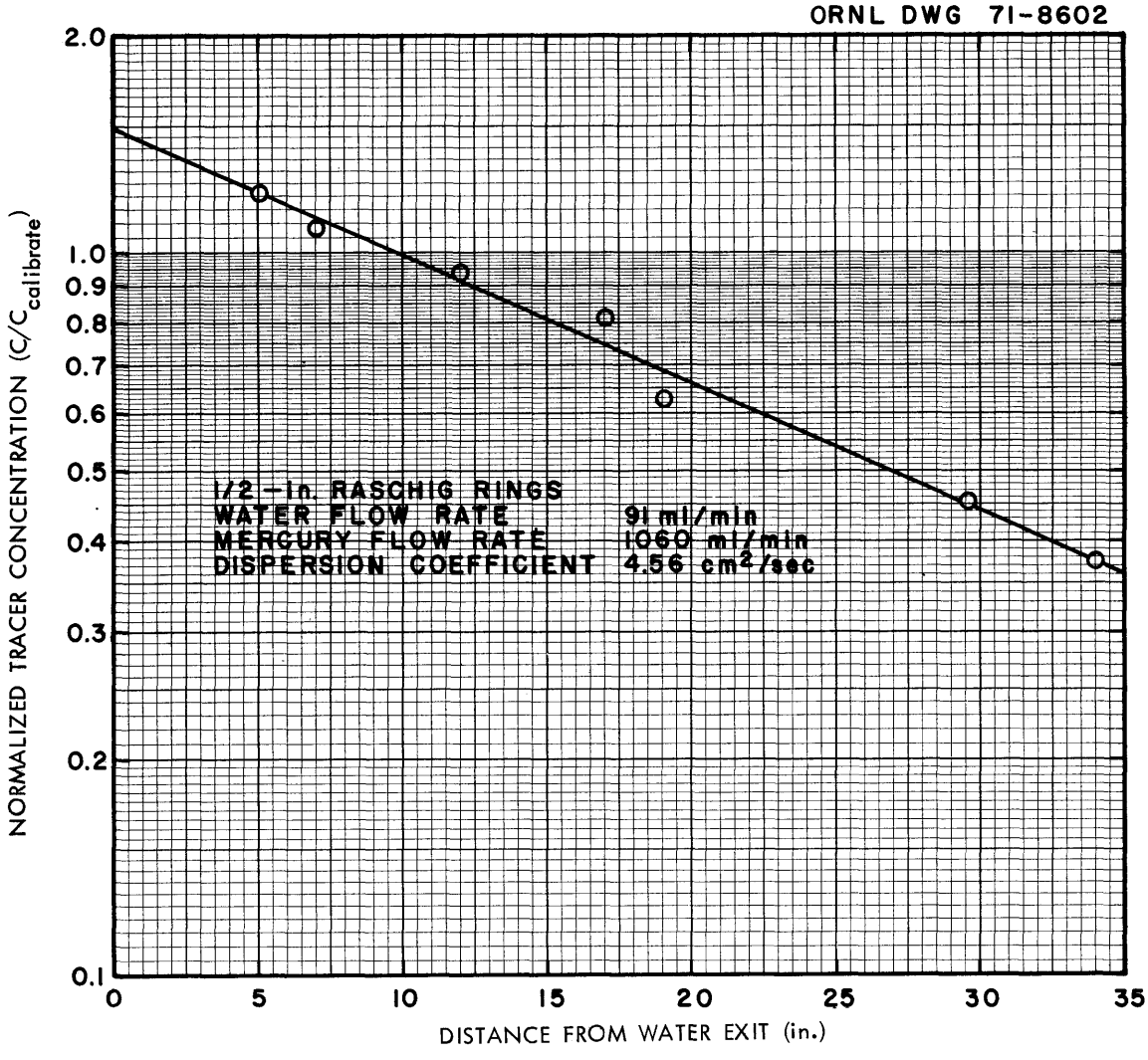

Fig. 42. Variation of Normalized Tracer Concentration with Distance Along 2-in.-diam Column Packed with 1/2-in. Raschig Ring Packing During Run 10.

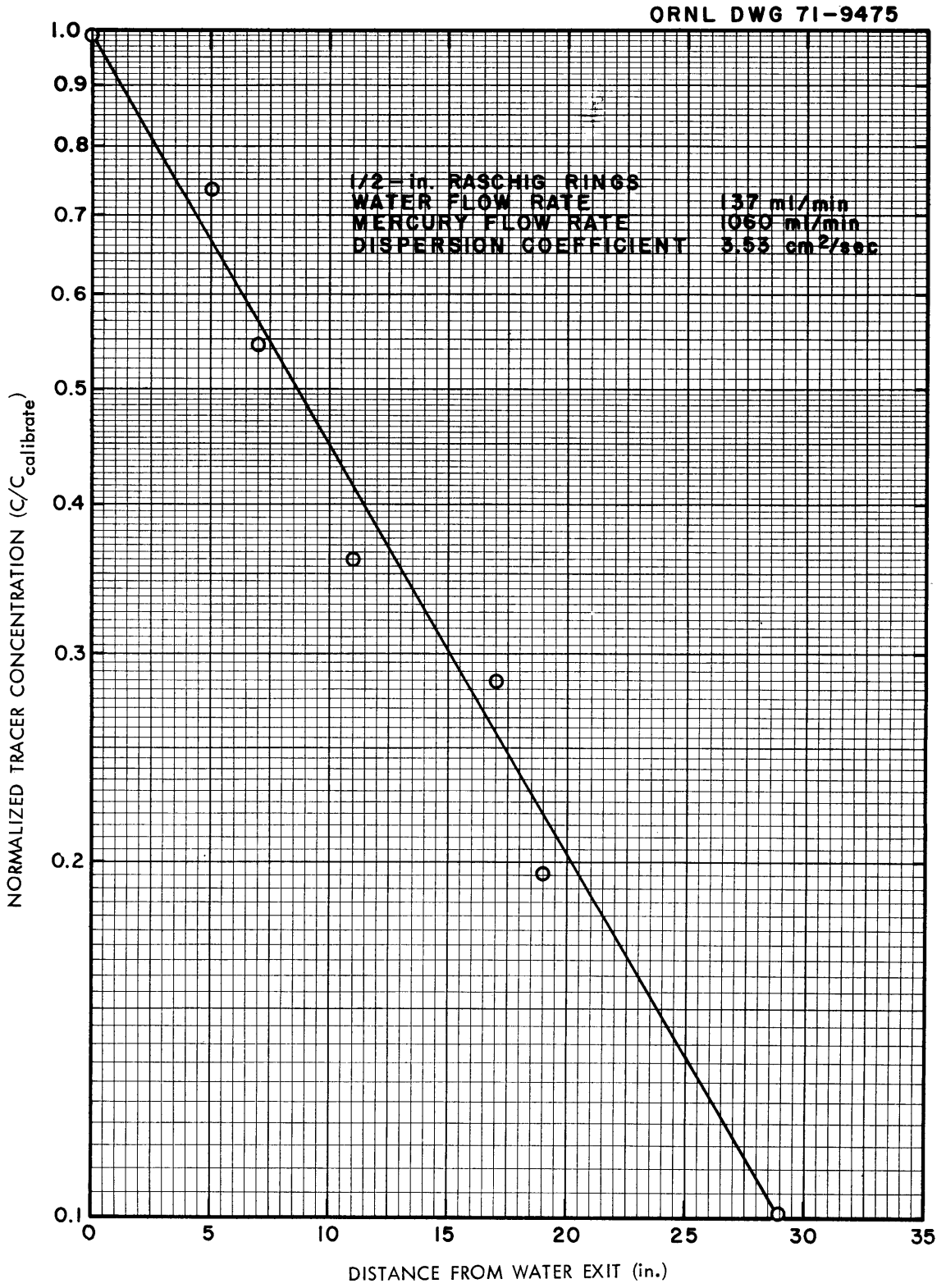

Fig. 43. Variation of Normalized Tracer Concentration with Distance Along 2-in.-diam Column Packed with 1/2-in. Raschig Ring Packing During Run 11.

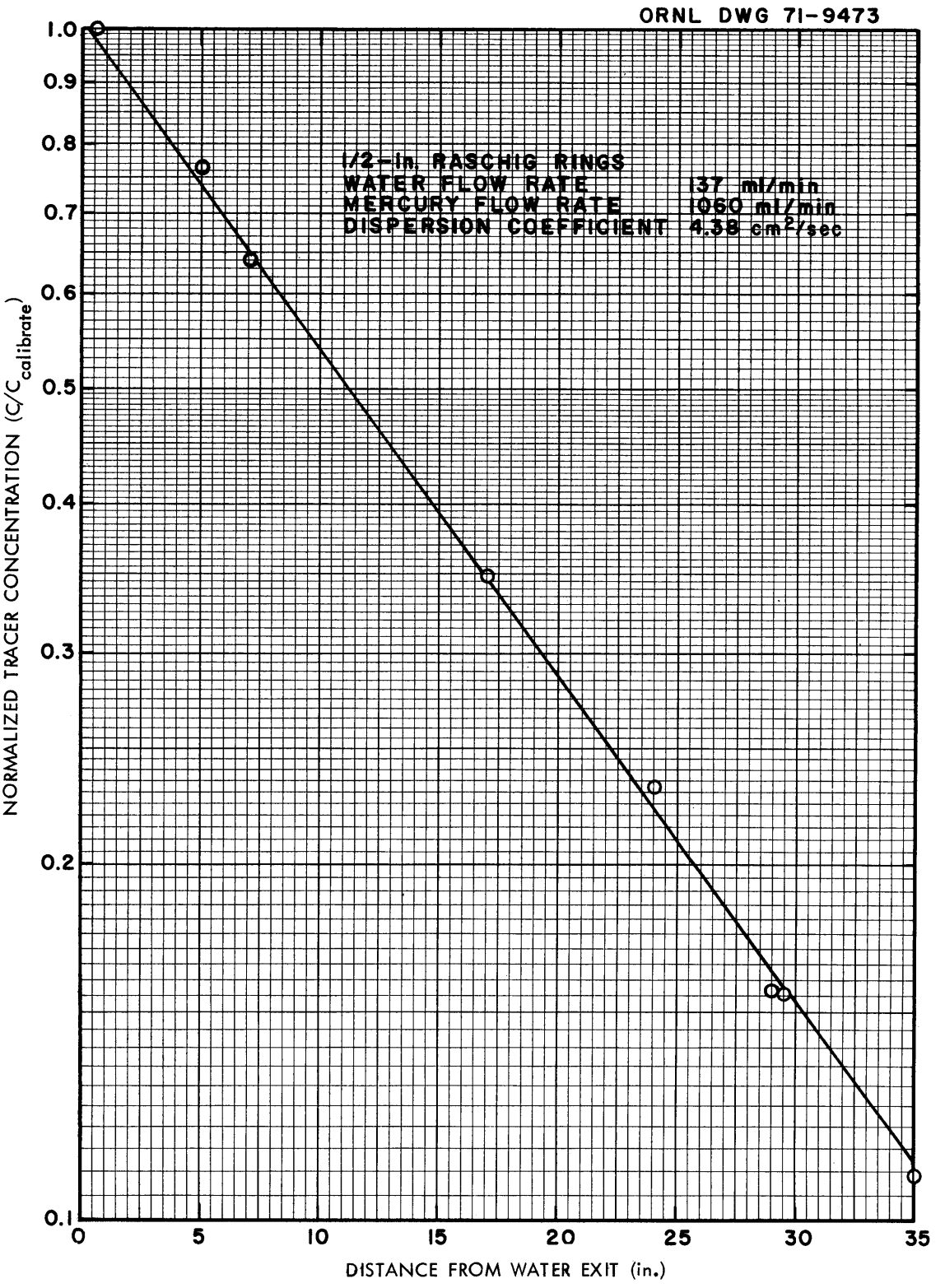

Fig. 44. Variation of Normalized Tracer Concentration with Distance Along 2-in.-diam Column Packed with 1/2-in. Raschig Ring Packing During Run 12.

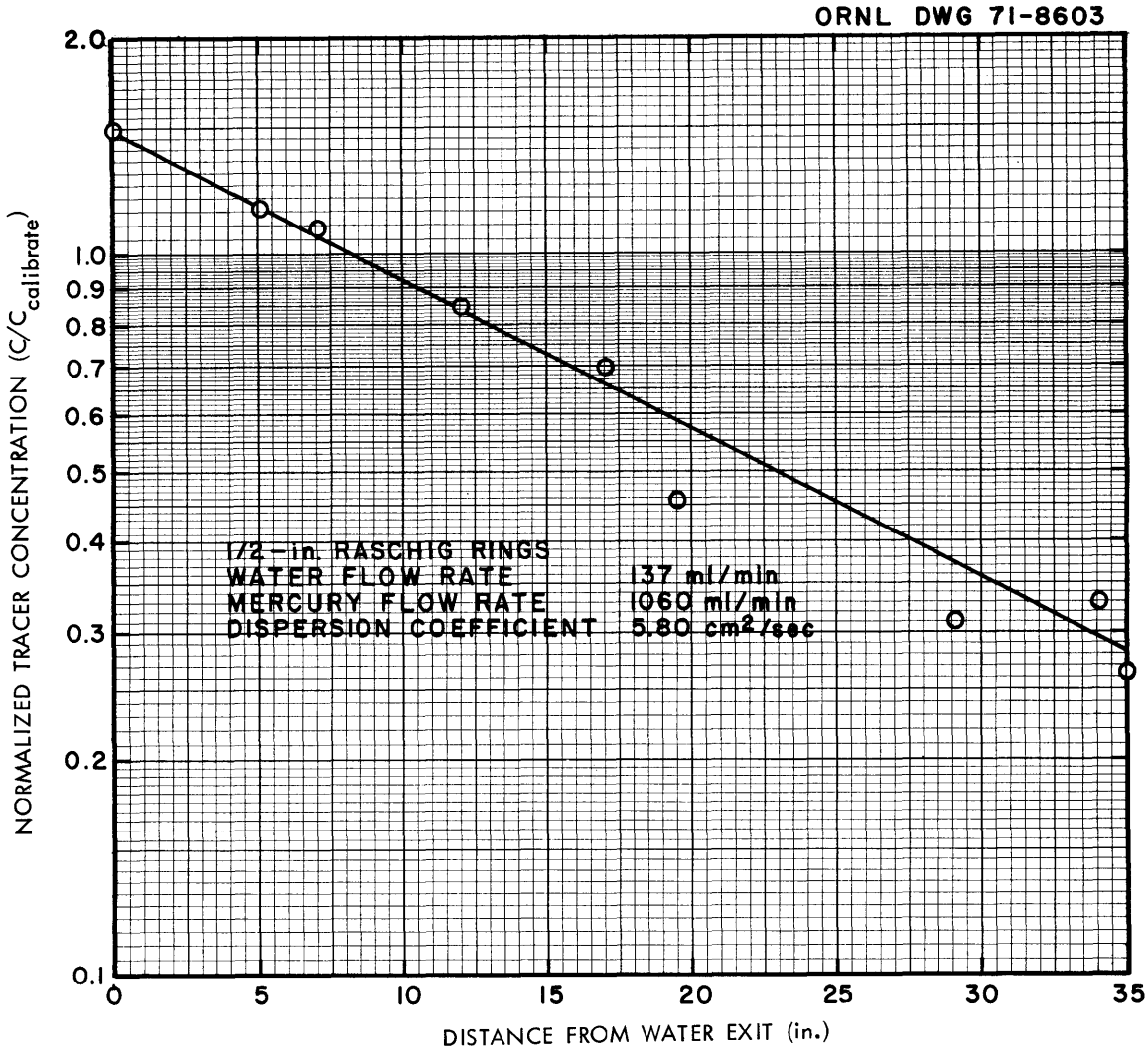

Fig. 45. Variation of Normalized Tracer Concentration with Distance Along 2-in.-diam Column Packed with 1/2-in. Raschig Ring Packing During Run 13.

Table 9. Summary of Axial Dispersion Measurements with 1/4-in. Solid Cylinders in a 2-in.-diam Column

Run	V_{Hg} (ml/min)	V_{H_2O} (ml/min)	D_e (cm^2/sec)
1	350	23	1.41
2	350	46	1.18
3	600	69	0.463
4	820	23	2.08
5	820	46	0.669

Table 10. Summary of Axial Dispersion Measurements with 1/4-in.-diam Raschig Rings in a 2-in.-diam Column

Run	V_{Hg} (ml/min)	V_{H_2O} (ml/min)	D_e (cm^2/sec)
1	350	22.8	2.05
2	350	47	1.33
3	350	68.4	0.918
4	820	22.8	2.16
5	820	45.6	1.88
6	820	64.8	1.03

Table 11. Summary of Axial Dispersion Measurements with 1/2-in.-diam Raschig Rings in a 2-in.-diam Column

Run	V_{Hg} (ml/min)	V_{H_2O} (ml/min)	D_e (cm^2/sec)
1	380	46	6.48
2	380	68	4.78
3	655	23	3.25
4	655	46	4.59
5	655	68	4.52
6	655	91	4.66
7	655	137	4.68
8	1060	46	6.23
9	1060	46	6.65
10	1060	91	4.56
11	1060	137	3.53
12	1060	137	4.38
13	1060	137	5.80

ORNL DWG 71-9545

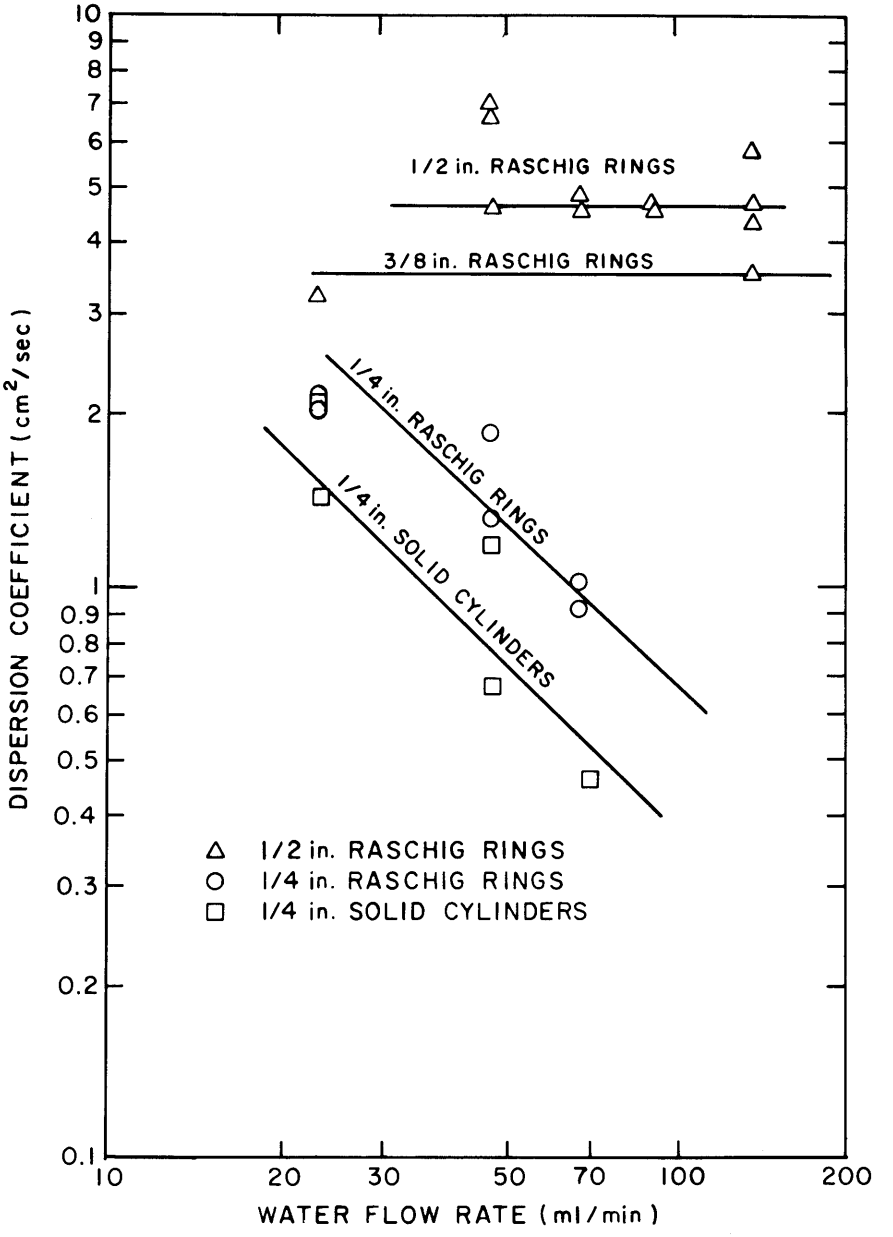

Fig. 46. Variation of Dispersion Coefficient with Water Flow Rate for Several Packing Materials in a 2-in.-diam Column.

the 1/4-in. packing indicate that the dispersion coefficient is inversely proportional to the continuous-phase flow rate. Differences between the dispersion coefficients for the two 1/4-in.-diam packing materials are probably related to the difference in the packing void fractions of these materials. The data appear to portray two types of behavior, one for 1/4-in. packing and one for larger packing.

7.2 Comparison of Results with a Published Correlation

Experimental data on axial dispersion in packed columns have been obtained by Vermeulen, Moon, Hennico, and Miyauchi,[16] who reported a correlation for predicting axial dispersion. Their study involved several fluids which had a range of physical properties and a number of packing materials; however, as the authors pointed out, the study did not include a sufficiently wide range of the difference in fluid densities to evaluate the effect of this variable. The data obtained during the present study afford a test of the Vermeulen correlation for fluids that have a large density difference.

The present data are compared with the correlation of Vermeulen, Moon, Hennico, and Miyauchi in Fig. 47, where the dimensionless quantity $\varepsilon V_c d_p/D_e$ is plotted against the dimensionless quantity $(\psi\nu/d_p V_c)^{1/2} V_d/V_c$. The agreement of the present experimental data with this correlation is remarkable since the correlation was developed from data obtained with systems having density differences between one and two orders of magnitude less than that of the mercury-water system. The scatter of the present data around the curve is not significantly greater than that of the earlier data.

Closer examination of the data reveals an apparent difference between the correlation and the present data with regard to the dependence of dispersion coefficient on the flow rates of the two phases. However, it was not possible to cover a sufficiently wide range of mercury and water flow rates to confirm the suspected dependence.

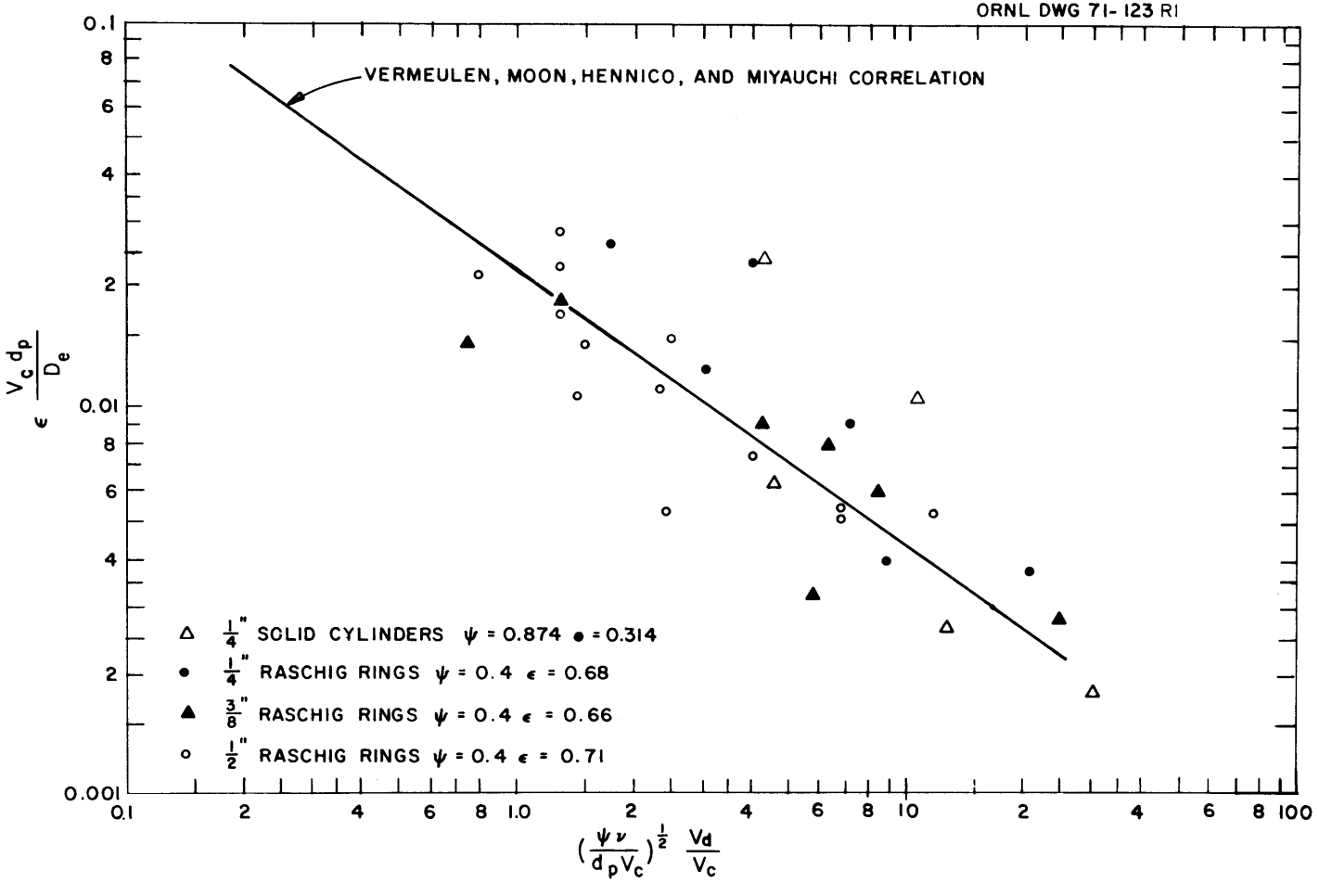

Fig. 47. Comparison of Mercury-Water Data Obtained in This Study With the Vermeulen, Moon, Hennico, and Miyauchi Correlation.

8. REFERENCES

1. M. J. Bell and L. E. McNeese, "MSBR Fuel Processing Using the Fluorination--Reductive Extraction and Metal Transfer Flowsheet," Engineering Development Studies for Molten-Salt Breeder Reactor Processing No. 6, ORNL-TM-3141 (in press).

2. L. M. Ferris, "Measurement of Distribution Coefficients in Molten Salt--Metal Systems," MSR Program Semiann. Progr. Rept. Aug. 31, 1970, ORNL-4622, p. 204.

3. R. W. Kessie et al., Process Design for Frozen-Wall Containment of Fused Salt, ANL-6377 (August 1961).

4. J. R. Hightower, Jr., C. P. Tung, and L. E. McNeese, "Use of Radio-Frequency Induction Heating for Frozen-Wall Fluorinator Development Studies," Engineering Development Studies for Molten-Salt Breeder Reactor Processing No. 6, ORNL-TM-3141 (in press).

5. S. Cantor (Ed.), Physical Properties of Molten Salt Reactor Fuel, Coolant, and Flush Salts, ORNL-TM-2316 (August 1968), p. 14.

6. J. W. Cook, MSR Program Semiann. Progr. Rept. Feb. 28, 1969, ORNL-4396, p. 122.

7. S. Cantor (Ed.), Op. Cit., p. 25.

8. P. G. Simpson, Induction Heating, McGraw-Hill, New York, 1960, p. 141.

9. E. L. Youngblood et al., "Metal Transfer Process Development," Engineering Development Studies for Molten-Salt Breeder Reactor Processing No. 6, ORNL-TM-3141 (in press).

10. MSR Program Semiann. Progr. Rept. Feb. 28, 1969, ORNL-4396, p. 284.

11. MSR Program Semiann. Progr. Rept. Feb. 28, 1970, ORNL-4548, p. 291.

12. R. B. Lindauer and L. E. McNeese, "Continuous Salt Purification Studies," Engineering Development Studies for Molten-Salt Breeder Reactor Processing No. 6, ORNL-TM-3141 (in press).

13. W. S. Pappas, Anal. Chem. 38, 615 (1966).

14. L. E. McNeese, Engineering Development Studies for Molten-Salt Breeder Reactor Processing No. 3, ORNL-3138, p. 34.

15. Ibid., p. 72.

16. T. Vermeulen, J. S. Moon, A. Hennico, and T. Miyauchi, Chem. Eng. Progr. 62, 96 (1966).

INTERNAL DISTRIBUTION

1. C. F. Baes
2. H. F. Bauman
3. S. E. Beall
4. M. J. Bell
5. M. R. Bennett
6. R. E. Blanco
7. F. F. Blankenship
8. G. E. Boyd
9. R. B. Briggs
10. R. E. Brooksbank
11. K. B. Brown
12. W. L. Carter
13. H. D. Cochran, Jr.
14. F. L. Culler
15. J. R. Distefano
16. W. P. Eatherly
17. D. E. Ferguson
18. L. M. Ferris
19. J. H. Frye
20. W. R. Grimes
21. A. G. Grindell
22. P. A. Haas
23. B. A. Hannaford
24. J. R. Hightower, Jr.
25. C. W. Kee
26. R. B. Lindauer
27. H. E. McCoy
28-38. L. E. McNeese
39. D. M. Moulton
40. J. P. Nichols
41. E. L. Nicholson
42. J. H. Pashley (K-25)
43. A. M. Perry
44-45. M. W. Rosenthal
46. A. D. Ryon
47. W. F. Schaffer, Jr.
48. Dunlap Scott
49. J. H. Shaffer
50. M. J. Skinner
51. F. J. Smith
52. D. D. Sood
53. Martha Stewart
54. O. K. Tallent
55. R. E. Thoma
56. D. B. Trauger
57. W. E. Unger
58. C. D. Watson
59. J. S. Watson
60. A. M. Weinberg
61. J. R. Weir
62. M. E. Whatley
63. J. C. White
64. W. M. Woods
65. R. G. Wymer
66. E. L. Youngblood
67-68. Central Research Library
69-70. Document Reference Section
71-73. Laboratory Records
74. Laboratory Records, RC
75. Y-12 Document Reference Section
76. ORNL Patent Office

EXTERNAL DISTRIBUTION

77. J. A. Accairri, Continental Oil Co., Ponca City, Oklahoma 74601
78. R. M. Bushong, UCC, Carbon Products Division, 12900 Snow Road, Parma, Ohio 44130
79. D. F. Cope, Atomic Energy Commission, RDT Site Office (ORNL)
80. C. B. Deering, Black & Veach, P. O. Box 8405, Kansas City, Missouri 64114
81. A. R. DeGrazia, USAEC, RDT, Washington, D.C. 20545
82. Delonde R. deBoisblanc, Ebasco Services, Inc., 2 Rector Street, New York, N.Y. 10006
83. D. Elias, RDT, USAEC, Washington, D.C. 20545
84. Norton Haberman, RDT, USAEC, Washington, D.C. 20545
85. T. R. Johnson, Argonne National Laboratory, 9700 S. Cass Avenue, Argonne, Illinois 60439

EXTERNAL DISTRIBUTION (Continued)

86. Kermit Laughon, Atomic Energy Commission, RDT Site Office (ORNL)
87-88. T. W. McIntosh, Atomic Energy Commission, Washington, D.C. 20545
89. E. H. Okrent, Jersey Nuclear Co., Bellevue, Washington 98004
90. R. D. Pierce, Argonne National Laboratory, 9700 S. Cass Avenue, Argonne, Illinois 60439
91. J. Roth, Combustion Engineering Inc., Prospect Hill Road, Windsor, Connecticut 06095
92. M. Shaw, Atomic Energy Commission, Washington, D.C. 20545
93. N. Srinivasan, Head, Fuel Reprocessing Division, Bhabha Atomic Research Center, Trombay, Bombay 74, India
94. C. L. Storrs, Combustion Engineering Inc., Prospect Hill Road, Windsor, Connecticut 06095
95. B. L. Tarmy, Esso Research and Engr. Co., P. O. Box 101, Florham Park, N.J. 07932
96. J. R. Trinko, Ebasco Services, Inc., 2 Rector Street, New York, N.Y. 10006
97. Laboratory and University Division, ORO
98-99. Division of Technical Information Extension, ORO, AEC